12-2015

A SPECIAL PROTECTION SCHEME UTILIZING TRAJECTORY SENSITIVITY ANALYSIS IN POWER TRANSMISSION

Dan Suriyamongkol
Clemson University, dsuriya@clemson.edu

A SPECIAL PROTECTION SCHEME UTILIZING TRAJECTORY SENSITIVITY ANALYSIS IN POWER TRANSMISSION

A Dissertation
Presented to
the Graduate School of
Clemson University

In Partial Fulfillment
of the Requirements for the Degree
Doctor of Philosophy
Electrical Engineering

---

by
Dan Suriyamongkol
December 2015

Accepted by:
Elham B. Makram, Committee Chair
Carl W. Baum
Mark E. Cawood
Richard E. Groff

ABSTRACT

In recent years, new measurement techniques have provided opportunities to improve the North American Power System observability, control and protection.

This dissertation discusses the formulation and design of a special protection scheme based on a novel utilization of trajectory sensitivity techniques with inputs consisting of system state variables and parameters. Trajectory sensitivity analysis (TSA) has been used in previous publications as a method for power system security and stability assessment, and the mathematical formulation of TSA lends itself well to some of the time domain power system simulation techniques.

Existing special protection schemes often have limited sets of goals and control actions. The proposed scheme aims to maintain stability while using as many control actions as possible.

The approach here will use the TSA in a novel way by using the sensitivities of system state variables with respect to state parameter variations to determine the state parameter controls required to achieve the desired state variable movements. The initial application will operate based on the assumption that the modeled power system has full system observability, and practical considerations will be discussed.

DEDICATION

I would like to express my deepest gratitude to my parents and my wife for their continued support and patience, and my teachers for the wisdom & lessons from their expertise and their experience. A student's education is a product of all the educators around the student as much as the student's efforts, resulting in my education becoming greater than the sum of its parts because of the educators around me.

ACKNOWLEDGMENTS

Dr. Adly A. Girgis and Dr. Brian Manhire have been educators who helped mold my successes, especially by showing their passion for this field, passion for education, and always bringing the best work out of the people around them.

Dr. Elham B. Makram has always kept her doors open and guided my work to the finish.

Dr. Hany A. Abdelsalam has been instrumental in helping refine my work with rigorous examination.

TABLE OF CONTENTS

Table of Contents (Continued)

Page

LIST OF TABLES

LIST OF FIGURES

List of Figures (Continued)

Page

List of Figures (Continued)

Page

List of Figures (Continued)

Page

List of Figures (Continued)

Page

CHAPTER 1

INTRODUCTION

This dissertation discusses the formulation and design of a special protection scheme based on a novel utilization of trajectory sensitivity techniques with power system state variables and physical model data as the main inputs. The work for the dissertation includes the formulation of the special protection scheme, the mathematical analysis leading up to the scheme design, and testing of the scheme using software simulation. In this introductory chapter, the research motivations and objectives, a brief review of relevant literature, the contributions of the dissertation, and the outline of the overall dissertation will be discussed.

1.1 Research Motivations and Objectives

The objective of this dissertation is to develop a special protection scheme for wide-area power systems, concentrating on the transmission level of the system. The special protection scheme will be designed to use power system state variables, and system data as inputs and utilize trajectory sensitivity analysis techniques to drive the protective and control actions.

Special protection schemes are different from conventional protection schemes. These schemes are designed to analyze the system state measurements and state estimates in order to determine whether the system is moving towards an unstable or unacceptable state and then take preventive actions. Instead of simply disconnecting equipment or switching some of the equipment, the special protection scheme is designed to evaluate

what protective and control actions are available and initiate the actions that have the most positive impact on the system state variables.

The state variables that are being evaluated and controlled include voltage and current magnitudes and angles, machine shaft speeds, and internal variables for the dynamic models of the power system components. For the purposes of this dissertation, the variables are imported from a time-domain simulation in a MATLAB environment. From a practical standpoint, some of the required data are available from synchrophasor outputs and the remainder can be derived using pseudo-measurements. These may include imported external device measurements, breaker status flags that can be used to determine changes to system topology, or equipment warning flags to detect overloading in key lines or transformers. The circuit topology and system equipment parameters such as machine inertia, exciter characteristics, etc., are also part of the input that will have to be available in order for the special protection scheme to evaluate the system trajectory correctly.

After the special protection scheme design is tested in software simulation, the scheme performance will be reviewed with considerations for the practical case where measurements are available from PMUs, but not at every bus on the system. Afterwards, a methodology is suggested for modifying the simulated case for application in an actual power system where perfect measurements cannot be assumed.

1.2 Brief Review of Topics Covered and Relevant Literature

1.2.1 Power System Dynamic Modeling

The simulations performed for this dissertation are done in a MATLAB environment, specifically utilizing the open-source PSAT toolbox [1]. All of the models and corresponding variables used are defined in the toolbox manual [1]. A summary of the models is shown below to clearly illustrate the calculation requirements.

Synchronous Machines

Synchronous machines are modeled as a sixth-order dynamic model. The differential and algebraic equations used in [1] follow the modeling equations in [2] which have the following state (x_{sync}) and algebraic (y_{sync}) variables.

$$x_{sync} = \left[\delta, \omega, e'_q, e'_d, e''_q, e''_d \right] \tag{1}$$

$$y_{sync} = \left[p_m, p_e, q_e \right] \tag{2}$$

Where

δ	Shaft angle of rotation
ω	Rate of rotation, per-unit
$e'_d, e'_q,$	Voltages behind transient reactances for *d* and *q* axes
e''_d, e''_q	Voltages behind sub-transient reactances
p_m	Mechanical power input for the machine
p_e, q_e	Electrical active (*p*) and reactive (*q*) power

The dynamic equations that model the behavior of the synchronous machine and the algebraic equations that model the machine terminal conditions as well as the other system parameters are shown in Chapter 2.

Automatic Voltage Regulators

Automatic Voltage Regulators (AVRs) are also known as Exciters or Excitation Systems, and are the control devices responsible for generating the voltage that is applied to the field circuit on the rotor. The field circuit appears in the equations as an input for the synchronous machine. The AVR model is IEEE Type II which is shown in Chapter 2 of this dissertation [1].

Power System Stabilizer

Power System Stabilizers (PSS) are control devices that are added to the synchronous machine in order to provide additional control for the speed or the voltage. The PSS model used for this dissertation is the model for speed control, and is applied to some but not all of the synchronous generators. The PSS model is Type II and is described by the state equations shown in Chapter 2.

Wind Generator

The wind turbine model simulated for this dissertation is comprised of a Weibull distribution speed model for the wind speed, a doubly-fed induction generator (DFIG) with a controller element representing speed, and pitch feedback to control the output power and voltage. The converter model is assumed to be lossless in order to simplify the calculations. The wind speed, turbine, and DFIG equations, including the voltage control equation containing the DFIG reference terminal voltage (V_{ref}), are discussed below. The basic circuit diagram for the DFIG is shown in Figure 1.1, reproduced from Milano [1].

The wind speed model includes constant air density which can be manually corrected based on altitude, and is assumed to be at sea level. The Weibull Distribution function that is used to determine the wind speed is shown in Chapter 2.

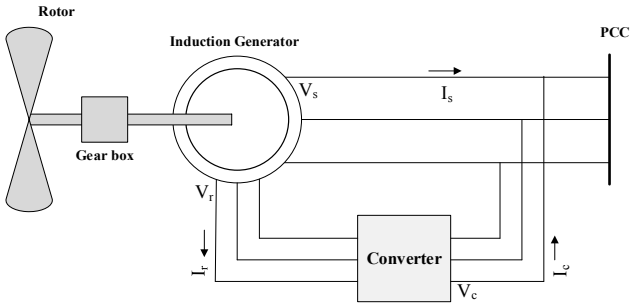

Figure 1.1: Block diagram of DFIG

The mechanical and electromechanical equations for the DFIG are based on the initial assumption that the converter controls decouple the generator from the grid. Generator complex power can be written from the rotor and stator currents. The rotor and stator currents and voltages are decomposed into direct- and quadrature-axes. [2]

The motion dynamic is based on a single shaft. The differential equations for the converter currents and pitch angle control are described in Chapter 2.

The existing literature and references that cover power system dynamic simulation are too numerous to list in detail. For the purposes of this dissertation, the dynamic modeling techniques are based on works by P.M. Anderson, et al [2], [3],and the programming references for PSAT in the MATLAB environment can be found in the bibliography of [1].

1.2.2 Trajectory Sensitivity Analysis

Beginning with sensitivity theory as described by Frank [4], dynamical systems with a state variable vector x, varying system parameters α, and system dynamics

function *F(x)* can be analyzed in terms of changes to the state variable with respect to changes in system parameters. These terms are called sensitivity functions *S(α)* and an approximate relationship between changes in system parameters and resulting changes in state variables is shown in equation (3) below.

$$\begin{aligned} &\dot{x} = f(x, \alpha, t, u), \quad x(t_0) = x_0 \\ &\Delta x \approx S(\alpha_0)\Delta\alpha \end{aligned} \tag{3}$$

Pai [5] applied sensitivity theory to power system transient stability assessment for power systems with the classical machine model where the only variables of concern were machine angles and generator shaft frequencies. TSA was used to create a dynamic security assessment tool to identify state parameters that have large effects on system stability and the state variables that will be affected. Laufenberg and Pai [6] then expanded the application to a differential-algebraic equation (DAE) representation of the power system.

Given a dynamical system with the state variable vector *x*, network variable vector *y*, and system parameters that are subject to change *α*, the system dynamics can be expressed as shown in equations (4) and (5).

$$\dot{x} = F(x, y, \alpha, t) \qquad x(t_0) = x_0 \tag{4}$$

$$0 = G(x, y, \alpha, t) \qquad y(t_0) = y_0 \tag{5}$$

The changes in the system parameters and variables with respect to system parameters can be expressed by augmenting the system equations (4) and (5) with the following equations (6) and (7).

$$\dot{w}_1 = \frac{\partial F}{\partial x} w_1 + \frac{\partial F}{\partial y} w_2 + \frac{\partial F}{\partial \alpha} \tag{6}$$

$$0 = \frac{\partial G}{\partial x} w_1 + \frac{\partial G}{\partial y} w_2 + \frac{\partial G}{\partial \alpha} \tag{7}$$

Where $w_1 = \partial x / \partial \alpha, \;\; w_2 = \partial y / \partial \alpha$

This set of equations can be solved using numerical techniques to analyze the effects of known disturbance or changes to the operating conditions, and have been used for dynamic security assessment purposes. While Laufenberg and Pai [5], [6] used the solved sensitivity functions as indicators of stability, Hou [7] used trajectory sensitivity techniques to estimate the trajectory of the state variables. Hou [7] then compared the estimated trajectory and actual trajectory during disturbances and found that the estimated state variable trajectory reasonably tracked the simulated state variable trajectories. These techniques will be utilized differently for the purposes of this dissertation and will be discussed further below.

For power systems, the state variables can include bus voltage magnitudes, bus voltage angles, line current magnitudes and angles, bus frequency, generator frequency and shaft angle, generator field voltage and current controls, power system stabilizer variables, as well as other variables. The amount of state variables may increase or decrease depending on the level of complexity of the models and the number of buses being considered. In [5] and [6], small system examples are provided, while the authors of [7] performed TSA on a large model that ended up requiring parallel computing to solve the simultaneous DAE sets.

Because the potential size and complexity of the TSA problems, it is important to select the state variables of interest, state parameters, as well as system models carefully. Shubhanga and Kulkarni [8] use TSA to improve transient stability using shunt/series compensation and preventive generator rescheduling. In Tang and McCalley [9], TSA applications in various areas of power systems are discussed. In addition, [9] used TSA for estimation accuracy refinement.

Distributed generation using synchronous generators with combustion turbines were studied by Chatterjee, et al [10] using the TSA technique to determine the critical values of different parameters and locate the distributed generation (DGs) in power systems. Mitra and Chatterjee [11] studied the impact of wind power (especially the DFIG) on the TSA for power system security assessment. Also, to the best of our knowledge none of the literature studied the self- and cross-interaction of DFIG variables.

1.2.3 Basics of Out-of-Step Protection and Special Protection Schemes

Out-of-step protection is a type of protection that is based on the apparent impedance calculations at a protective device or measurement point located on a device that is deemed critical to power system operations such as a major transmission line where a loss of power transmission across the line will result in catastrophic system failure. Anderson [12] provides a basic overview to the philosophy as well as some examples. The North American Electric Reliability Corporation (NERC) publishes requirements for designing, assessing, operating, and maintaining special protection

schemes [13 - 16], and these requirements are enforced by the Federal Energy Regulatory Committee (FERC).

A protective relay can calculate the apparent impedance (Z_{app}) of the device it is protecting by using the measured voltage and current as shown in equation (8).

$$\bar{Z}_{app} = \left(\left| \bar{V}_{relay} \right| / \left| \bar{I}_{relay} \right| \right) \angle \left(\theta_V - \theta_I \right) \tag{8}$$

Where the θ symbol denotes the phasor angles and the bar above the variables indicate that the variables are phasors.

Out-of-step relay settings are established by performing a power system stability analysis via simulation. Scenarios where the protected device becomes unstable are determined, and the apparent impedances in these scenarios are used to create the settings of out-of-step relays. An example and application to the test systems in this dissertation will be shown in subsequent chapters.

The apparent impedance is continuously calculated by the relay for various functions, primarily the main protection settings, as well as for any local calculations. In some cases when the relay requires calculated impedance or measurements, communication methods such as phasor measurements are required.

Because of the status of out-of-step (OOS) protection schemes as a special protection scheme type, OOS are often deployed by utilities to solve localized problems or very specific scenarios that destabilize the power system. Examples of these schemes have been published from South Africa [17] to Texas [18] and several areas in between. The OOS analysis has become more important due to the increased presence of wind energy resources [18], because wind turbines have smaller amounts of stored energy in

the rotating mass, which in turn generates sub-synchronous swings in power systems that were not present in past synchronous machine-dominated systems.

In addition to the older definitions and settings of OOS protection, researchers and engineers have also worked on various methods of enhancing OOS protection. This includes implementing adaptive protection schemes so that the settings can adapt to the changing conditions of the power system around the relays [19], setting up relay blocking schemes that prevent inadvertent tripping when the power system conditions are swinging into the protection setting zone but will return to stability [20 – 22]. Lastly, the development of synchrophasor technology allowed for new and more accurate measurements as well as auxiliary functionalities to be applied as enhancement of OOS schemes [23 – 24].

1.2.4 Phasor Measurement Unit Basics

Phasor Measurement Units (PMUs, also called synchrophasors) are a class of measurement equipment that is defined by IEEE standard number C37.118.1^{TM}-2011 [25] and C37.118.2^{TM}-2011 [26]. The current version of the standard's two volumes was modified from the 2005 version to provide additional specifications and to make the format of the standard consistent with IEC standards in anticipation of the IEEE standard being adopted for use by IEC.

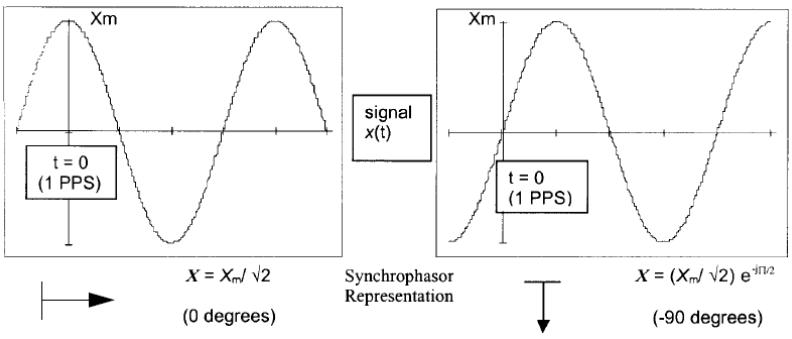

Figure 1.2: IEEE C37.118.1-2011 standard phasor representation of a sinusoidal signal

PMUs utilize time synchronized sampling of an analog signal and the samples are processed to estimate phasor representations of the measured analog signal as shown in Figure 1.2. There are several manufacturers that utilize different methods of signal processing to produce the phasor estimates, but the IEEE standard specifies the format of the output, the quality of the measurements, and the message packet contents for communication purposes. This assures that the PMUs output uniform measurements across vendors. Figure 1.3 shows the standard message format for PMUs.

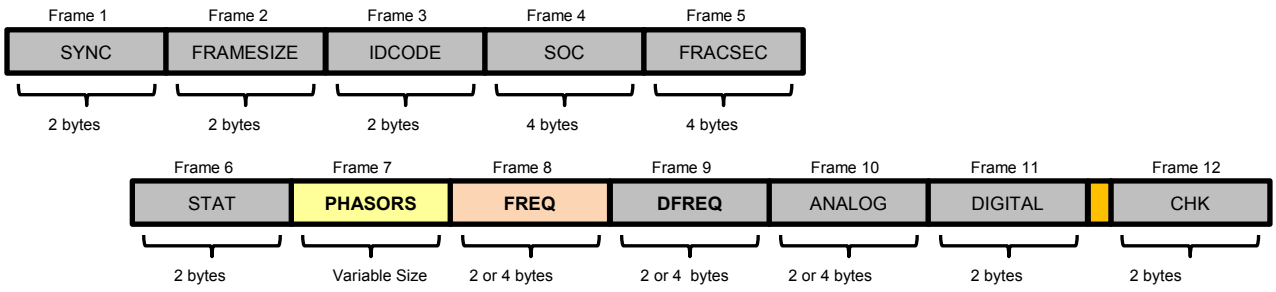

Figure 1.3: IEEE C37.118.2-2011 standard message format

The information included in each message frame is listed below.

SYNC: Frame synchronizing word.

FRAMESIZE: Total number of bytes in the frame.

IDCODE: PMU ID Number.

SOC: GPS time stamp.

FRACSEC: Fraction of Second and Time Quality.

STAT: Status flags.

PHASORS: Actual phasor measurement results. (See more details below)

FREQ: Frequency.

DFREQ: Rate of change of frequency.

ANALOG: Analog data that can be added to the message.

DIGITAL: Digital data that can be added to the message.

CHK: CRC error check.

The PHASORS, FREQ, DFREQ, ANALOG, and DIGITAL frames can be repeated for the number of PMU measurements to be included in the message, and the number of PMU measurements included in a message is specified in the SYNC frame. Messages coming from a phasor data concentrator can have dozens or hundreds of PMU measurements within one message. The phasors for each PMU can include voltages and/or currents, it can be expressed in polar or rectangular form, and can be positive sequence only or three-phase quantities. Analog and digital data frames can include other measurement data, equipment status bits or digital communication data as the user deems necessary.

One of the practical considerations of the special protection scheme is the case where PMUs are not located at every bus, the trajectory sensitivity and special protection scheme equations will be modified accordingly. This is a consideration because it is not practical for PMUs to be located at every bus. Buses that do not have PMUs installed are

usually handled in terms of pseudo-measurements that are calculated from adjacent buses with PMUs.

1.3 Contributions of the Dissertation

Previous literature used trajectory sensitivity analysis to perform security assessments to determine if a disturbance will result in undesired state variable values. This research uses those techniques and extends the use of trajectory sensitivity analysis to determine how to reach a desired outcome or desired state variable values.

Existing special protection schemes often have limited sets of goals and control actions, such as controlling capacitor switching to maintain voltage stability or controlling generation parameters to maintain angular stability. The proposed scheme aims to maintain both voltage and angular stability simultaneously, while using as many control actions as necessary.

1.4 Methodology

1.4.1 Determine Unstable Scenarios

Using the PSAT toolbox to simulate a large power system, the IEEE 68-Bus Test System, one of the main tie lines between two major sub-systems are analyzed for its role in maintaining stability and preventing the two sub-areas from separation. Cases with separation of the two sub-areas are considered catastrophically unstable scenarios because the smaller systems that remain have large mismatches between generation capacity and loads.

Instability can also be detected by analyzing the mode of oscillation of bus angle and frequency measurements. Tools that utilize this technique are already commercially

available in some of the newer relays and phasor data concentrators. The measurement of the angle and frequency (δ, ω) are analyzed over a window of time and evaluated curve-fitted time functions to determine if the variables appear underdamped, critically damped or undamped (unstable cases) or well-damped (stable). The mode of oscillation is a complex number that can be transmitted from the relays/PDCs by appending the values to the synchorphasor message.

1.4.2 Selecting the Protective & Control Actions

When the power system is characterized as sets of dynamic state equations and power flow equations, the voltages, angles, frequencies, and power flows are the state variables that are being monitored. Keeping these state variable values within acceptable ranges is the goal of the special protection scheme and it can be achieved by using protective and control actions on the power system. The protective and control actions include switching on reactive power assets (changes to Q_c), connecting or disconnecting lines (changes to Y_{bus}, Z_{bus}), changes to excitation and PSS controls (changes to ω_{ref}, V_{gen}, E_{field}) and changes to generator output power ($P_{gen,ref}$, $P_{turbine.ref}$).

In the power flow equations and system dynamic equations, these values are characterized as either state equation inputs or system parameters. Using the trajectory sensitivity analysis, we can determine which parameters have the highest sensitivity coefficients and determine which variables should be manipulated to restore stability and prevent any existing out-of-step protection from disconnecting a line, thereby causing the catastrophic failure.

CHAPTER 2

MATHEMATICAL FORMULATION OF TSA

In this chapter, the mathematical formulations of the trajectory sensitivity analysis (TSA) will be presented in greater details. This will take the form of the application to power systems starting from a simple example and expanding to a larger generalized system. The TSA model will then be revised further to accommodate the fact that the system information is not a true set of measurements but rather discrete simulation outputs. This exercise is performed first for a simple classical machine system, then a larger 9-bus power system, and last with a 68-bus system. The 68-bus system will become the focus of the out-of-step protection design. Finally, the logic diagram of the special protection scheme is developed to include the results of the previous sections.

2.1 TSA Equation Formulation

2.1.1 Simple Dynamical System

As seen from equations (3) through (7) in Chapter 1, the TSA equations result in the sensitivity factors becoming additional state variables that must be solved after the original state variables are solved. In the cases of simple dynamical systems, the system can be modeled purely with dynamical equations and do not have any algebraic equations or other mathematical constraints. This corresponds to systems that can be described by a system similar to equation (3). The process for calculating the sensitivity coefficients is shown in Figure 2.1 in the next page. This means that for n state variables and m parameters of interest, there are n state equations and $m \times n$ sensitivity equations that need to be solved, or a total of $n \times (m+1)$ equations.

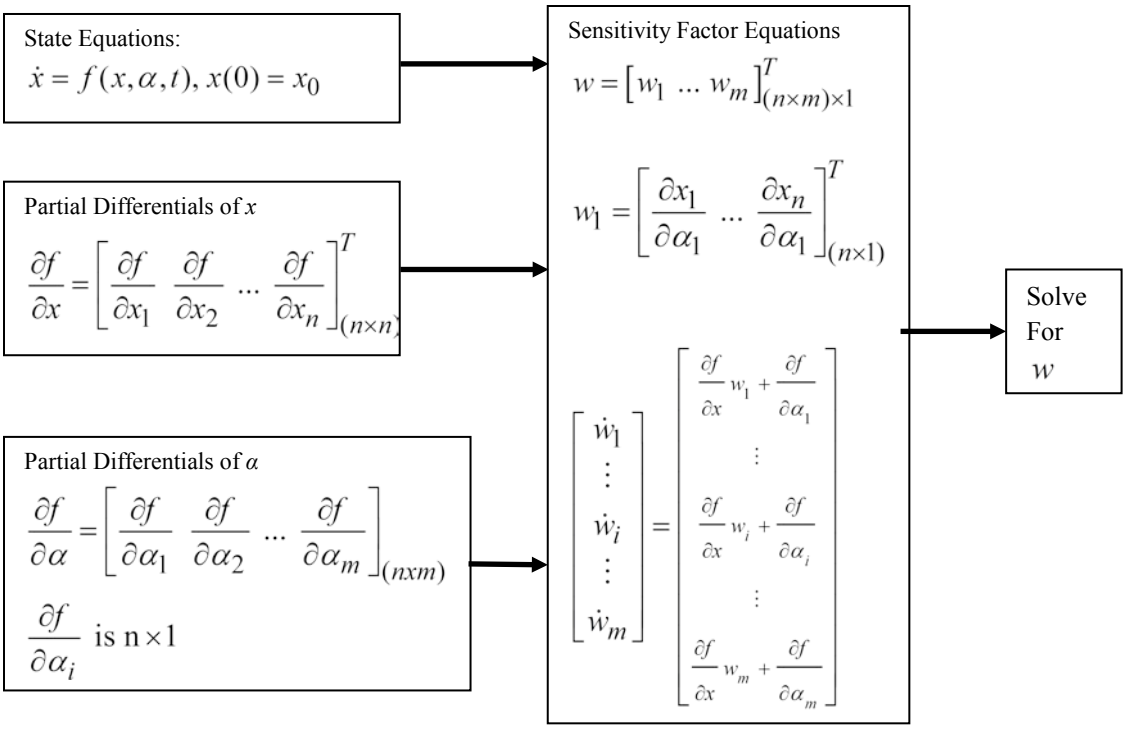

Figure 2.1: Process for calculating sensitivity factors of a dynamical system

From the process and equations shown in Figure 2.1, it can be seen that the sensitivity coefficients – members of the w vector – are calculated independently of solving for the state variables, but they will require the state variables to be solved in the cases where the partial differentials contain state variable terms. The trajectory sensitivity analysis above is based on the system dynamic containing continuous functions that are not being subjected to sudden changes in the structure of the system. This is discussed in greater detail by Frank [4]. When the system experiences sudden changes in system topology, and when the system exhibits hybrid differential-algebraic-discrete structure (such as a power system), the application of trajectory sensitivity analysis has to be adjusted to account for the system properties and the borders between discrete system changes. This treatment is introduced by Hiskens and Pai [27].

2.1.2 Systems with Dynamic and Algebraic Equations

Systems that exhibit dynamical properties while also being constrained by algebraic equations are exemplified in equations (4) and (5) in Chapter 1. The system will also contain state variables (x) and system outputs (y) that are dependent on each other, which means that taking partial differentials will result in cross-coupled terms. These terms when expanded using the first order Taylor series will result in the solution form in equations (6) and (7). Sections 2.2.2 and 2.2.3 show two different approaches to solving these coefficients with two different types of time domain simulation.

2.2 TSA Application for Power Systems

2.2.1 Simple Dynamical System

In this section, a very simple electric machine model and swing equation will be used as an example of TSA analysis. The synchronous machine is modeled as a rotating mass with an inertia constant H, electrically modeled as an impedance connected in series to a constant EMF. Using one machine connected to an infinite bus model shown in Figure 2.2, the swing equation is shown below. The system and its related equations are examined in further details by Anderson and Fouad [2].

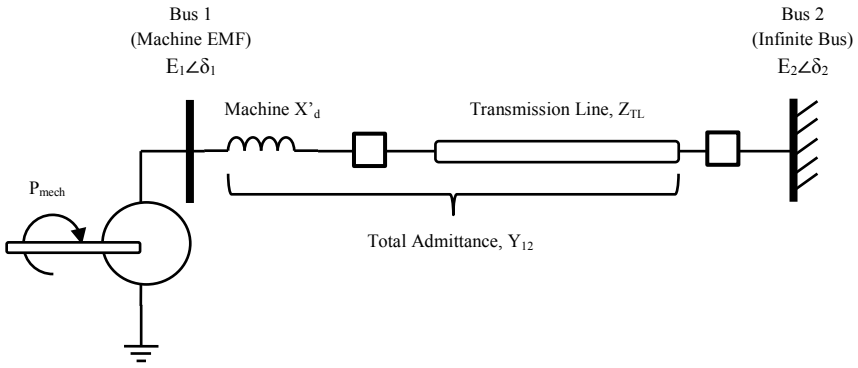

Figure 2.2: Simple system with synchronous machine connected to an infinite bus

$$\dot{\delta}_1 = \omega_1 - \omega_R$$
$$\frac{2H}{\omega_R}\frac{d\omega_1}{dt} + D\omega_1 = P_{mech} - E_1 E_2 Y_{12}\cos(\theta_{12} - \delta_1) \tag{9}$$

Where, in per-unit unless stated otherwise, the variables are:

H	Machine's Inertia Constant
D	Machine's Damping Constant
ω_1	Speed of Rotation, p.u.
ω_R	System's Rated Speed of Rotation, radians/sec. ($2\pi f$, or 1 p.u.)
$E_1\angle\delta_1$	Machine's EMF in p.u. and angle in radians (bus 1)
$E_2\angle\delta_2$	Infinite Bus Voltage with angle of zero (bus 2, $\delta_2=0$)
P_{mech}	Mechanical Power Input to the Generator
$Y_{12}\angle\theta_{12}$	Admittance Between Buses 1 and 2

The system shown in Figure 2.2 and equation (9) can be further simplified by assuming the transmission line is purely reactive ($\theta_{12}=90°$). The state variables for this system will include the machine's rotor angle $\delta_1(t)$ and the speed of rotation $\omega_1(t)$. This results in the following nonlinear state equations. $P_{e,max}$ is the maximum power transfer across the line, or $E_1E_2Y_{12}$.

$$\begin{bmatrix} x_1 \\ x_2 \end{bmatrix} = \begin{bmatrix} \delta_1 \\ \omega_2 \end{bmatrix}$$
$$\dot{x}_1 = x_2 - 1 \tag{10}$$
$$\dot{x}_2 = \frac{\omega_R P_{mech}}{2H} - \frac{\omega_R D}{2H}x_2 - \frac{\omega_R P_{e,\max}}{2H}\sin(x_1)$$

The partial derivatives with respect to the state variables (Jacobian) can be easily determined.

$$\frac{\partial f}{\partial x} = \begin{bmatrix} 0 & 1 \\ -\dfrac{\omega_R P_{e,\max}}{2H}\cos(x_1) & -\dfrac{\omega_R D}{2H} \end{bmatrix} \tag{11}$$

The parameters that will be studied for trajectory sensitivity include the mechanical power, machine damping constant, and the maximum power transfer. The partial derivatives with respect to the system parameters can then be determined.

$$\begin{aligned} \alpha &= \begin{bmatrix} P_{mech} & D & P_{e,\max} \end{bmatrix}^T \\ \frac{\partial f}{\partial \alpha} &= \begin{bmatrix} 0 & 0 & 0 \\ \dfrac{\omega_R}{2H} & -\dfrac{\omega_R}{2H}x_2 & -\dfrac{\omega_R}{2H}\sin(x_1) \end{bmatrix} \end{aligned} \tag{12}$$

The parts are now in place to calculate the sensitivity factors using the process shown in Figure 2.1 (page 16).

$$\begin{bmatrix} w_1 & w_2 & w_3 \end{bmatrix} = \begin{bmatrix} \partial x_1/\partial P_{mech} & \partial x_1/\partial D & \partial x_1/\partial P_{e,\max} \\ \partial x_2/\partial P_{mech} & \partial x_2/\partial D & \partial x_2/\partial P_{e,\max} \end{bmatrix} \tag{13}$$

$$\dot{w}_1 = \frac{\partial f}{\partial x} w_1 + \begin{bmatrix} 0 \\ \dfrac{\omega_R}{2H} \end{bmatrix} \tag{14}$$

$$\dot{w}_2 = \frac{\partial f}{\partial x} w_2 + \begin{bmatrix} 0 \\ -\dfrac{\omega_R}{2H}x_2 \end{bmatrix} \tag{15}$$

$$\dot{w}_3 = \frac{\partial f}{\partial x} w_3 + \begin{bmatrix} 0 \\ -\dfrac{\omega_R}{2H}\sin(x_1) \end{bmatrix} \tag{16}$$

With the system equations setup above, a numerical example with the following parameters is evaluated using MATLAB. The machine has an inertia constant of 1.25 p.u., a damping constant of 0.25 p.u., an EMF of 1.05, the initial combined line and machine reactance is 0.125 p.u., the infinite bus voltage is 1.00 p.u., the system rated frequency is 60 Hz., and the initial electrical and mechanical power in p.u. is 2.0. This results in the initial $P_{e,max}$ value of 8.4 p.u., $\omega(0)$ is 1 p.u., and $\delta(0)$ is 0.24 radian. The system is simulated as a faulted system where $P_{e,max}$ suddenly drops to 5. This results in the following set of equations. The initial values of w_1, w_2, w_3 can be calculated by evaluating equations (14) through (16) at the initial conditions of x and setting the left hand side of these equations to zero.

$$\dot{x}_1 = x_2 - 1, \qquad x_1(0) = 0.24$$
$$\dot{x}_2 = 0.8 - 0.2x_2 - 2\sin(x_1), \qquad x_2(0) = 1$$
$$\frac{\partial f}{\partial x} = \begin{bmatrix} 0 & 1 \\ -2\cos(x_1) & -0.2 \end{bmatrix}$$
$$\dot{w}_1 = \begin{bmatrix} 0 & 1 \\ -2\cos(x_1) & -0.2 \end{bmatrix} w_1 + \begin{bmatrix} 0 \\ 0.4 \end{bmatrix}, \qquad w_1(0) = \begin{bmatrix} 0 \\ 0.2059 \end{bmatrix}$$
$$\dot{w}_2 = \begin{bmatrix} 0 & 1 \\ -2\cos(x_1) & -0.2 \end{bmatrix} w_2 + \begin{bmatrix} 0 \\ -0.4x_2 \end{bmatrix}, \qquad w_2(0) = \begin{bmatrix} 0 \\ -0.2059 \end{bmatrix}$$
$$\dot{w}_3 = \begin{bmatrix} 0 & 1 \\ -2\cos(x_1) & -0.2 \end{bmatrix} w_3 + \begin{bmatrix} 0 \\ -0.4\sin(x_1) \end{bmatrix}, \qquad w_3(0) = \begin{bmatrix} 0 \\ -0.049 \end{bmatrix}$$

The results of this simulation are shown in the figures below. Figure 2.3 shows the phase plot of the angle (x_1) versus frequency (x_2) and the plot of the state variables with respect to time. Note that the initial conditions and the post-fault system combine to result in the state variables being well within the stable operating region. Figure 2.4

shows the plots of the calculated sensitivity coefficients, sorted by the state variables associated with each coefficient.

There are a few observations that can be quickly made based on this simple example. However, the electric machine model used here is the most simplistic and the power flow and voltage equations have not been addressed yet. In the following section, a system with more detailed models is analyzed.

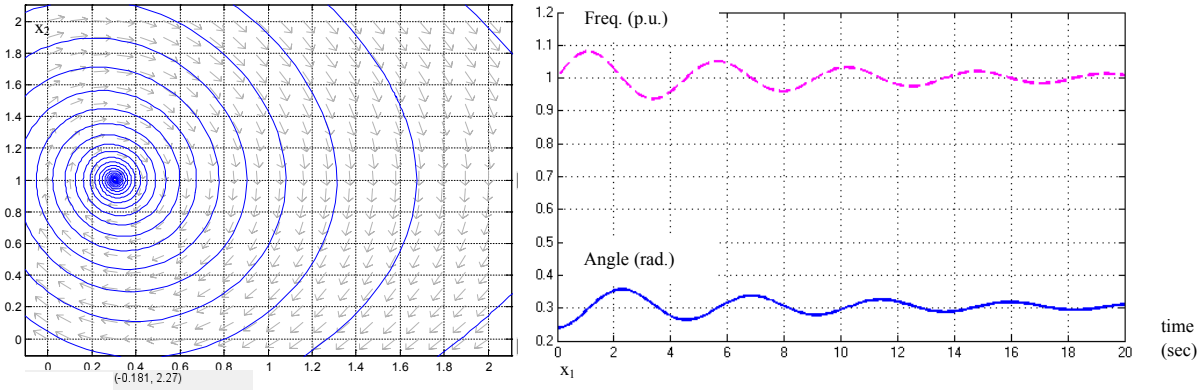

Figure 2.3: Phase-plane plot of machine angle vs. frequency (left) and time plot of machine angle (solid line) and frequency (right).

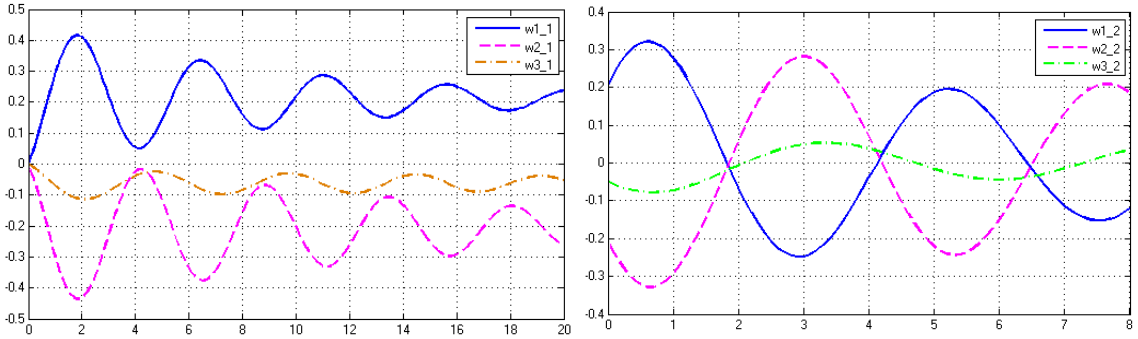

Figure 2.4: Plots of $\partial\delta/\partial P_{mech}$, $\partial\delta/\partial D$, $\partial\delta/\partial P_{e,max}$ against time, labeled w1_1, w2_1, and w3_1 respectively (left) and plots of $\partial\omega/\partial P_{mech}$, $\partial\omega/\partial D$, $\partial\omega/\partial P_{e,max}$ against time, labeled w1_2, w2_2, and w3_2 respectively.

2.2.2 TSA Application for Small Power System Model with DAE System Equations

Power systems in practice are modeled as a hybrid system as defined by Hiskens and Pai [27], where parts of the state equations are differential equations and parts are algebraic equations. In this section, an example using the nine bus system from Anderson and Fouad [2] is used to derive TSA equations when the system is modeled in greater detail.

First, the power system equations now include an algebraic component as well as differential equations, as expressed in equations (4) through (7) in the first chapter.

In this section, the synchronous machine is represented as the one-axis model with armature and field resistances neglected as well as field voltage equation. For a simple example of one machine connected to an infinite bus, with the infinite bus represented as V_∞ and an angle of zero, the system equations are shown below.

$$\dot{\delta} = \omega - \omega_R \tag{17}$$

$$\dot{\omega} = \frac{\omega_R}{2H}\left[P_{mech} - \left(E_q^{'} I_q + \left(x_q - x_d^{'} \right) I_d I_q + D\left(\omega - \omega_R \right) \right) \right] \tag{18}$$

$$\dot{E}_q^{'} = \frac{1}{\tau_{d0}^{'}}\left(-E_q^{'} + \left(x_d - x_d^{'} \right) I_d + E_{fd} \right) \tag{19}$$

$$\dot{E}_{fd} = \frac{1}{\tau_A}\left(-E_{fd} + \left(V_{ref} - V_t \right) K_A \right) \tag{20}$$

$$0 = x_q I_q - V_t \sin(\delta - \theta) \tag{21}$$

$$0 = E_q^{'} - V_t \cos(\delta - \theta) - x_d^{'} I_d \tag{22}$$

$$0 = -R_e I_d + X_e I_q + V_t \sin(\delta - \theta) - V_\infty \sin\delta \tag{23}$$

$$0 = -X_e I_d - R_e I_q + V_t \cos(\delta - \theta) - V_\infty \cos\delta \tag{24}$$

Equations (17) through (20) are the dynamic equations with the machine rotor angle δ, speed of rotation ω, q-axis armature voltage E'_q, and field voltage E_{fd} as the state variables. Because the q-axis and field voltages are parameters that are not usually measured directly, equations (21) and (22) are the decomposition of the q-axis and d-axis currents with respect to the terminal voltage V_t. Equations (23) and (24) are the Ohm's Law equations that govern the behavior of the terminal voltage decomposed along the d-axis and the q-axis. In larger systems this will be replaced by power flow equations or injected current equations.

During the simulation, the state variables (x) include δ, ω, E'_q, and E_{fd}, while the auxiliary variables (y) include I_d and I_q, and the variables that are analyzed for sensitivity include the system transmission impedances, shunt admittances, load admittance and generator input mechanical power. The system used for this analysis is shown in Figure 2.5 on the next page. The machine and other data are provided in chapter 2 of Anderson & Fouad [2]. The system equations then become the set of equations listed on the next page.

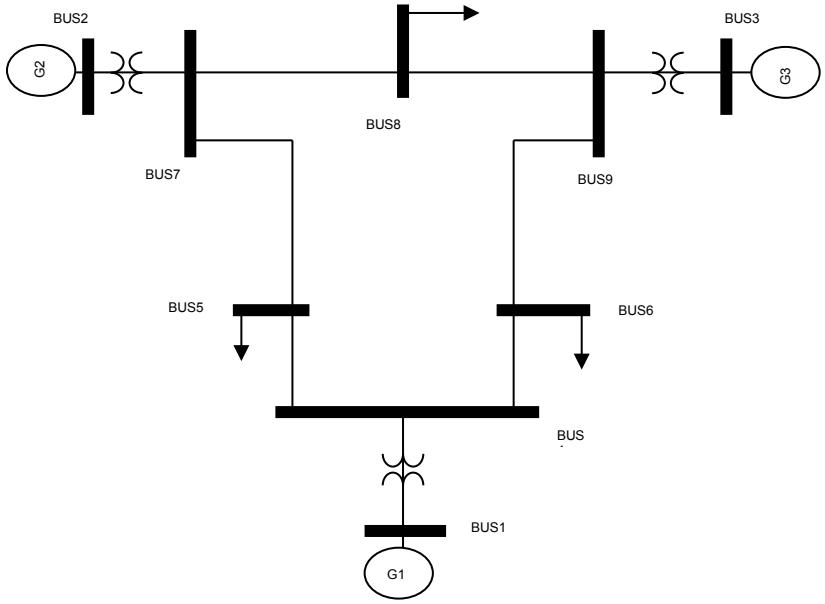

Figure 2.5: Nine bus system from Anderson & Fouad [2]

System parameters shown below are based on the values listed in [2] but with the base power converted to 100 MVA.

$$\dot{\delta}_1 = \omega_1 - 1 = f_1(x, y, \alpha, t) \qquad \dot{\delta}_2 = \omega_2 - 1 = f_2(x, y, \alpha, t) \qquad \dot{\delta}_3 = \omega_3 - 1 = f_3(x, y, \alpha, t)$$

$$\dot{\omega}_1 = \frac{1}{47.28}\left[0.716 - \left(E'_{q1} I_{q1} + (0.03915 - 0.02457) I_{d1} I_{q1} + 0.80808(\omega_1 - 1)\right)\right] = f_4(x, y, \alpha, t)$$

$$\dot{\omega}_2 = \frac{1}{12.8}\left[1.63 - \left(E'_{q2} I_{q2} + (0.45026 - 0.0624) I_{d2} I_{q2} + 1.04167(\omega_2 - 1)\right)\right] = f_5(x, y, \alpha, t)$$

$$\dot{\omega}_3 = \frac{1}{6.02}\left[0.85 - \left(E'_{q3} I_{q3} + (0.98266 - 0.14164) I_{d3} I_{q3} + 1.5625(\omega_3 - 1)\right)\right] = f_6(x, y, \alpha, t)$$

$$\dot{E}'_{q1} = \frac{1}{8.96}\left(-E'_{q1} + (0.05899 - 0.02457) I_{d1} + E_{fd1}\right) = f_7(x, y, \alpha, t)$$

$$\dot{E}'_{q1} = \frac{1}{6}\left(-E'_{q2} + (0.46656 - 0.0624) I_{d2} + E_{fd2}\right) = f_8(x, y, \alpha, t)$$

$$\dot{E}'_{q3} = \frac{1}{5.89}\left(-E'_{q3} + (1.02539 - 0.14164) I_{d3} + E_{fd3}\right) = f_9(x, y, \alpha, t)$$

$$\dot{E}_{fd1} = \frac{1}{0.02}\left(-E_{fd1} + (1.040 - V_{t1})100\right) = f_{10}(x, y, \alpha, t)$$

$$\dot{E}_{fd2} = \frac{1}{0.2}\left(-E_{fd2} + (1.025 - V_{t2})25\right) = f_{11}(x, y, \alpha, t)$$

$$\dot{E}_{fd3} = \frac{1}{0.2}\left(-E_{fd3} + (1.025 - V_{t3})25\right) = f_{12}(x, y, \alpha, t)$$

The set of equations above are the state variable equations for the system dynamics. Each equation is given an $f_i(x,y,\alpha,t)$ designation corresponding to its position in $F(x,y,\alpha,t)$. For this analysis, the generator stator resistances are assumed zero ($r_a << X'_d, X'_q$) and the generator terminal voltages and currents are solved using the techniques for analyzing the terminal conditions introduced in chapters 4 and 5 of Anderson & Fouad [2]. The equations below are given $g_i(x,y,\alpha)$ designations corresponding to their positions in $G(x,y,\alpha)$.

$$0 = x_{q1} I_{q1} - V_{t1} \sin(\delta_1 - \theta_1) = g_1(x, y, \alpha)$$

$$0 = x_{q2} I_{q2} - V_{t2} \sin(\delta_2 - \theta_2) = g_2(x, y, \alpha)$$

$$0 = x_{q3} I_{q3} - V_{t3} \sin(\delta_3 - \theta_3) = g_3(x, y, \alpha)$$

$$0 = E'_{q1} - V_{t1} \cos(\delta_1 - \theta_1) - x'_{d1} I_{d1} = g_4(x, y, \alpha)$$

$$0 = E'_{q2} - V_{t2} \cos(\delta_2 - \theta_2) - x'_{d2} I_{d2} = g_5(x, y, \alpha)$$

$$0 = E'_{q3} - V_{t3} \cos(\delta_3 - \theta_3) - x'_{d3} I_{d3} = g_6(x, y, \alpha)$$

The following equations are the voltage drop and KCL equations that will relate the power flow restrictions to the system state variables. The I_a variables represent the generator terminal currents solved by the power flow. For this particular system, the

generator currents travel through the transformers where the transformer shunt elements and resistances are ignored before entering the high voltage buses that are connected to the load buses. Therefore, one way to create the zero-sum functions is to derive the KCL equations around the high voltage buses nearest to the generators. Then the equations are decomposed along the d-axis and q-axis of each machine. The angle term γ_{ij} represent the angles of the admittance between buses i and j.

Phasor KCLs:

$$\bar{I}_{a1} = \left(\bar{V}_5 - \bar{V}_4\right)\bar{Y}_{45} + \left(\bar{V}_6 - \bar{V}_4\right)\bar{Y}_{46} + \bar{V}_4\bar{Y}_{44}$$

$$\bar{I}_{a2} = \left(\bar{V}_8 - \bar{V}_7\right)\bar{Y}_{78} + \left(\bar{V}_5 - \bar{V}_7\right)\bar{Y}_{57} + \bar{V}_7\bar{Y}_{77}$$

$$\bar{I}_{a3} = \left(\bar{V}_8 - \bar{V}_9\right)\bar{Y}_{89} + \left(\bar{V}_6 - \bar{V}_9\right)\bar{Y}_{69} + \bar{V}_9\bar{Y}_{99}$$

Decomposed KCLs form the remainder of the *G(x,y,α)* functions:

$$g_7(x,y,\alpha) = 0 = -I_{q1} - |V_4||Y_{45}|\cos(\theta_4 + \gamma_{45} - \delta_1) - |V_4||Y_{46}|\cos(\theta_4 + \gamma_{46} - \delta_1) + |V_4||Y_{44}|\cos(\theta_4 + \gamma_{44} - \delta_1) + \ldots$$
$$|V_5||Y_{45}|\cos(\theta_5 + \gamma_{45} - \delta_1) + |V_6||Y_{46}|\cos(\theta_6 + \gamma_{46} - \delta_1)$$

$$g_8(x,y,\alpha) = 0 = -I_{d1} - |V_4||Y_{45}|\sin(\theta_4 + \gamma_{45} - \delta_1) - |V_4||Y_{46}|\sin(\theta_4 + \gamma_{46} - \delta_1) + |V_4||Y_{44}|\sin(\theta_4 + \gamma_{44} - \delta_1) + \ldots$$
$$|V_5||Y_{45}|\sin(\theta_5 + \gamma_{45} - \delta_1) + |V_6||Y_{46}|\sin(\theta_6 + \gamma_{46} - \delta_1)$$

$$g_9(x,y,\alpha) = 0 = -I_{q2} - |V_7||Y_{57}|\cos(\theta_7 + \gamma_{57} - \delta_2) - |V_7||Y_{78}|\cos(\theta_7 + \gamma_{78} - \delta_2) + |V_7||Y_{77}|\cos(\theta_7 + \gamma_{77} - \delta_2) + \ldots$$
$$|V_5||Y_{57}|\cos(\theta_5 + \gamma_{57} - \delta_2) + |V_8||Y_{78}|\cos(\theta_8 + \gamma_{78} - \delta_2)$$

$$g_{10}(x,y,\alpha) = 0 = -I_{d2} - |V_7||Y_{57}|\sin(\theta_7 + \gamma_{57} - \delta_2) - |V_7||Y_{78}|\sin(\theta_7 + \gamma_{78} - \delta_2) + |V_7||Y_{77}|\sin(\theta_7 + \gamma_{77} - \delta_2) + \ldots$$
$$|V_5||Y_{57}|\sin(\theta_5 + \gamma_{57} - \delta_2) + |V_8||Y_{78}|\sin(\theta_8 + \gamma_{78} - \delta_2)$$

$$g_{11}(x,y,\alpha)=0=-I_{q3}-|V_9||Y_{69}|\cos(\theta_9+\gamma_{69}-\delta_3)-|V_9||Y_{89}|\cos(\theta_9+\gamma_{89}-\delta_3)+|V_9||Y_{99}|\cos(\theta_9+\gamma_{99}-\delta_3)+\ldots$$
$$|V_6||Y_{69}|\cos(\theta_6+\gamma_{69}-\delta_3)+|V_8||Y_{89}|\cos(\theta_8+\gamma_{89}-\delta_3)$$

$$g_{12}(x,y,\alpha)=0=-I_{d3}-|V_9||Y_{69}|\sin(\theta_9+\gamma_{69}-\delta_3)-|V_9||Y_{89}|\sin(\theta_9+\gamma_{89}-\delta_3)+|V_9||Y_{99}|\sin(\theta_9+\gamma_{99}-\delta_3)+\ldots$$
$$|V_6||Y_{69}|\sin(\theta_6+\gamma_{69}-\delta_3)+|V_8||Y_{89}|\sin(\theta_8+\gamma_{89}-\delta_3)$$

The initial conditions for E_{fd}, δ, and E'_q can be calculated using the equations below, with ϕ_i representing the power angle between the terminal voltage and armature current of generator at bus i.

$$\delta_{i,0}=\tan^{-1}\left[\frac{V_{i,0}\sin\theta_i+I_{ai,0}x'_{qi}\sin(\phi_i+90^\circ)}{V_{i,0}\cos\theta_i+I_{ai,0}x'_{qi}\cos(\phi_i+90^\circ)}\right] \tag{25}$$

$$E'_{qi,0}=|V_{ai,0}|\cos(\delta_{i,0}-\theta_{i,0})+x'_q|I_{ai,0}|\cos(\phi_{i,0}+90-\delta_{i,0})-(x'_d-x'_q)I'_{di,0} \tag{26}$$

$$E_{fdi,0}\cong|V_{ai,0}|\cos(\delta_{i,0}-\theta_{i,0})+x_q|I_{ai,0}|\cos(\phi_{i,0}+90-\delta_{i,0})-(x_d-x_q)I_{di,0} \tag{27}$$

$$I_{d1}=-I_{a1}\sin\delta_1 \qquad I_{d2}=-I_{a2}\sin\delta_2 \qquad I_{d3}=-I_{a3}\sin\delta_3$$

$$I_{q1}=I_{a1}\cos\delta_1 \qquad I_{q2}=I_{a2}\cos\delta_2 \qquad I_{q3}=I_{a3}\cos\delta_3 \tag{28}$$

In order to begin the sensitivity coefficient analysis, the system state variables (x), auxiliary variables (y), and parameters of interest (α) are defined below.

$$x=\begin{bmatrix}\delta_1 & \delta_2 & \delta_3 & \omega_1 & \omega_2 & \omega_3 & E'_{q1} & E'_{q2} & E'_{q3} & E_{FD1} & E_{FD2} & E_{FD3}\end{bmatrix} \tag{29}$$

$$y=\begin{bmatrix}I_{d1} & I_{d2} & I_{d3} & I_{q1} & I_{q2} & I_{q3}\end{bmatrix} \tag{30}$$

$$\alpha=\begin{bmatrix}P_{mech1} & P_{mech2} & P_{mech3} & Y_{44} & Y_{77} & Y_{99}\end{bmatrix} \tag{31}$$

The mechanical power and shunt admittances at the substation buses are chosen as the parameters under analysis in order to see if manipulation of switched shunts is more or less effective than manipulating the turbine controls. We then form the sensitivity coefficient equations using equations (4) and (5), with the *F* functions being the dynamic functions, and the *G* functions being the KCL and terminal current equations. The sensitivity coefficients for each of the α parameters can be further derived below, with the index w_{1j} refers to the sensitivity of state variable with respect to the parameter α_j as follows.

$$w = \begin{bmatrix} w_1 \\ w_2 \end{bmatrix} = \left[\begin{bmatrix} w_{11} \\ w_{21} \end{bmatrix}, \begin{bmatrix} w_{12} \\ w_{22} \end{bmatrix}, \begin{bmatrix} w_{13} \\ w_{23} \end{bmatrix}, \begin{bmatrix} w_{14} \\ w_{24} \end{bmatrix}, \begin{bmatrix} w_{15} \\ w_{25} \end{bmatrix}, \begin{bmatrix} w_{16} \\ w_{26} \end{bmatrix} \right] \tag{32}$$

For example, $j=1$ so $\alpha_1=P_{mech1}$, and the sensitivity coefficients with respect to P_{mech1} are calculated with equations (33) and (34) below.

$$\dot{w}_{11} = \frac{\partial F}{\partial x} w_{11} + \frac{\partial F}{\partial y} w_{21} + \frac{\partial F}{\partial \alpha_1} \tag{33}$$

$$0 = \frac{\partial G}{\partial x} w_{11} + \frac{\partial G}{\partial y} w_{21} + \frac{\partial G}{\partial \alpha_1} \tag{34}$$

Each element of equations (33) and (34) are from the Jacobian matrices of the state equations, and the solutions for all the members of *w* in equation (32) can be done in each time step. The Jacobian matrices are updated at each time step, and the matrices are sparse. The ∂F/∂x matrix has 18 nonzero terms, the ∂F/∂y matrix has 9 nonzero terms, the ∂G/∂x matrix has 15 nonzero terms, and finally ∂G/∂y has 12 nonzero terms. Of those terms, a total 33 terms are constants. A brief linear algebra analysis of the Jacobian

matrices indicate that the equations for the sensitivity coefficients are not underdetermined.

The format of equations (33) and (34) can be adjusted in order to calculate the sensitivity coefficients on a time-step basis. This is done by using the coefficients of the previous time step $(w_{1,t-}, w_{2,t-})$ to calculate for the $\dot{w}_1$ rates of change using equation (33). Then the coefficients at the end of the time step $(w_{1,t+})$ can be estimated by basic trapezoidal integration and finally the $(w_{2,t+})$ coefficients are calculated using equation (34).

The calculation steps and results below are based on time simulation of the aforementioned 9-bus system using PSS/E software. The flowcharts in Figures 2.6 and 2.7 show the calculations required to process the PSS/E outputs into formats that can be used to calculate the coefficients as well as the steps to calculate the coefficients.

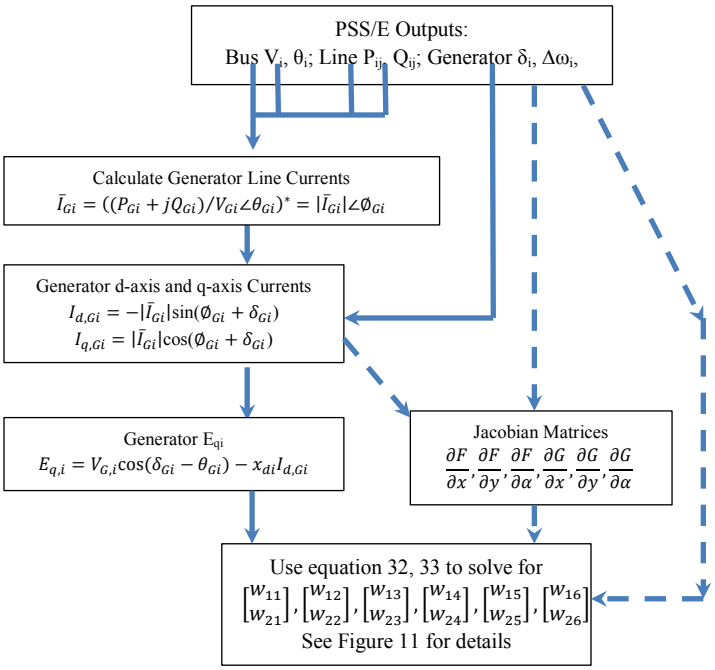

Figure 2.6: Flowchart of data used for calculating the sensitivity coefficients

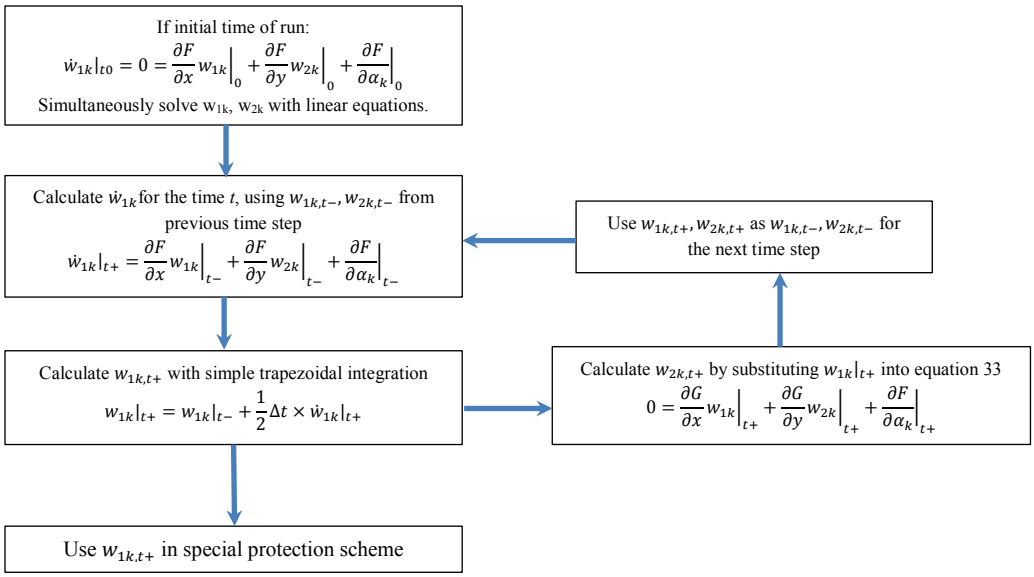

Figure 2.7: Steps for calculating the coefficients with equations 33 and 34. The index *k* represents the α parameters, *k=1..6*.

2.2.3 TSA Application for Larger Power Systems with DAE Equations

In order to analyze how TSA and the special protection scheme in this dissertation will perform, modeling with larger systems must be done in order to achieve a reasonable simulation of a real system. For most of the discussions and results in the remainder of this dissertation, the IEEE 68-Bus test system will be used. The system model is a 16-machine five-area study system, shown in Figure 2.8, is considered for this study. The limited number of buses allows for reasonable debugging and troubleshooting during the development of the methodology. The algorithm being tested is written with generic and expandable formatting such that expansion to system models with a larger amount of buses can be achieved. This system contains five sub-areas [28], with two areas represented by a group of generators whereas each of the three remaining regions is

represented by an equivalent generator. The system data is obtained from Kundur [28]. Area #1 is the only area with AVRs, as the generators in other areas are reduced only to the synchronous machine models for simplicity. Only one PSS is modeled as a wash out block and two lead-lag blocks (Type II) and installed at G9 to ensure the base system stability (for the simulation purpose).

The IEEE 68-Bus test system will later be modified by adding wind generation modeled as wind turbines with doubly-fed induction generators (DFIG). The system is modified by replacing the synchronous machines with the wind generators at bus 1 and bus 12. The DFIG parameters are taken from the model properties in one of the time domain simulation test cases [10]. The system topology with the modification is shown in Figure 2.8.

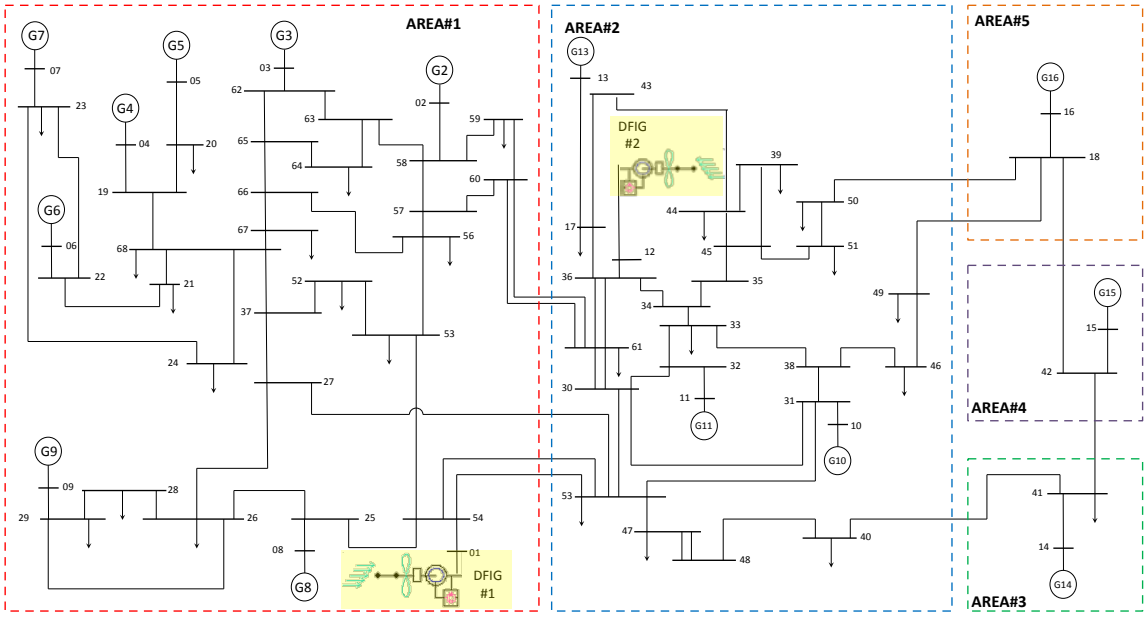

Figure 2.8: Modified IEEE 68-Bus test system with two wind generators at bus 1 and bus 12 (highlighted).

The model state equations for each of the power system components are listed in the equations and variables below. It would become obvious that the level of complexity and volume of equations that have to be solved are much greater than the small system in the previous section.

Synchronous Machines

With the synchronous machine models described in Chapter 1, the equations for the synchronous machines are shown in equations (35) through (43). The motion equations (35), (36) govern the transfer from mechanical power transmitted through the shaft to the electrical power and accounts for the inertia of the rotating mass. Equations (37) to (40) model the mutual electromagnetic interactions between the rotor and stator circuits transferred that govern the electromotive forces and stator currents. Equations (41) to (43) describe the circuit conditions and power output of the generator, known collectively as the generator terminal conditions.

$$\dot{\delta} = \omega_b \left(\omega - 1\right) \tag{35}$$

$$\dot{\omega} = \left(p_m - p_e - D\left(\omega - 1\right)\right) / M \tag{36}$$

$$\dot{e}_q^{'} = \left(-f_s\left(e_q^{'}\right) - \left(x_d - x_d^{'} - \frac{T_{d0}^{''}}{T_{d0}^{'}} \frac{x_d^{''}}{x_d^{'}} \left(x_d - x_d^{'} \right) \right) i_d + \left(1 - \frac{T_{AA}}{T_{d0}^{'}} \right) v_f \right) / T_{d0}^{'} \tag{37}$$

$$\dot{e}_d^{'} = \left(-e_d^{'} + \left(x_q - x_q^{'} - \frac{T_{q0}^{''}}{T_{q0}^{'}} \frac{x_q^{''}}{x_q^{'}} \left(x_q - x_q^{'} \right) \right) i_q \right) / T_{q0}^{'} \tag{38}$$

$$\dot{e}_q^{''} = \left(-e_q^{''} + e_q^{'} - \left(x_d - x_d^{'} - \frac{T_{d0}^{''}}{T_{d0}^{'}} \frac{x_d^{''}}{x_d^{'}} \left(x_d - x_d^{'} \right) \right) i_d + \left(1 - \frac{T_{AA}}{T_{d0}^{'}} \right) v_f \right) / T_{d0}^{''} \tag{39}$$

$$\dot{e}_d^{'} = \left(-e_d^{''} + e_d^{'} + \left(x_q - x_q^{'} - \frac{T_{q0}^{''}}{T_{q0}^{'}} \frac{x_q^{''}}{x_q^{'}} \left(x_q - x_q^{'} \right) \right) i_q \right) / T_{q0}^{''} \tag{40}$$

$$p_e = \left(v_q + r_a i_q \right) i_q + \left(v_d + r_a i_d \right) i_d \tag{41}$$

$$0 = v_q + r_a i_q - e_q^{''} + \left(x_d^{''} - x_l \right) i_d \tag{42}$$

$$0 = v_d + r_a i_d - e_d^{''} + \left(x_q^{''} - x_l \right) i_q \tag{43}$$

The following list defines variables and parameters that are not previously noted.

ω_b Base rate of rotation, radians per second

M Moment of Inertia

D Droop characteristic constant

v^*_f Field voltage, per unit

T_{d0}, T'_{d0}, T''_{d0} Direct-axis electromagnetic time constants

T_{q0}, T'_{q0}, T''_{q0} Quadrature-axis electromagnetic time constants

T_{AA} Field circuit time constant

x_d, x'_d, x''_d Steady-state, transient, sub-transient direct-axis circuit reactances

x_q, x'_q, x''_q Steady-state, transient, sub-transient quadrature-axis circuit reactances

x_l Leakage reactance

$f_s(e'_q)$ Magnetic saturation function

Automatic Voltage Regulator (AVR, or Exciters)

The AVR control model is based on the IEEE type II standard, and the model block diagram is shown in Figure 2.9, reproduced from Milano [1]. The model output (field circuit voltage, v_f) is then linked to the field-induced elements in the synchronous

machine model modeled in equations (37) and (39). The field circuit generates the electromagnetic field that emits from the rotor of the synchronous machine.

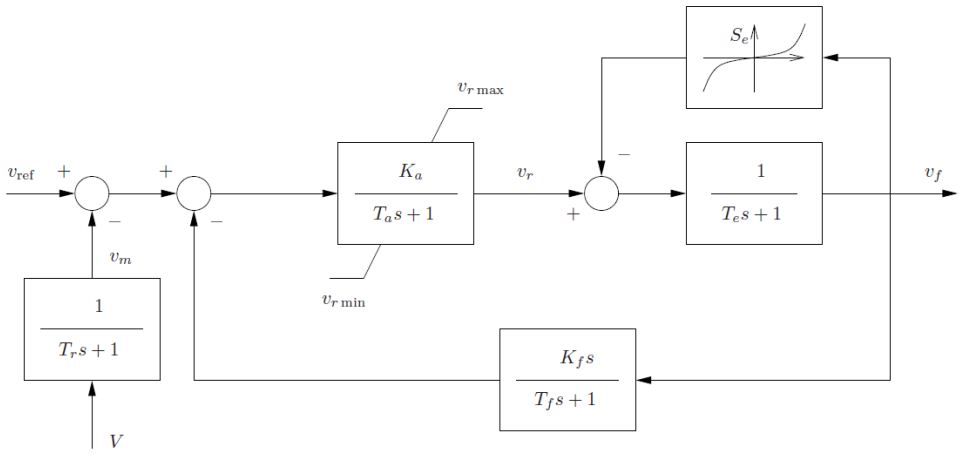

Figure 2.9: IEEE Type II Automatic Voltage Regulator (AVR, or Exciter) model block diagram. Reproduced from Milano [1].

$$\dot{v}_m = (V - v_m)/T_r \tag{44}$$

$$\dot{v}_{r1} = \left(K_a(v_{ref} - v_m - v_{r2} - \frac{K_f}{T_f} v_f) - v_{r1} \right) / T_r \tag{45}$$

$$v_r = \begin{cases} v_{r1} \text{ if } v_{r,\min} \le v_{r1} \le v_{r,\max} \\ v_{r,\max} \text{ if } v_{r1} > v_{r,\max} \\ v_{r,\min} \text{ if } v_{r1} < v_{r,\min} \end{cases} \tag{46}$$

$$\dot{v}_{r2} = -\left(\frac{K_f}{T_f} v_f + v_{r2} \right) / T_f \tag{47}$$

$$\dot{v}_f = -\left(v_f \left(1 + S_e(v_f) \right) - v_r \right) / T_e \tag{48}$$

Where

V Machine terminal voltage

v_m	Machine measured voltage (after measurement block)
T_r	Measurement time constant
K_a	Amplifier gain
v_{ref}	Reference voltage
v_{r1}, v_{r2}	Regulator signals
K_f	Stabilizer gain
T_f	Stabilizer time constant
$S_e(v_f)$	Saturation function

Power System Stabilizers (PSS)

The PSS control model is based on the IEEE type II standard, and the model block diagram is shown in Figure 2.10, also reproduced from Milano [1]. The model output (stabilizing signal, v_s) is then summed into the reference voltage of the AVR in equation (45). The dynamic equations of the PSS are shown in equations (49) through (52).

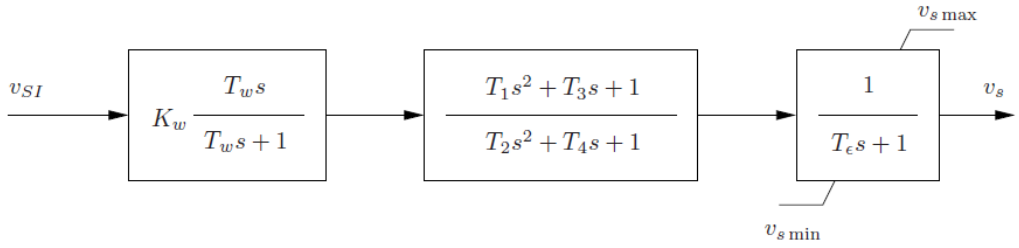

Figure 2.10: IEEE Type II Power System Stabilizer (PSS) model block diagram. Reproduced from Milano [1].

$$\dot{v}_1 = -(K_\omega v_{SI} + v_1)/T_\omega \tag{49}$$

$$\dot{v}_2 = \left(\left(1 - \frac{T_1}{T_2} \right) \left(K_\omega v_{SI} + v_1 \right) - v_2 \right) / T_2 \tag{50}$$

$$\dot{v}_3 = \left(\left(1 - \frac{T_3}{T_4} \right) \left(v_2 + \left(\frac{T_1}{T_2} \left(K_\omega v_{SI} + v_1 \right) \right) \right) - v_3 \right) / T_4 \tag{51}$$

$$\dot{v}_S = \left(v_3 + \frac{T_3}{T_4} \left(v_2 + \frac{T_1}{T_2} \left(K_\omega v_{SI} + v_1 \right) \right) - v_S \right) / T_\varepsilon \tag{52}$$

Where

v_1, v_2, v_3	First, second, and third stabilizer outputs
v_s	Stabilizer output signal
v_{SI}	Stabilizer input signal
K_ω	Stabilizer gain
T_1, T_2, T_3, T_4	First through fourth Stabilizer time constants
T_ω	Wash-out time constant
T_ε	Stabilizer output time constants

Wind Turbine and DFIG Models

The wind turbine model used in this dissertation is comprised of a Weibull distribution speed model for the wind speed, a DFIG with a controller element representing speed, and pitch feedback to control the output power and voltage. The converter model is assumed to be lossless in order to simplify the calculations. The Weibull Distribution function that is used to determine the wind speed is shown in equations (53) and (54).

$$f(v_w, c, k) = \frac{k}{c^k} v_w^k e^{-\left(v_w/c\right)^k} \tag{53}$$

$$v_w(t) = \left(-\frac{\ln \ell(t)}{c} \right)^{1/k} \tag{54}$$

Where

$\ell(t)$ Random number generator function.

v_w Wind speed

c Scale factor in Weibull Distribution

k Shape factor in Weibull Distribution

v_{wa} Average wind speed

The mechanical and electromechanical equations for the DFIG are based on the initial assumption that the converter controls decouple the generator from the grid. Generator complex power can be written from the rotor and stator currents in equations (55) and (56). The rotor and stator currents and voltages are decomposed into direct- and quadrature-axes. The motion dynamic (57) is based on a single shaft. The differential equations for the converter currents and pitch angle control are described in (58) through (60) below.

$$P = v_{ds} i_{ds} + v_{qs} i_{qs} + v_{dr} i_{dr} + v_{qr} i_{qr} \tag{55}$$

$$Q = v_{qs} i_{ds} - v_{ds} i_{qs} + v_{qr} i_{dr} - v_{dr} i_{qr} \tag{56}$$

$$\dot{\omega} = \left(T_m - T_e\right) / 2H_m \tag{57}$$

$$\dot{i}_{qr} = (-\frac{x_s + x_m}{x_m V} \mathrm{P}_w(\omega_m) / \omega_m - i_{qr}) / T_\varepsilon \tag{58}$$

$$\dot{i}_{dr} = K_V (V - V_{ref}) / x_m - i_{dr} \tag{59}$$

$$\dot{\theta}_p = \left(K_p \phi \left(\omega_m - \omega_{ref} \right) - \theta_p \right) / T_p \tag{60}$$

Where

ω_m	Shaft speed
T_e	Electrical torque
T_m	Mechanical torque
P_w	Mechanical power extracted from wind
θ_p	Pitch angle, radians
i_{dr}, i_{ds}	Direct axis rotor (r) and stator (s) currents
i_{qr}, i_{qs}	Quadrature axis rotor (r) and stator (s) currents
v_{dr}, v_{ds}	Direct axis rotor (r) and stator (s) voltages
v_{qr}, v_{qs}	Quadrature axis rotor (r) and stator (s) voltages
V_{ref}	Reference voltage
x_m	Magnetizing reactance
H_m	Rotor inertia
K_p	Pitch control gain
T_p	Pitch control time constant
K_V	Voltage control gain
T_ε	Power control time constant

Φ Pitch control step function

Based on all of the models and equations listed above, the resulting system equations of the IEEE 68-bus system will result in 129 dynamic equations and 207 algebraic equations. This volume of interconnected equations and variables is too large to directly derive and solve for the TSA coefficients. For larger systems in this dissertation, the TSA coefficients will be calculated using the method described below.

Due to programming flexibility and availability of resources, the TSA coefficients in the system described in this section are calculated using a modified version of the Power System Analysis Toolbox (PSAT) [1] in MATLAB. PSAT is chosen because of its availability as an open-source tool with detailed documentation, which lends itself well to modifications to add TSA calculation modules to the existing time-domain simulation structure. The data used in the simulations for this dissertation is slightly modified from the system studied by Abdelsalam [29].

The TSA algorithm begins with the execution of a conventional time domain algorithm [10] where the TSA specific variables are initiated. The time domain algorithm solves for the state variables (x) and outputs (y) for the power system models. The TSA coefficient calculation algorithm is written to utilize the results and variables of the PSAT simulation within the MATLAB environment [1]. The time domain algorithm also generates partial differential matrices that are used for the TSA calculation. These matrices include $\partial F/\partial x$, $\partial F/\partial y$, $\partial G/\partial x$ and $\partial G/\partial y$ which are slightly modified to become the partial differential matrices in (6) and (7). The remaining $\partial F/\partial \alpha$ and $\partial G/\partial \alpha$ are

extracted from system simulation variables by defining α as a variable that is already in the time domain model environment and evaluated.

The algorithm and the passing of variables and matrices between the time domain and TSA calculation environments are shown in Figure 2.11. In Figure 2.11, Δt denotes the time increment and t denotes the time at which the simulation is running. The TSA coefficients w_1 and w_2 are obtained by solving the DAE in (6) and (7).

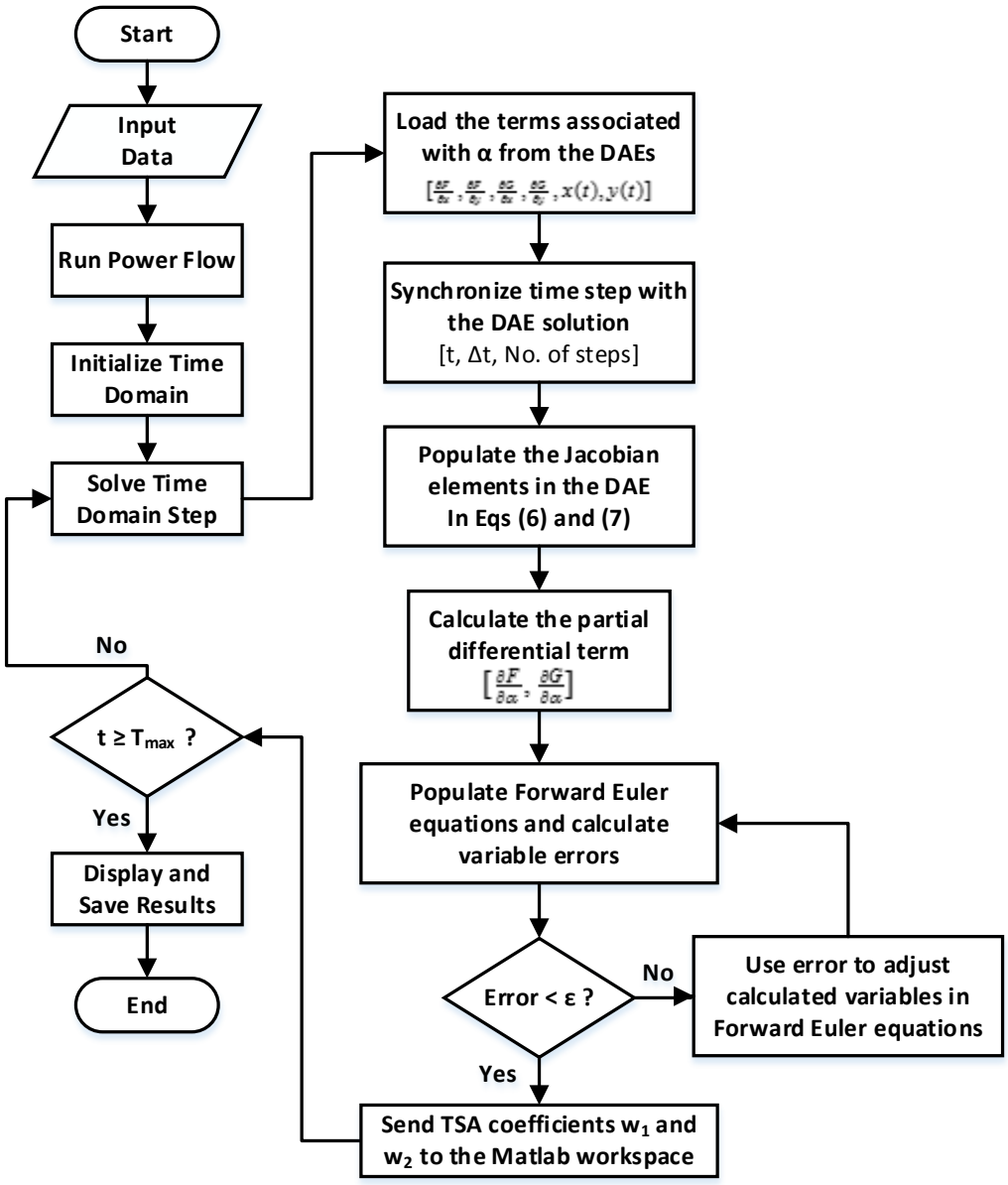

Figure 2.11: Flow chart of Time Domain Simulation and TSA Coefficients calculations and their interfaces.

2.3 Determining Out-Of-Step (OOS) Relay Settings

The OOS settings are dependent on the calculated apparent impedance seen by the relay, which is based on the measured voltage and current at the relay, and it is usually taken from the relays that are placed at the terminals of transmission lines. OOS

protection schemes primarily monitor the movements of the apparent impedance in relation to the fault protection settings.

As described by Blackburn and Domin [30] the apparent impedance calculated by the relay will abruptly encroach the protection setting zones during a fault or major disturbance, while the same impedance will travel along a trajectory in a progressive fashion in the case of a power swing across the monitored line. This can be illustrated by using a simple two-area system with a transmission line between them, as shown in Figure 2.12.

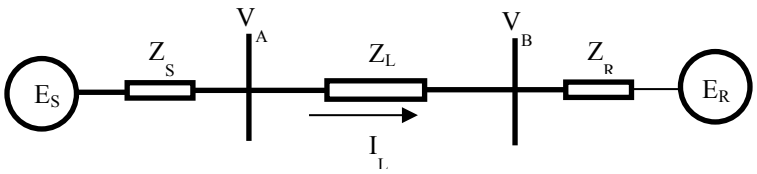

Figure 2.12: Simple 2-area system used for illustrating out-of-step conditions.

In this example system, the two areas are reduced to an equivalent voltage source (S for sending end, R for receiving end) have the source voltages of E_S and E_R, respectively, as well as system equivalent impedances Z_S and Z_R. The transmission line that transfers power between the two is connected to buses A and B, and the line impedance Z_L allows the current I_L to flow from system S to R. All of these quantities are complex numbers or phasors representing the magnitudes and angles. For this case, the relay is considered to be installed at bus A. This means that the relay will simply calculate the apparent impedance as seen in equation (61).

$$Z_{app} = V_A / I_L \tag{61}$$

Let's also assume that the angle difference between the source voltages E_S and E_R phasors is δ_{SR}. The resulting equation for the apparent impedance becomes equation (62).

$$Z_{app} = \frac{E_S\left(Z_S + Z_L + Z_R\right)}{E_S - E_R} - Z_S \tag{62}$$

The trajectory for the apparent impedance seen by the relay as the angle between the source voltages is varied, when plotted on an X-R plane, can be seen in Figure 2.13.

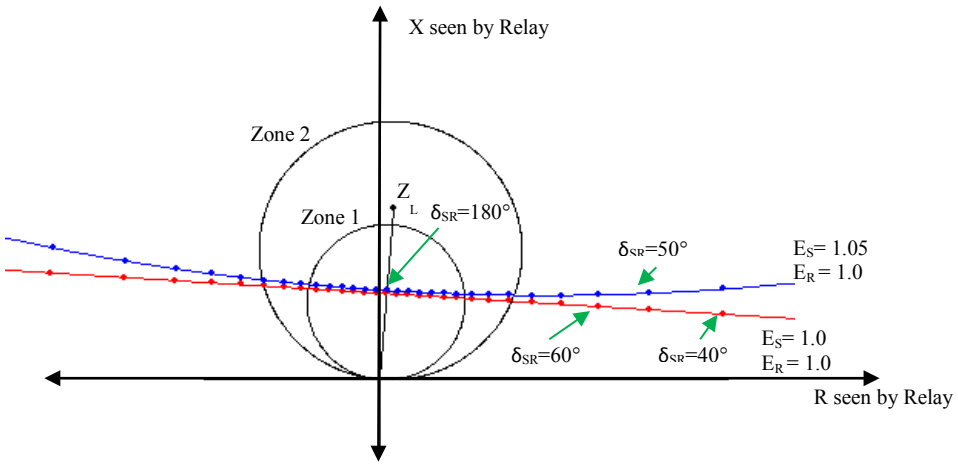

Figure 2.13: Apparent impedance seen by the relays at bus A of the system shown in Figure 2.12.

Note that the trajectory of the impedance is determined almost completely by the angle between the two systems as long as the voltages remain stable. The purpose of OOS protection is to disconnect the system before the apparent impedance reaches a zone that represents undesirable operating conditions. This can be achieved in several different ways that depends on the operator's protection philosophy as well as specific system conditions that are expected during disturbances. Anderson [12] and Kundur [28] as well as Blackburn and Domin [30] all have shown different examples of OOS philosophies

including using OOS to disconnect an unstable transmission line in order to prevent overloading or equipment damage during the high-magnitude portions of the swings, as well as using OOS to block certain system operations in order to prevent further perturbations in the system.

The characteristics of the OOS relay tripping zones are also varied, and can look like overlapping circles as seen in Figure 2.13 or concentric circles [30], or other types of zones established to correspond with the expected impedance trajectory during unstable conditions. Additional considerations may include preventing tripping when the angle across the line is at the maximum, such as when δ_{SR} approaches 180 degrees in Figure 16. Disconnections during this type of conditions will result in severe transient conditions around the switching equipment, especially transient recovery voltages, which could result in devices being exposed to very high voltages and suffering further damages. The principles and detailed discussions of transient recovery voltages are shown in Greenberg [31].

Another consideration when setting OOS relays is load encroachment. This can be reviewed by plotting the apparent impedance seen by the relay as it corresponds to various loading conditions in both magnitude and power factor. The more power is transmitted through a line, the lower the apparent impedance becomes, and it is the responsibility of the protection engineer to avoid having OOS relays trip during heavy loading events that are stable.

For the purposes of this dissertation, the transmission lines being considered to apply OOS relays and the special protection scheme will have to be evaluated and the

impedance trajectories during disturbances will be reviewed in order to determine the OOS relay settings. For simplicity, the OOS relay settings for the transmission lines in the IEEE 68-bus system will be set as single boundary based on the simulated unstable encroachment. The single boundary scheme will have the basic apparent impedance shape as shown in Figure 2.14, where the boundary may be two parallel lines or a geometric shape surrounding the protection zone.

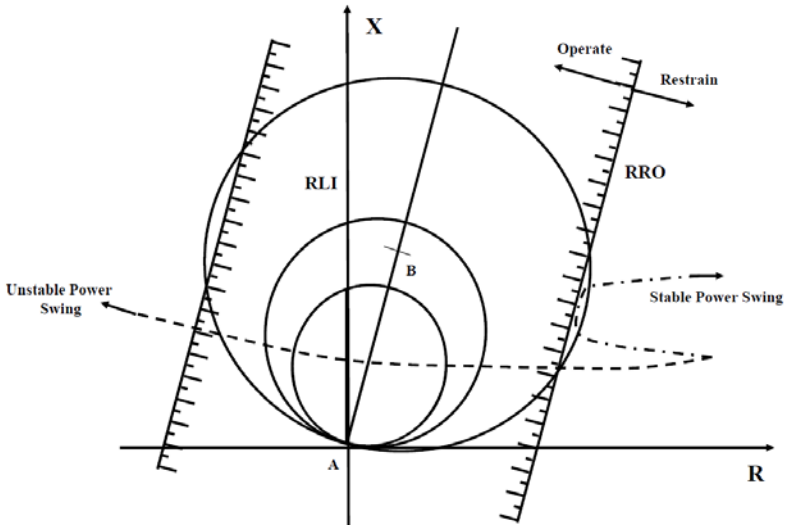

Figure 2.14: Single blinder OOS relay characteristic.

2.4 Planning The Special Protection Scheme.

As required by NERC regulations [13 – 16], any new special protection scheme cannot interfere or degrade other protection systems unintentionally. This means that all of the other essential protection schemes such as fault protection or OOS cases where the special protection scheme will worsen the system must not result in the OOS operation. The general outline of the special protection scheme uses the philosophy outlined in Figure 2.15.

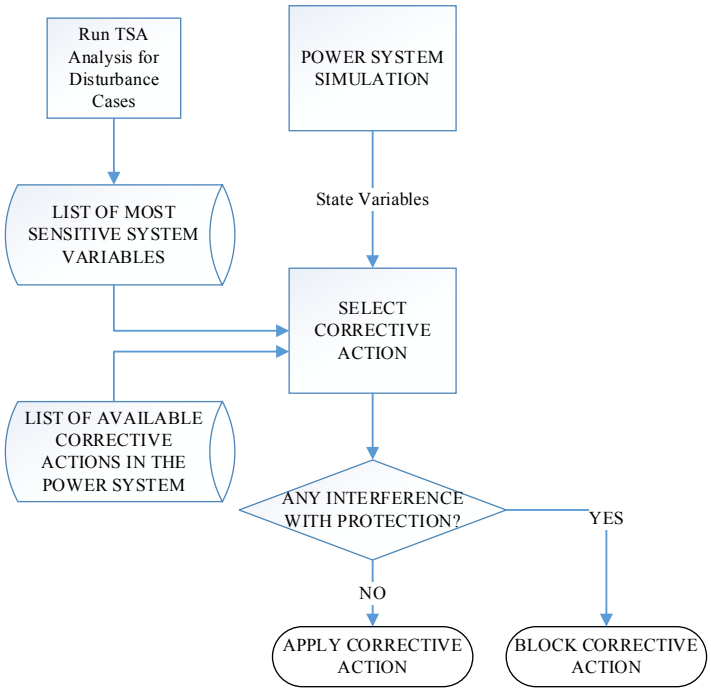

Figure 2.15: Special protection scheme operating philosophy.

CHAPTER 3

SIMULATION AND CALCULATION RESULTS

For this chapter, the results of simulations outlined in Chapter 2 are shown and discussed. First, the TSA coefficient results from the smaller 9-bus test system are shown and briefly discussed in order to establish the viability of calculating TSA coefficients in power systems. The following section shows the TSA coefficient results for the IEEE 68-bus system. Afterwards, the apparent impedances calculated for the buses connected to the main transmission tie lines in the IEEE 68-bus sytem are examined. Finally, the conventional out-of-step relay setting is established and the settings for the special protection schemes are developed using the simulation results.

3.1 TSA Coefficient Results for the 9-Bus Test System

Simulation generator angles (δ_i), bus voltages at generator terminals (V_i), and frequency ($\Delta\omega_i$) are shown in Figures 3.1 through 3.3, and some of the trajectory coefficients are shown in Figure 3.4. Discussion of the results is presented in the following section. Note that the disturbance is presented as a 20% increase in load MVA at bus 8.

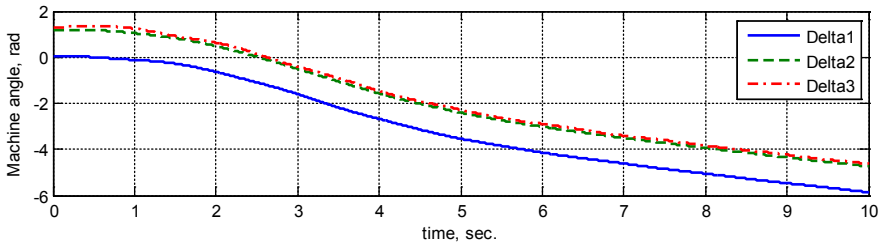

Figure 3.1: Machine angles with respect to time during simulation.

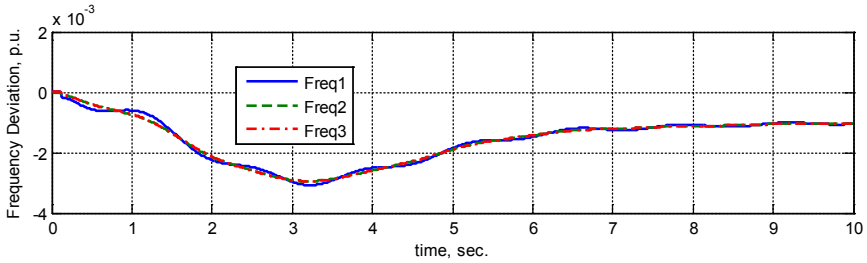

Figure 3.2: Bus frequency deviation with respect to time during simulation.

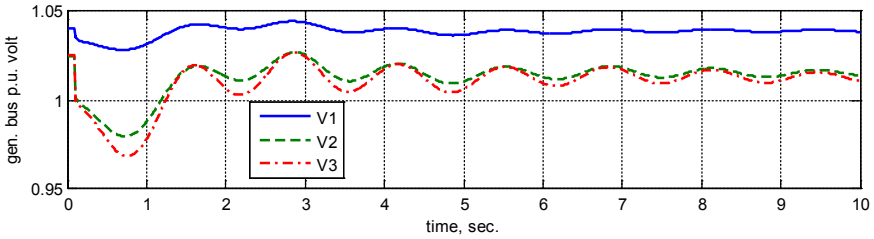

Figure 3.3: Bus voltages with respect to time during simulation.

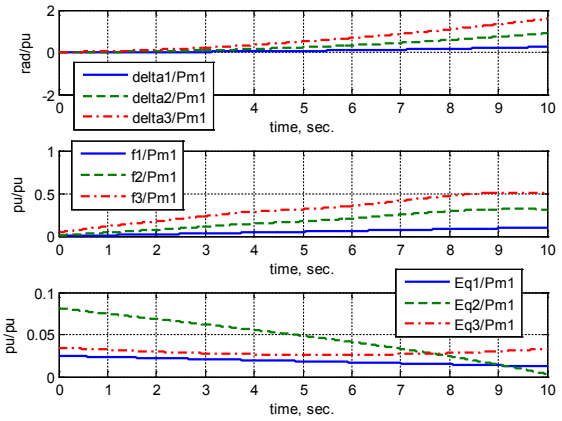

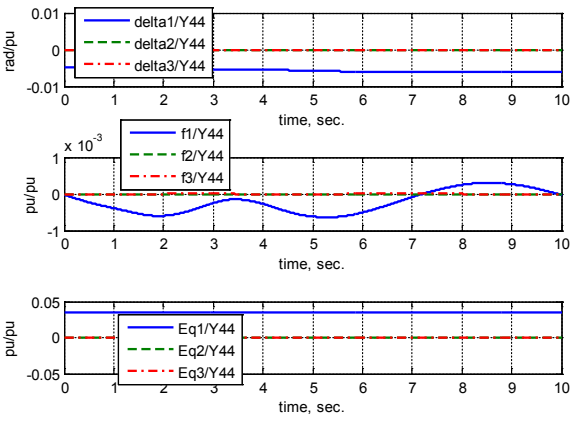

3.4a – coefficients wrt. P_{mech1} 3.4b – coefficients wrt. Y_{44}

Figure 3.4: Sensitivity coefficients with respect to bus 1 mechanical power (3.4a) and bus 4 shunt admittance (3.4b) for the simulation shown in Figures 3.1 through 3.3.

The sensitivities with respect to shunt admittances in Figures 3.4b and 3.5a and 3.5b are shown in order to illustrate the effects that changes in other system parameters beyond the dynamic models can also influence the system state variables.

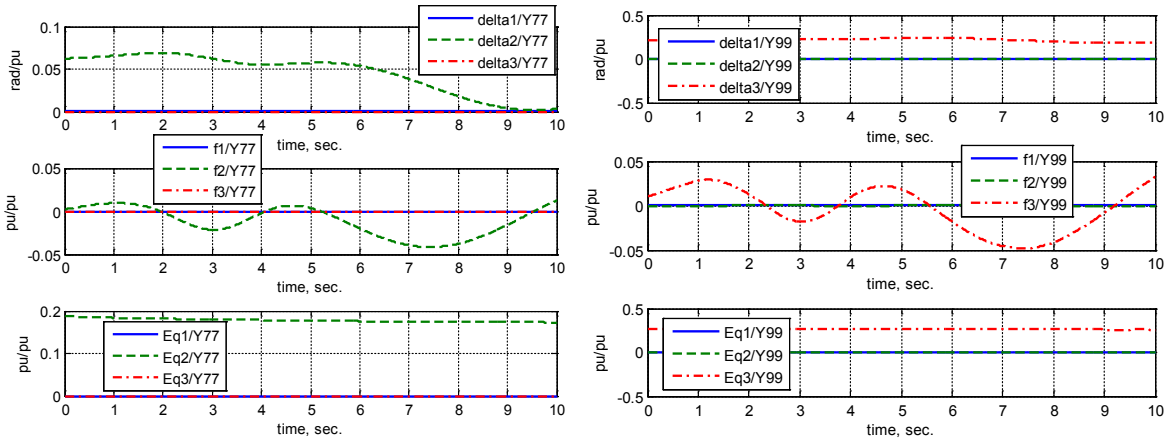

3.5c – coefficients wrt. Y_{77} 3.5d – coefficients wrt. Y_{99}

Figure 3.5**:** Sensitivity coefficients with respect to bus 7 shunt admittance (3.5a) and bus 9 shunt admittance for the simulation shown in Figure 3.1 (3.5b).

The system state variables by themselves, such as machine rotor angles, shaft speeds, voltages, etc., all provide insight into local stability for the aspects of the system surrounding that particular state variable. Unlike most systems, the power system has the ability to survive local instability by disconnecting the unstable parts to maintain operation in the stable areas. This is achieved using power systems protection techniques, as well as islanding techniques.

In order to determine if a locally unstable state variable (say, the frequency of one machine) can be recovered or is causing system separation that requires protective action, it is important to be able to see the local state variable's trajectory with respect to other related state variables. This is most commonly expressed in power system operations as the bus voltage angle differences across pairs of important buses. This means that the angle differences ($\delta_{ij} = \delta_i - \delta_j$) or rotor speed differences ($\omega_{ij} = \omega_i - \omega_j$) are as useful

as the individual state variables. This can also be applied to products of individual variables, such as the magnitudes apparent power being products of measured voltages and currents.

Sensitivity theory, as described by Frank [4], defines the sensitivity coefficients as partial derivatives of the state variables with respect to the system parameters. If all derivatives exist, the following rules can be applied.

$$\frac{\partial\left(x_1 + x_2\right)}{\partial\alpha} = \frac{\partial x_1}{\partial\alpha} + \frac{\partial x_2}{\partial\alpha} \tag{63}$$

$$\frac{\partial\left(x_1 x_2\right)}{\partial\alpha} = x_2(0)\frac{\partial x_1}{\partial\alpha} + x_1(0)\frac{\partial x_2}{\partial\alpha} \tag{64}$$

Where x_i and x_j are two state variables in the system and α is the system parameter of interest, and the derivatives on the right hand side of equations (63) and (64) exist.

With this in mind, the sensitivity coefficients of the angular separation ($\delta_{ij} = \delta_i - \delta_j$) and frequency separation ($\omega_{ij} = \omega_i - \omega_j$) can be calculated based on the previously calculated sensitivity coefficients of the individual angles and frequencies. This ability is important from a power systems protection standpoint, as the difference between bus angles is one of the key determinants of the power transfer between the buses, and the frequency difference between buses indicates whether the angles will further separate. There are several conventional and special protection schemes that explicitly monitor bus angles and frequencies, because large angle separation leads to the power system being unable to transfer power in a phenomenon known as out-of-step swing.

The results shown in Figures 3.1 through 3.5 can then be modified to show the differences between machine angles and machine frequency deviations. The modified results are shown in Figures 3.6 and 3.7 below.

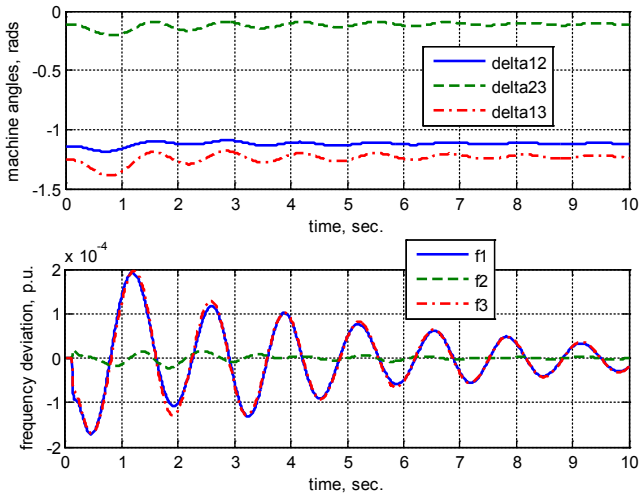

Figure 3.6: Machine angle differences between pairs of generators in radians (top) and differences in frequency deviations in per-unit (bottom) with respect to time.

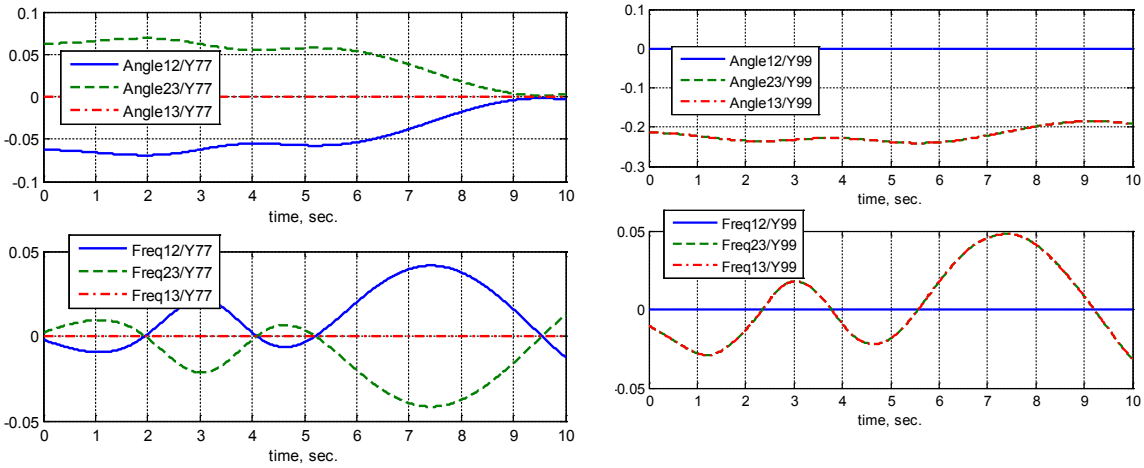

3.7a – coefficients wrt. Y_{77} 3.7b – coefficients wrt. Y_{99}

Figure 3.7: Sensitivity coefficients with respect to bus 7 shunt admittance (3.7a) and bus 9 shunt admittance (3.7b) for the simulation shown in Figure 3.6.

From Figures 3.1 through 3.5, it can be seen that the power system stabilizes in the short term but with the frequency level settling below nominal there will be a shaft speed difference between the input mechanical torque and the rotor speed. Having different mechanical input speed and generator rotor speed is an unacceptable condition physically for most turbine operations. This is reflected in the frequency relay standard published by the IEEE and NERC regulations for maintaining system frequency [32].

It can also be seen that the sensitivity coefficients of bus frequencies with respect to shunt admittances in Figures 3.5 and 3.7 have oscillating characteristics while the sensitivity coefficients with respect to mechanical power have a more stable characteristic. This suggests that changing the shunt admittances are not suitable for influencing the frequencies. However, the sensitivity coefficients of angles with respect to mechanical power appear to rise uncontrollably while the sensitivity coefficients of angles with respect to shunt admittances seem to have bounded responses. Figures 3.5 and 3.7 indicate that the influence of Y_{77} diminishes to zero over time, while the influence of Y_{44} is an order of magnitude smaller than Y_{99}.

Similar analyses of the sensitivity coefficients can be made for various disturbances and patterns of the coefficient characteristics coupled with the state variable responses can be used to determine the severity of the disturbance as well as determine the most influential system parameter that can be used to manipulate the state variables.

The example 9-bus system described above was further simulated and analyzed for several disturbance cases, and the results were compared and reviewed to see if any patterns emerge. A partial list of results is shown in Table 3.1 as follows.

Disturbance Case	Angle and Frequency State Variable Responses	Sensitivity Coefficient Reponses
3-phase bus fault at bus 4 for 2 cycles, reclose successful	After initial pertubations, system recovers to different operating point.	$\partial f_{ij}/\partial Y_{kk}$ and $\partial \delta_{ij}/\partial Y_{kk}$ do not oscillate but some coefficients are unstable.
Large load step-down, bus 5	ω_i settle above nominal, V_i is poorly damped but settle above initial points.	$\partial f_{ij}/\partial Y_{kk}$ all oscillate but are offset from 0, $\partial \delta_{ij}/\partial Y_{kk}$ are large for Y_{77} and Y_{99}.
Large load step-down, bus 6	ω_i settle above nominal, V_i is poorly damped but settle above initial points.	$\partial f_{ij}/\partial Y_{kk}$ all oscillate but are offset from 0, $\partial \delta_{ij}/\partial Y_{kk}$ are large and become unstable for Y_{77} and Y_{99}.
Large load step-down, bus 8	ω_i settle above nominal, V_i is poorly damped but settle above initial points.	$\partial f_{ij}/\partial Y_{kk}$ all oscillate but are offset from 0, $\partial \delta_{ij}/\partial Y_{kk}$ are large and become unstable for Y_{77} and Y_{99}.
Large load step-up, bus 5	ω_i settle below nominal, V_i is poorly damped but settle below initial points.	$\partial f_{ij}/\partial Y_{kk}$ all oscillate about 0, $\partial \delta_{ij}/\partial Y_{kk}$ are small except for Y_{99}.
Large load step-up, bus 6	ω_i settle below nominal, V_i is poorly damped but settle below initial points.	$\partial f_{ij}/\partial Y_{kk}$ all oscillate about 0, $\partial \delta_{ij}/\partial Y_{kk}$ start out small except for Y_{99}, but $\partial \delta_{ij}/\partial Y_{99}$ diminishes after t=7s.
Large load step-up, bus 8	ω_i settle below nominal, V_i is poorly damped but settle below initial points.	$\partial f_{ij}/\partial Y_{kk}$ all oscillate about 0, $\partial \delta_{ij}/\partial Y_{kk}$ are small except for Y_{99}.

Table 3.1: Comparison of state variables and sensitivity coefficients for various simulations.

3.2 Discussion of Results in Section 3.1

Based on the results of the 9-bus example system, a few observations can be made about the sensitivity coefficients and the applications that can be used.

3.2.1 Weakly linked parameter/variable pairs

The sensitivity coefficients of systems that are mathematically weakly linked to the parameters of interest will become zero. This shows up in all the plots for field EMF (E_{FD}) in all the cases. This is partly due to the nature of the field control and partly due to the assumptions taken in the calculations. *It is important to note that this does not mean that E_{FD} will not be affected by parameter changes, but only that the mathematical formulation has them weakly linked.*

The electrical properties at the buses (angles, frequencies) are more susceptible to changes in parameters that are closer to the buses of interest. In the 9 bus model the generators are too electrically far apart (admittances between generators are too high) for changes near one generator to greatly affect other generators. The coefficients are on the order of 10^{-9} per unit change in state variable per each unit change in parameters for devices that are far apart electrically, such as being separated by 2 or more buses with a large amount of impedances between them.

3.2.2 Oscillating sensitivity coefficients exist

During power swings there are coefficients that will swing about an axis either in-phase or out-of-phase with the angle and frequency state variables. This is especially pronounced if the electrical machines are assumed to be operating as the Classical Model with a constant EMF and rotating mass. These coefficients are not immediately suitable

for protection or feedback applications because the latency of the real communication and data handling systems will result in any decisions made based on these coefficients will significantly lag the actual parameter in the system. Any application using these coefficients will have to be timed to take effect at the appropriate part of the swing. For example, in Figure 3.7, all three coefficients with respect to the system frequency oscillate about zero. The implication of this characteristic is that system latency can cause a decision based on a positive coefficient can be applied during the negative coefficient, and result in a reverse of the intended impact.

3.3 TSA Coefficient Results for the IEEE 68-Bus System

Two disturbances are simulated and analyzed for TSA coefficients: a three-phase fault at bus 60, and a line disconnection for one of the two parallel lines between buses 60-61. The system network data are listed in Appendix A. The locations of these disturbances are selected since they both affect the power transfer and interconnection between Area #1 and Area #2 shown in Chapter 2, Figure 2.8.

The two areas have two sets of double-circuited tie-lines, with the faulted bus in the 3-phase fault case located on one end of the tie line between buses 60-61 and the wind generator at bus 12 is in close proximity to the other tie line. Extended time simulation indicates that both the fault and a persistent disconnection of one of the parallel lines will eventually destabilize the system by degrading the ability to transfer power between Area #1 and Area #2. With the tie line near the fault diminished, the remaining tie line will gain a more important role in recovering the system operating conditions.

The other disturbance being investigated is a line trip that disconnects one line between buses 60-61. In the cases where the line is not reclosed, the system eventually separates, but in the case where the line is reclosed within a certain amount of time, the system will recover.

Figure 3.8 shows the angles across the three transmission lines that connect Area #1 and Area #2 in the IEEE 68-bus system in the three-phase fault case with no protection and with wind generation present. Figure 3.9 shows the angles across the transmission lines in the case where one of the two parallel lines between buses 60 and 61 is tripped permanently. Figure 3.10 shows the angles across the lines in the case where the line in the previous case is tripped and then reclosed.

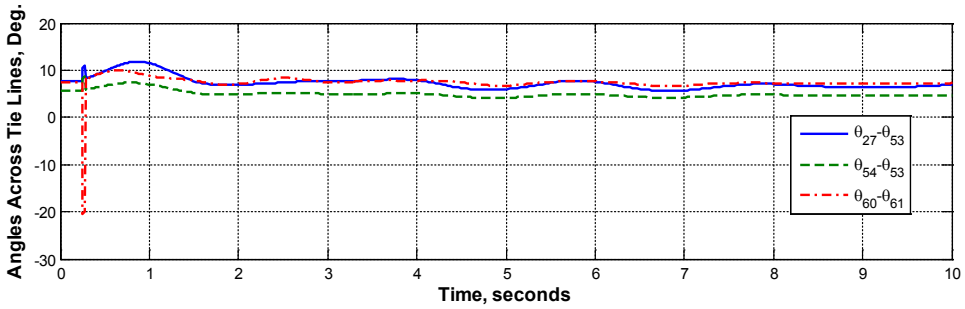

Figure 3.8: Angle differences across three tie lines of the 3-phase fault at bus 60 case.

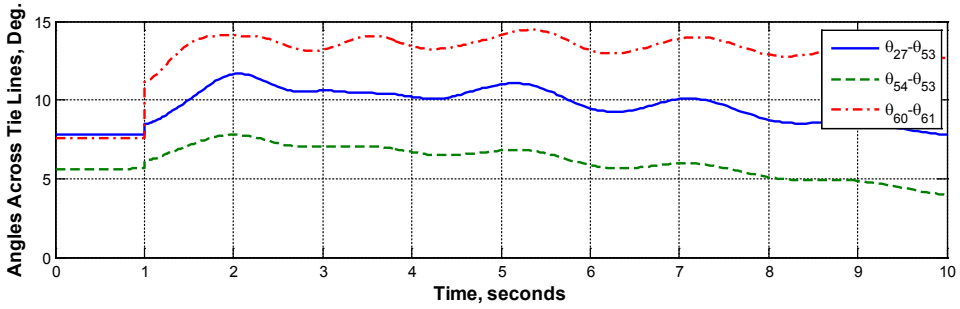

Figure 3.9: Angle differences across three tie lines due to a permanent line trip on one of the parallel lines between buses 60-61.

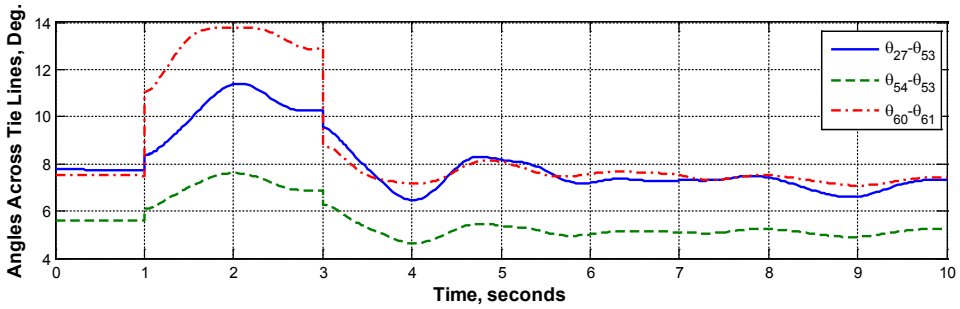

Figure 3.10: Angle differences across three tie lines in the event of a permanent line trip on one of the parallel lines between buses 60-61.

From Figure 3.8, it can be seen that the short duration of the fault resulted in the angles across the tie lines eventually stabilizing, but in this case the voltage suppression in Area #1 where the fault occurs eventually collapse. Figures 3.9 and 3.10 compare two contrasting scenarios with the same line-tripping disturbance, where Figure 3.9 shows one step change in the simulation corresponding to the line trip and Figure 3.10 shows two step changes corresponding to the line trip and then the line reclosing.

The TSA coefficients were calculated for all three cases above, with the α-parameter being the terminal voltage set-point (V_{ref}) for the DFIGs at the two wind generators in the system. By examining the sensitivity coefficients associated with the wind generator, it can be determined whether the wind generator can be used to improve operating conditions.The simulations for these two disturbances were run and analyzed in six cases as follows.

Simulation Case A: 3-Phase Fault at bus 60, α-parameter studied for TSA coefficients is the $V_{ref,DFIG1}$, the voltage control set-point for the wind turbine located at Bus 12. The

fault is cleared quickly within 2 cycles, but the disturbance is severe enough to cause persistent tie line oscillations and eventual separation between the Areas 1 and 2.

Simulation Case B: The same 3-Phase Fault at bus 60 as in case A, but with α-parameter studied for TSA coefficients is the $V_{ref,DFIG2}$, the voltage control set-point for the wind turbine located at Bus 1.

Simulation Case C: One of the parallel lines between buses 60 and 61 is permanently tripped, α-parameter studied for TSA coefficients is the $V_{ref,DFIG1}$. In this simulation case, area #1 separates from the rest of the system.

Simulation Case D: One of the parallel lines between buses 60 and 61 is permanently tripped, α-parameter studied for TSA coefficients is the $V_{ref,DFIG2}$.

Simulation Case E: One of the parallel lines between buses 60 and 61 is tripped and reclosed after 2 seconds, α-parameter studied for TSA coefficients is the $V_{ref,DFIG1}$. This case and case F below are analyzed to contrast the two scenarios after the initial disturbance. In cases C and D, the line trips and does not reclose, while in cases E and F the line does reclose.

Simulation Case F: One of the parallel lines between buses 60 and 61 is tripped and reclosed after 2 seconds, α-parameter studied for TSA coefficients is the $V_{ref,DFIG2}$.

In all of the cases above, the simulation applies the disturbance at 1 second, and is run for 10 seconds. The TSA coefficients for state variable sensitivities with respect to the corresponding α-parameter are calculated and examined. The resulting matrix dimensions of these sensitivities are 129×k for w_1 and 207×k for w_2, where k is the number of simulation time steps. Due to the large numbers of these coefficients, the

results are not presented here in full. However the most sensitive variables and their characteristics are presented in Table 3.2 through Table 3.5.

Type	Description	Representative Example Plot
Result Type 1	A spike in sensitivity occurs immediately after the time of the disturbance and oscillates noticeably (spikes on both positive and negative values), but also quickly damps down to zero or oscillates near-zero. Damping time is less than 0.5 seconds.	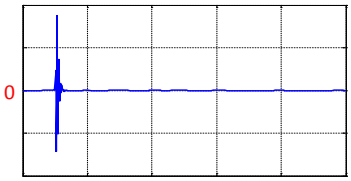
Result Type 2	Sensitivity coefficients oscillate within a consistent zone, offset below zero (negative value in the vast majority of the plot).	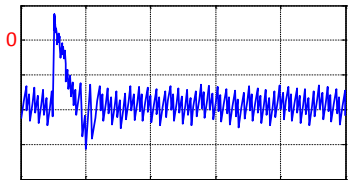
Result Type 3	Sensitivity coefficients oscillate within a consistent zone, offset above zero (positive value in the vast majority of the plot).	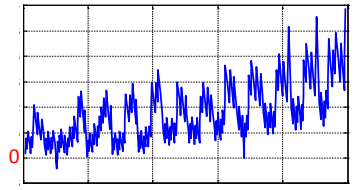
Result Type 4	Sensitivity coefficients oscillate around zero (may be skewed towards positive or negative values).	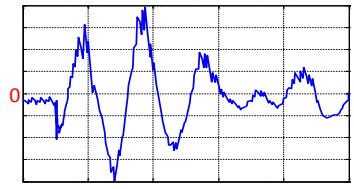
Result Type 5	A spike in sensitivity occurs immediately after the time of the disturbance and oscillates (spikes on either positive or negative values), but also immediately damps down to zero or oscillates near-zero. Damping time is less than 0.5 seconds.	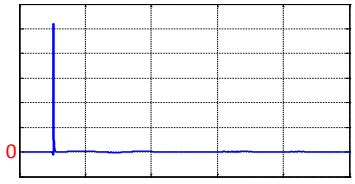

Table 3.2: Summary of the characteristics of the sensitivity coefficients of the variables for cases A-F.

After completing the simulations and analyzing the results it became clear that the sensitivity coefficients will exhibit characteristics that can be grouped together. These types of characteristics are summarized in Table 3.2. The types and categories shown

here are defined for the purposes of convenience only and do not reflect a standardized definition as none exists at this time for TSA analysis in power systems.

	CASE A, Fault @ Bus 60 $\alpha = V_{ref,DFIG1}$		CASE B, Fault @ Bus 60 $\alpha = V_{ref,DFIG2}$	
System State Variable	Maximum/Minimum Sensitivity Coefficient Value	Characteristic Type	Maximum/Minimum Sensitivity Coefficient Value	Characteristic Type
$V_{r1,Exc1}$	0.8254	Type 1	-0.9496	Type 1
$V_{r1,Exc2}$	0.6581	Type 1	-0.7582	Type 1
$V_{r1,Exc3}$	0.1589	Type 1	-0.1816	Type 1
$V_{r1,Exc4}$	-0.1065	Type 1	-0.1232	Type 1
$V_{r1,Exc5}$	0.1525	Type 1	-0.1759	Type 1
$V_{r1,Exc6}$	0.1190	Type 1	-0.1374	Type 1
$V_{r1,Exc7}$	-0.2631	Type 1	-0.3015	Type 1
$I_{dr,DFIG1\ (bus\ 12)}$	-0.1413	Type 2	-	-
$I_{qr,DFIG1\ (bus\ 12)}$	-	-	0.0694	Type 5
$I_{dr,DFIG2\ (bus\ 1)}$	-	-	-0.1410	Type 2
$I_{qr,DFIG2\ (bus\ 1)}$	0.2170	Type 1	0.2606	Type 5
System Output	Maximum/Minimum Sensitivity Coefficient Value	Characteristic Type	Maximum/Minimum Sensitivity Coefficient Value	Characteristic Type
$P_{elec,Gen2}$	-	-	0.0544	Type 3
$P_{elec,Gen3}$	0.2459	Type 4	0.1671	Type 4
$V_{f,Gen7}$	-0.0821	Type 1	-0.0580	Type 1
$Q_{elec,Gen7}$	-	-	0.0660	Type 1
$V_{f,Gen8}$	0.0649	Type 1	-	-
$P_{elec,Gen8}$	-0.0552	Type 4	-	-
$P_{elec,Gen13}$	-	-	0.0482	Type 3

Table 3.3: Summary of the most sensitive system variables and outputs for Case A (Fault @ Bus 60, $\alpha = V_{ref,DFIG1}$) and for Case B ($\alpha = V_{ref,DFIG2}$).

System State Variable	Maximum/Minimum Sensitivity Coefficient Value	Characteristic Type	Maximum/Minimum Sensitivity Coefficient Value	Characteristic Type
$I_{dr,DFIG1\ (bus\ 12)}$	-0.3274	Type 2		
$I_{dr,DFIG2\ (bus\ 1)}$			-0.1606	Type 2
System Output	Maximum/Minimum Sensitivity Coefficient Value	Characteristic Type	Maximum/Minimum Sensitivity Coefficient Value	Characteristic Type
$P_{elec,Gen3}$			-0.0546	Type 4
$Q_{elec,Gen3}$	-0.2215	Type 2		
$P_{elec,Gen13}$			0.0394	Type 3

Table 3.4: Summary of the most sensitive system variables and outputs for Case C (Trip @ Line 60-61, $\alpha = V_{ref,DFIG1}$) and for Case D ($\alpha = V_{ref,DFIG2}$).

System State Variable	Maximum/Minimum Sensitivity Coefficient Value	Characteristic Type	Maximum/Minimum Sensitivity Coefficient Value	Characteristic Type
$I_{dr,DFIG1\ (bus\ 12)}$	-0.1796	Type 2		
$I_{dr,DFIG2\ (bus\ 1)}$			-0.1320	Type 2
System Output	Maximum/Minimum Sensitivity Coefficient Value	Characteristic Type	Maximum/Minimum Sensitivity Coefficient Value	Characteristic Type
$P_{elec,Gen3}$			0.0667	Type 4
$Q_{elec,Gen3}$	-0.2215	Type 2		

Table 3.5: A summary of the most sensitive system variables and outputs for Case E (Trip @ Line 60-61 with reclose, $\alpha = V_{ref,DFIG1}$) and for Case F ($\alpha = V_{ref,DFIG2}$).

3.4 Discussion of Results in Section 3.3

The tables above indicate that the internal variables of some AVRs (V_{r1}) can have large magnitude sensitivity coefficients with respect to the DFIG voltage set-point, but these coefficients are also quickly damped out (all Type 1). This is consistent with observations and derivations made in [4] with respect to the sensitivities of the variables in a well-damped system. A stably controlled subsystem will tend to drive its own internal states to a stable point and therefore exhibit small values for sensitivity coefficients.

This analysis is intended to evaluate whether TSA is suitable for security assessment, and the plotted shapes of the calculated coefficients indicate that the state variables of the AVRs by themselves are not suitable candidates for determining the stability or security of a power system. The reasoning is twofold. First, the variables are quickly damped and only spike during large disturbances which does not exhibit noticeable changes during oscillations in the system. Second, these variables are internal to a model representation of the AVRs, which means that they cannot be directly

measured and additional state estimation would be required to estimate their values from measurable variables such as terminal voltages or field voltages. Lastly, when the disturbance is not a fault or does not suppress voltages, the magnitudes of these sensitivities are no longer among the highest, which is why they do not appear on Tables 3.3 through 3.5.

The sensitivity coefficients of the DFIG generator q-axis current, d-axis current, and synchronous machine real and reactive power are variables that can be either directly measured or estimated using relatively simple pseudo-measurements, and present more interesting opportunities for expanding the research in utilizing TSA in power systems. The sensitivity coefficients of these variables usually exhibit low-frequency oscillatory characteristics, with no offset or an offset above or below zero. The difference between fast-damping and slow-oscillating coefficients is illustrated in Figure 3.11.

For the exact same disturbance, analyzing the sensitivity coefficients with respect to two different α-parameters can yield interesting observations. This is illustrated by reviewing the coefficients with respect to $V_{ref,DFIG1}$ and $V_{ref,DFIG2}$, as shown Figures 3.12 and 3.13.

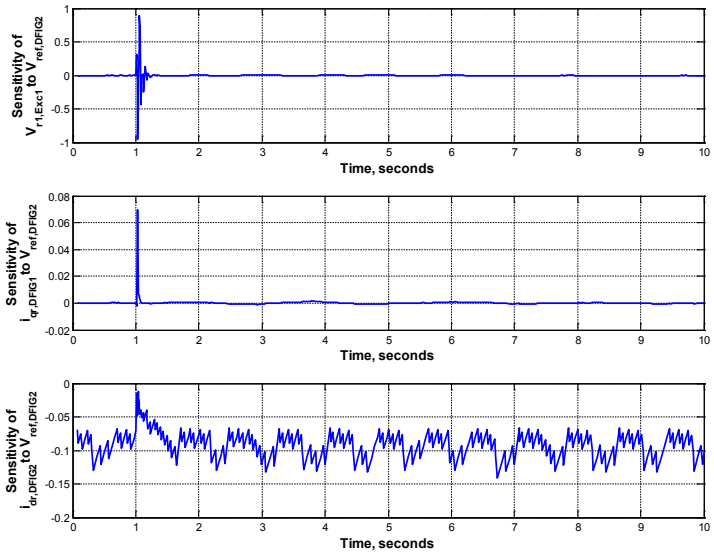

Figure 3.11: Sensitivity coefficients of exciter V_{r1} at AVR1 (top), DFIG q-axis current (middle) and d-axis current (bottom) with respect to the DFIG terminal voltage setting $V_{ref,DFIG2}$. Plots taken from Case B.

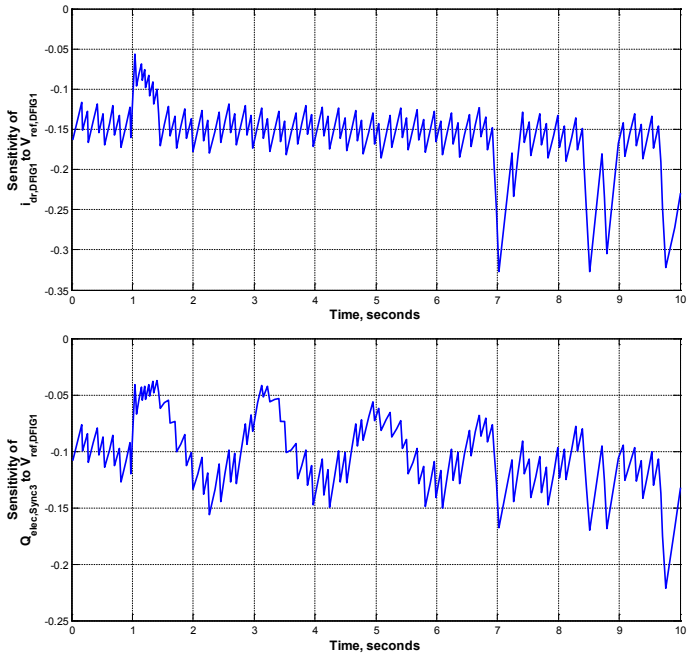

Figure 3.12: Sensitivity coefficient of DFIG1 d-axis rotor current (top) and G3 reactive power (bottom) with respect to $V_{ref,DFIG1}$. Simulated Case C.

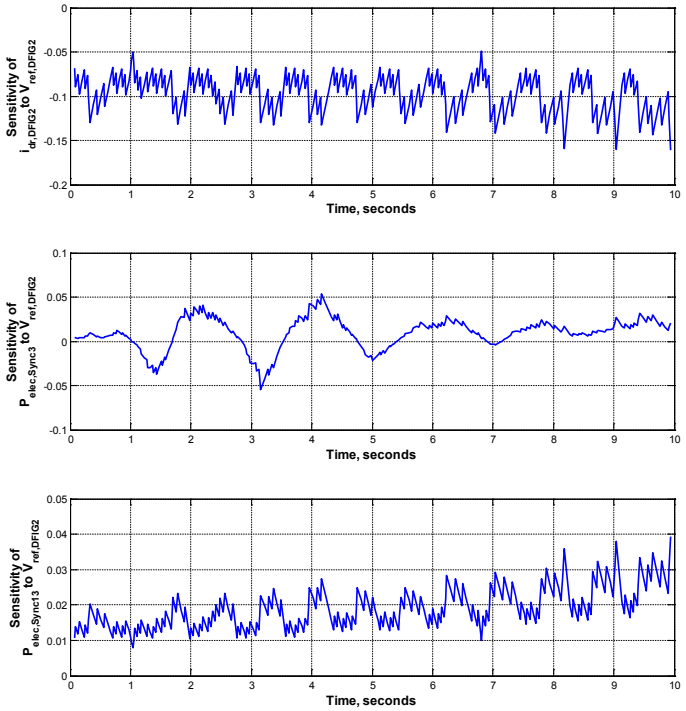

Figure 3.13: Sensitivity coefficient of $DFIG_2$ q-axis rotor current (top) and real power output from G_3 (middle) and G_{13} (bottom) with respect to $V_{ref,DFIG2}$. Simulated Case D

The comparison between simulation cases with the same disturbance but different α-parameters is useful for determining which general zones of the power system are subject to more severe instability, and provides clues as to which areas of the power system would benefit more from corrective or preventive control actions. For example, the sensitivities of real power at two synchronous generators shown in Fig. 3.12 are beginning to trend towards instability (under-damped), which suggests that the power transfer within the system is becoming unstable. This can be compared to the simulation cases where the same conditions as those shown in Fig. 3.12 and 3.13, but with a successful reclose of the tripped line.

Figure 3.14 shows the same sensitivity coefficients as the ones shown in Figure 3.12, except that for simulation case C the tripped line does not reclose while the simulation case E recloses. The plots in these two cases have the same general characteristics, but the plots in Figure 3.12 trend away from the starting values while the plots in Figure 3.14 appear to be bounded. The plots of Figures 3.13 and 3.15 can be compared to analyze the differences in responses between a case where the disturbance is not reclosed (Figure 3.13) and the case where the disturbance is reclosed (Figure 3.15). The perturbations in the cases with reclosing appear to return to stability sooner or have smaller deflection between minimum and maximum.

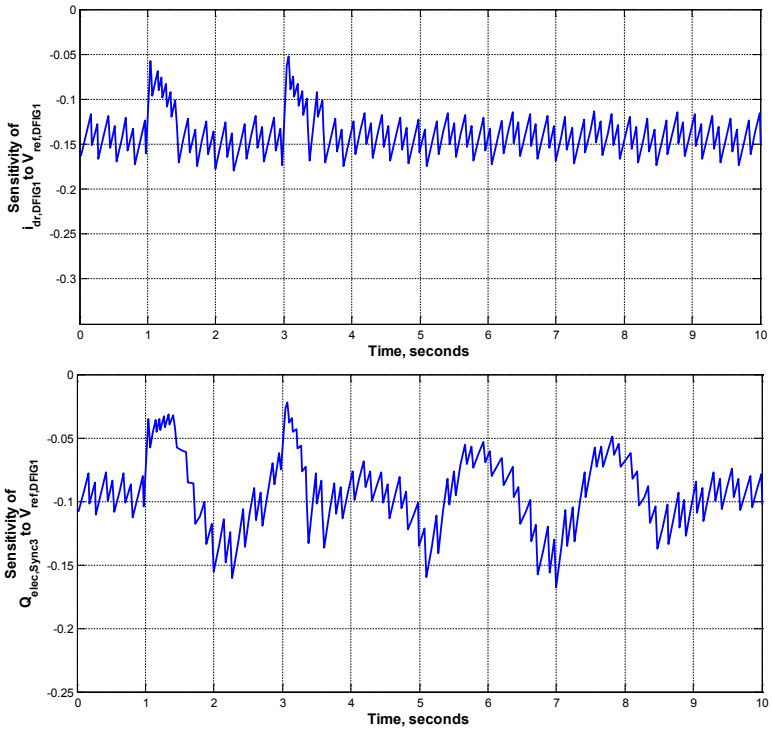

Figure 3.14: Sensitivity coefficient of DFIG1 d-axis rotor current (top) and reactive power output of G3 (bottom) with respect to $V_{ref,DFIG1}$. Simulated Case E.

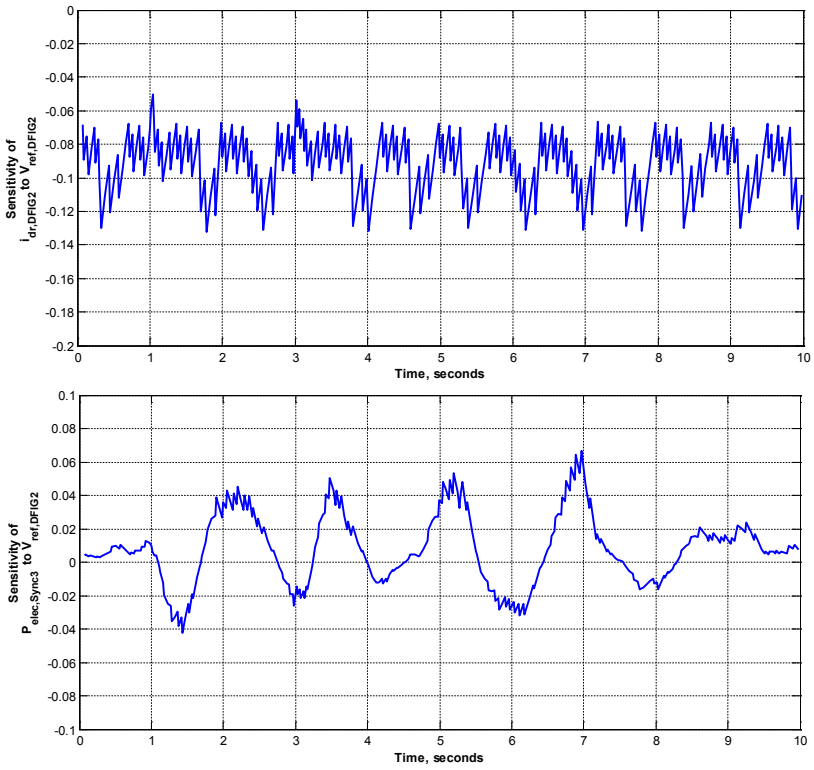

Figure 3.15: Sensitivity coefficient of DFIG2 d-axis rotor current (top) and real power output from G3 (bottom) with respect to $V_{ref,DFIG2}$ (Case F).

The interactions between DFIG variables, either within the same DFIG or between different DFIGs in the power system, can be analyzed to determine possible relationships that may affect control or protection considerations. In Figure 3.16, the cross-sensitivities, variables of one DFIG w.r.t. the other DFIG (such as $\partial i_{qr,DFIG1}/\partial V_{ref,DFIG2}$) of the DFIG d-axis currents are presented. In contrast, Figure 3.17 shows the self-sensitivities of the d-axis currents. Similar comparison plots of the DFIG q-axis currents are shown in Figures 3.18 and 3.19.

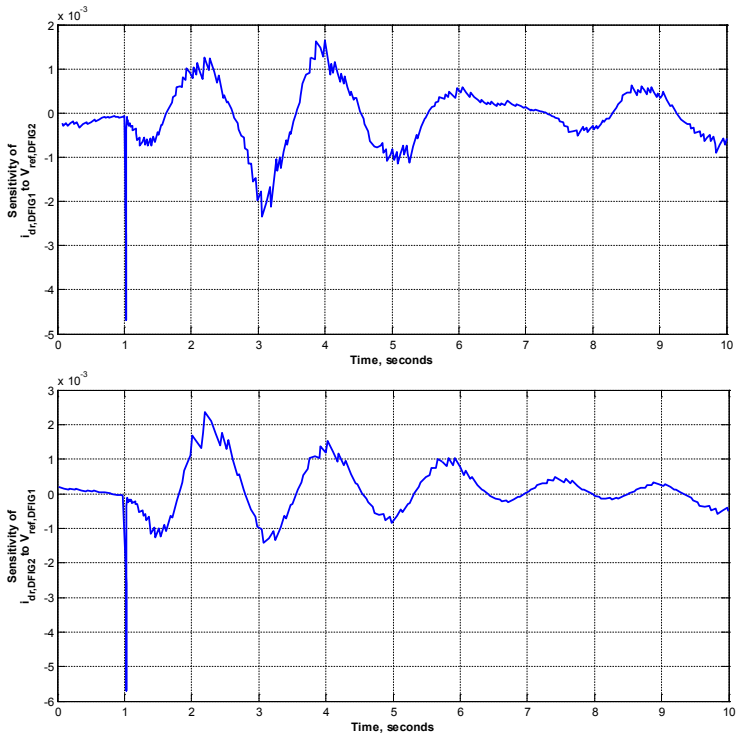

Figure 3.16: Sensitivity coefficients $\partial i_{dr,DFIG1}/\partial V_{ref,DFIG2}$ and $\partial i_{dr,DFIG2}/\partial V_{ref,DFIG1}$, in the 3-phase fault case.

The i_{dr} and i_{qr} sensitivities can be analyzed further by examining the mathematical models of the respective machines. The model of each DFIG corresponds to equations (55) through (60) in Chapter 2, with (58) governing the i_{qr} behavior and (59) governing i_{dr}. When extracting the relevant sub-equations from the partial derivatives shown in equations (6) and (7) after substituting the model equations in (58) and (59), the solutions for $\partial i_{dr}/\partial V_{ref,DFIG}$ will have the general form of a differential equation with $\partial F/\partial i_{dr}$ terms, $\partial G/\partial i_{dr}$ terms, $\partial F/\partial V_{ref,DFIG}$ terms, and other mutual terms cross-coupled to the other system variables and outputs. The same principle applies in the i_{qr} cases.

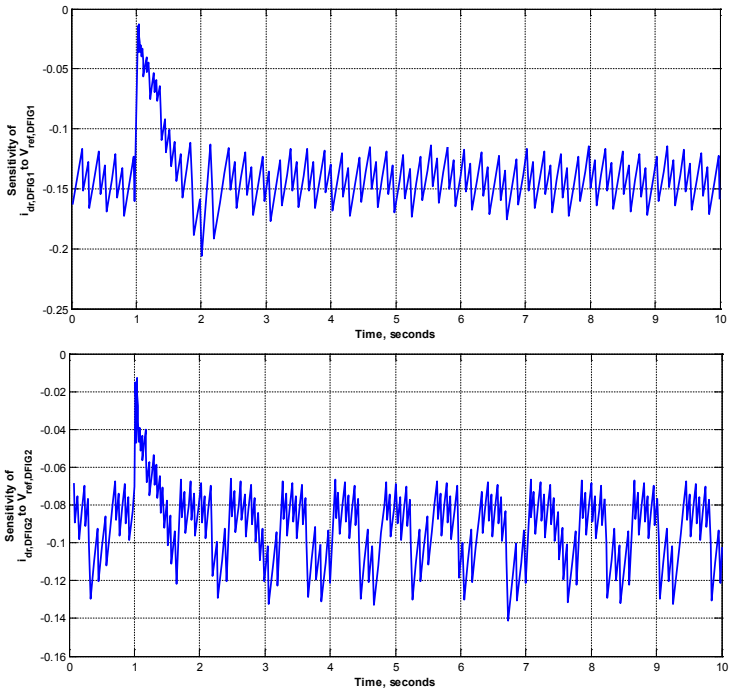

Figure 3.17: Sensitivity coefficient of each DFIG d-axis current with respect to the DFIG terminal voltage setting $V_{ref,DFIG}$ of the same DFIG, in the 3-phase fault case.

By further evaluating the equations, the time differential of $\partial i_{qr}/\partial V_{ref,DFIG}$ and $\partial i_{dr}/\partial V_{ref,DFIG}$ contain terms that are multiplied by the DFIG terminal voltage after the calculated power is decomposed into i_{qr} and i_{dr} parts, but only $\partial i_{dr}/\partial V_{ref,DFIG}$ contains a constant term from $\partial F/\partial V_{ref,DFIG}$.

These differences in the solutions resulted in the difference in responses shown in Figures 3.16 through 3.19. The coefficient $\partial i_{qr}/\partial V_{ref,DFIG}$ has the largest magnitude when the voltage is suppressed, and returns to a small value as soon as the voltage recovers. On the other hand, $\partial i_{dr}/\partial V_{ref,DFIG}$ has a similarly sudden change due to the DFIG terminal voltage presences in the differential equations, but has a steady-state value based on the constant term in the partial differential which is scaled by other operating conditions.

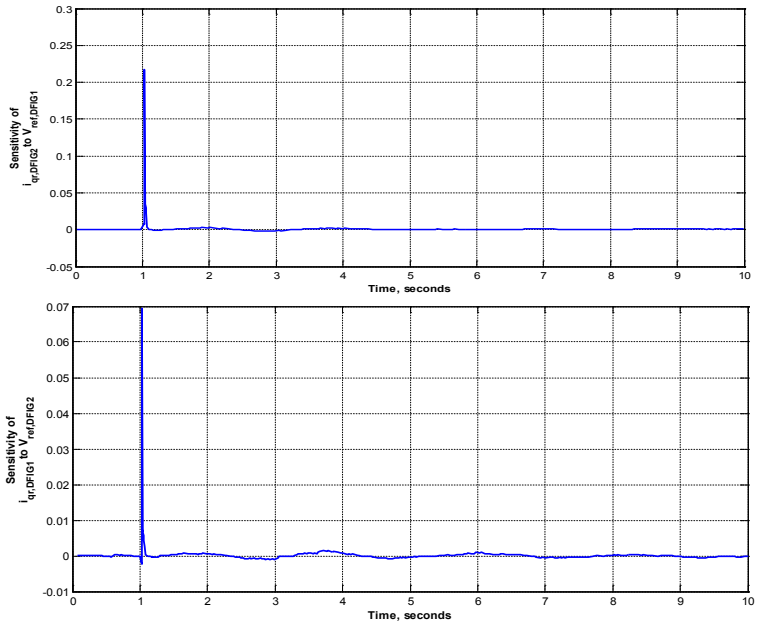

Figure 3.18: Sensitivity coefficient of each DFIG q-axis current with respect to the DFIG terminal voltage setting $V_{ref,DFIG}$ of the other DFIG, in the 3-phase fault case.

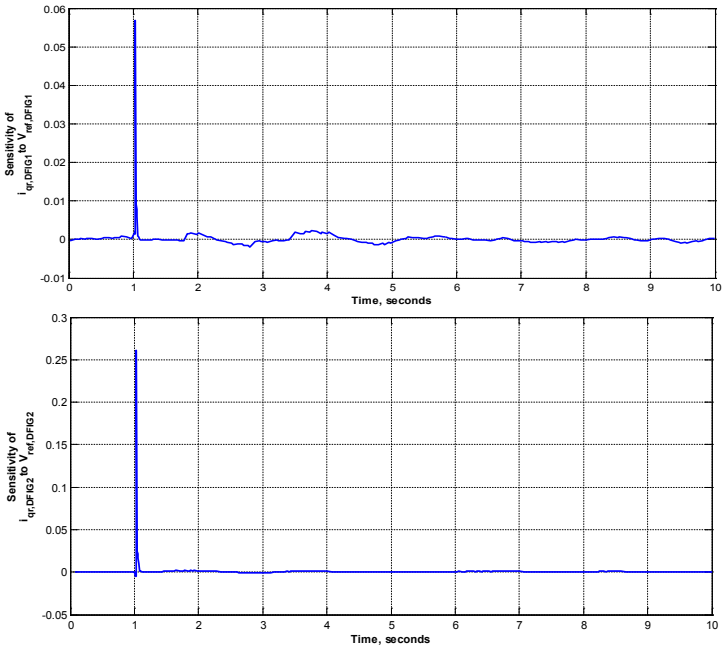

Figure 3.19: Sensitivity coefficient of each DFIG q-axis current with respect to the DFIG terminal voltage setting $V_{ref,DFIG}$ of the same DFIG, in the 3-phase fault case.

For comparison with the 3-phase fault case, Figures 3.20 and 3.21 shows the same plots for the line trip disturbance, where the disturbance does not include voltage suppression. When voltage suppression does not occur during the disturbance, the dominant components of the $\partial i_{qr}/\partial V_{ref,DFIG}$ coefficients disappear and the remaining values have smaller magnitudes on the order of 10^{-3}.

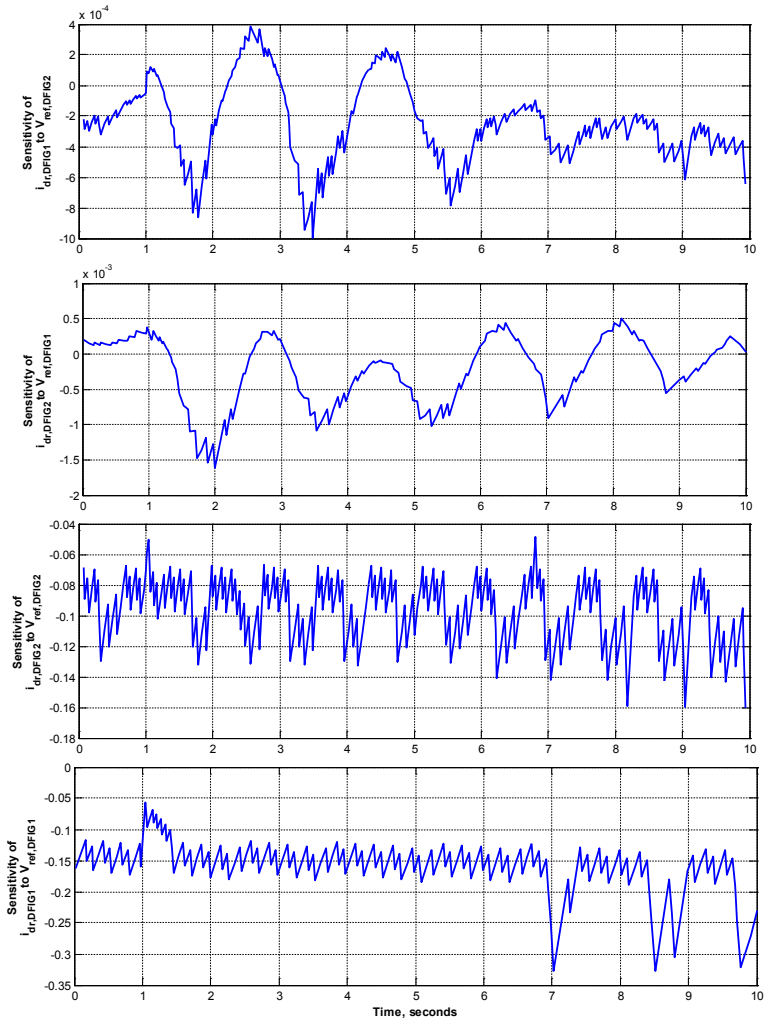

Figure 3.20: Sensitivity coefficient of each DFIG d-axis current with respect to the DFIG terminal voltage setting $V_{ref,DFIG}$ of the other DFIG (top 2 plots) and same DFIG (bottom 2 plots), in the line trip case.

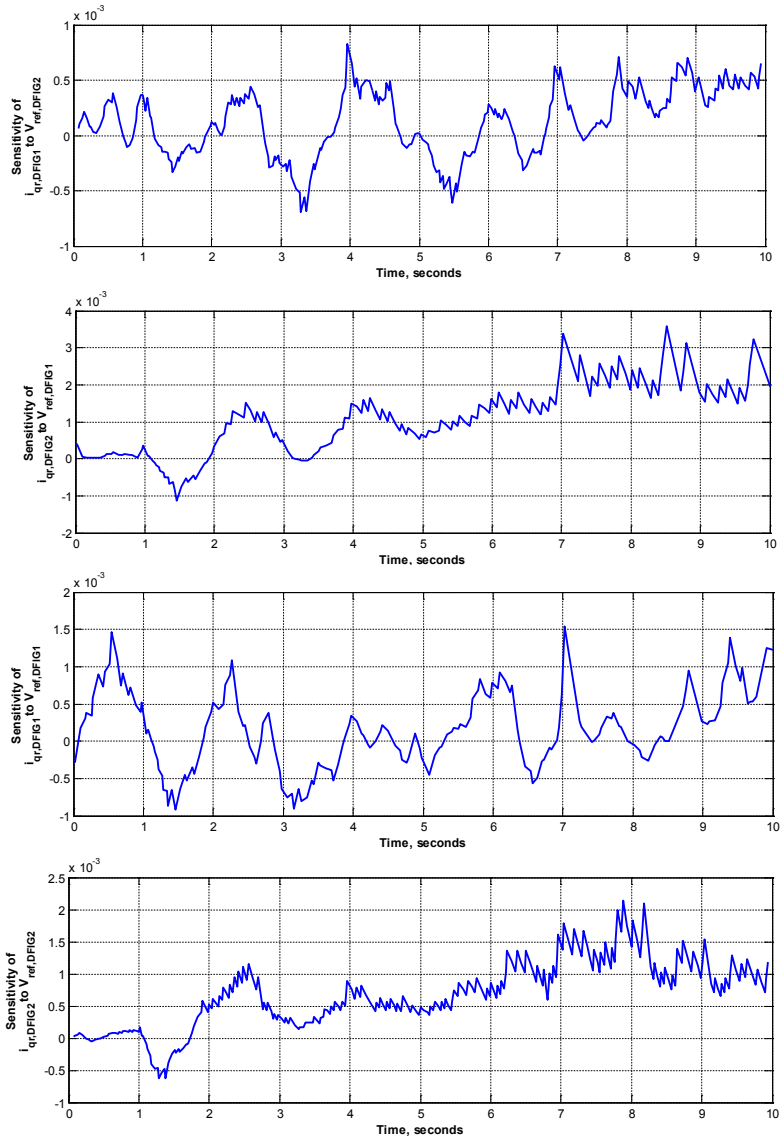

Figure 3.21: Sensitivity coefficient of each DFIG q-axis current with respect to the DFIG terminal voltage setting $V_{ref,DFIG}$ of the other DFIG (top 2 plots) and of the same DFIG (bottom 2 plots), in the line trip case.

3.5 Apparent Impedances in Cases Discussed in 3.4

The output data from the time domain PSAT simulation includes bus voltages and bus voltage angles. The apparent impedance at various points can be calculated using the voltage and line data all in per-unit [33]. Equation (65) shows the phasor calculation of the apparent impedance at bus *i*, as seen by a relay protecting the line between buses *i*-*j*.

$$Z_{app,i_{ij}} = \frac{V_i}{I_{ij}} = \frac{V_i Z_{ij}}{\left(V_i - V_j\right)} \tag{65}$$

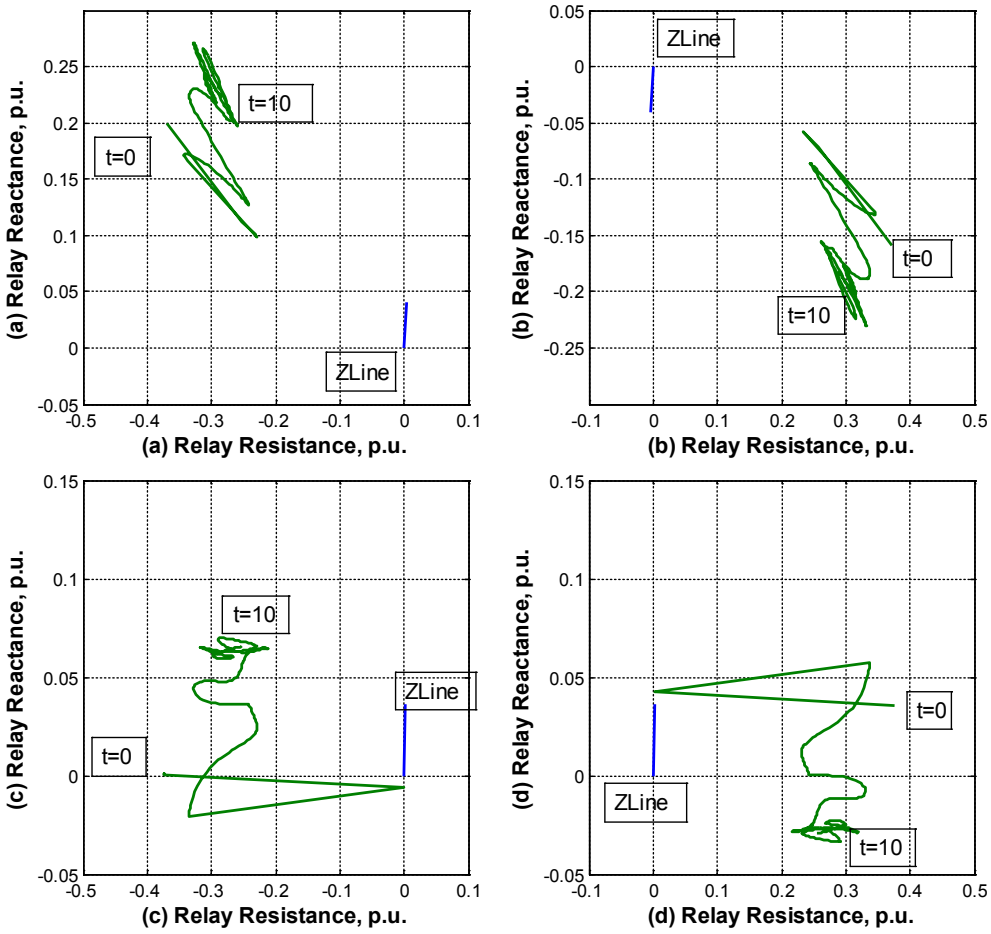

Figure 3.22: Apparent impedances in the 3-phase fault case – (a) bus 53 looking into line 53-54; (b) bus 54, line 53-54; (c) bus 61, line 61-60; (d) bus 60, line 61-60.

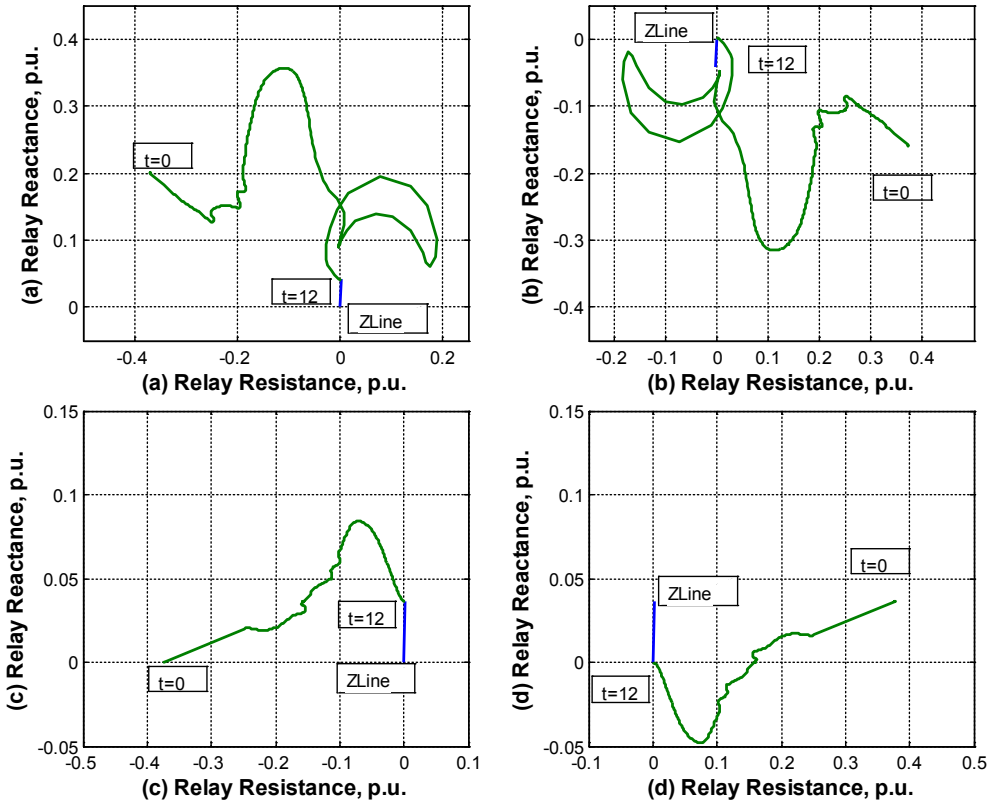

Figure 3.23: Apparent impedances in the line trip fault case – (a) bus 53 looking into line 53-54; (b) bus 54, line 53-54; (c) bus 61, line 61-60; (d) bus 60, line 61-60.

Figure 3.22 in the previous page shows the apparent impedance plots in the case of a 3-phase fault as seen from the four buses on both ends of two of the main tie lines between Area #1 and Area #2. The corresponding plots from the case where one of the two lines between buses 60-61 is tripped.

The straight line in each of the plot marked with "ZLine" represents the impedance of the transmission line connected to the bus. In Figures 3.22 (a) and (b) the plots reflect the impedance seen by relays at buses 53 and 54. Since the 53-54 line is not involved with the fault, the apparent impedance only reflects the angle and voltage fluctuations. On the other hand, Figures 3.22 (c) and (d) show the apparent impedance on

the faulted bus (60) and the bus on the other end of a line connected to the faulted bus (61). The apparent impedances in these cases immediately shows the effect of the fault where the impedance drops sharply and the calculated impedance in 3.22 (c) and (d) move to areas associated visually with the impedance of the line before entering the recovery oscillation.

The apparent impedances for the line trip case in Figure 41 show what unstable swings and system separations look like. The apparent impedances all swing in towards the line impedance and do not recover. This is further illustrated in Figure 3.24 which expands the time frame of Figure 3.9 to the time period where the instability becomes very obvious.

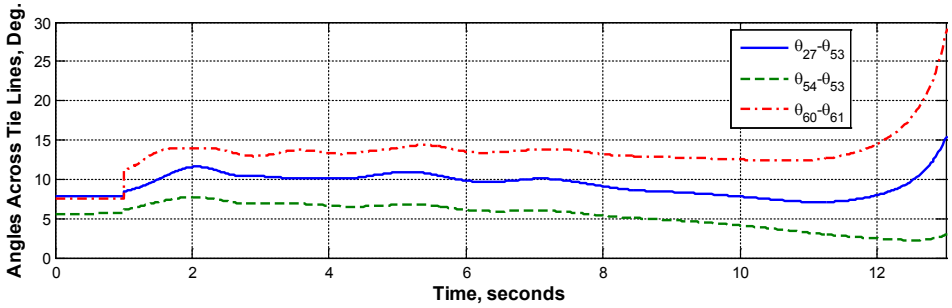

Figure 3.24: Plots of angle differences from Figure 3.9, but with extended simulation time to illustrate the instability.

The conditions in which the power system do not recover and the apparent impedances obviously approach a zone near the transmission line impedance are conditions that are suitable candidates for out-of-step relaying, which would make these cases the basis for the following chapter where a normal out-of-step relay setting is determine and then the special protection scheme using TSA will be added to improve the out-of-step protection performance and improve the system response to disturbances.

CHAPTER 4

OUT-OF-STEP SETTINGS AND SPECIAL PROTECTION SCHEME

This chapter begins with the establishment of normal out-of-step relay settings for the transmission tie lines presented in Chapter 3. The settings will be based on the recommendations in Blackburn and Domin [30]. The process starts with determining basic distance relay settings [30] which would provide the protection setting perimeter that guides the out-of-step (OOS) settings. The OOS settings will in turn be evaluated against the apparent impedance plots from the disturbances discussed at the end of Chapter 3. This evaluation will then lead to the determination of the special protection settings and the chapter will be concluded with the simulation result after implementing the special protection scheme.

4.1 Out-of-Step Relay Settings

The OOS relay settings require the settings of standard distance relays to be established for detecting regular faults in order for the OOS settings to have a perimeter where the OOS relay should not encroach. If the OOS relay characteristics overlap with the distance relays, then there is a chance that the combination of the two protection types may operate incorrectly. These conditions can be tested and ameliorated by using blocking logic to prevent incorrect operation.

4.1.1 Distance Relay Setting

There are no standardized rules for setting distance relays, and each utility or regulatory entity has to be responsible for establishing a protection philosophy and settings guidelines. The settings are then studied internally to ensure that they are

properly coordinated and subsequently submitted to the applicable regulatory body. The distance relays in this case will follow the general recommendations from Blackburn and Domin [30], which is 90% of the impedance value of the transmission line for the primary zone, and 150% of the line for the back-up zone. The distance relay zones are shown in Figures 4.1, which only show the distance relay characteristics from the Area #1 side of each line.

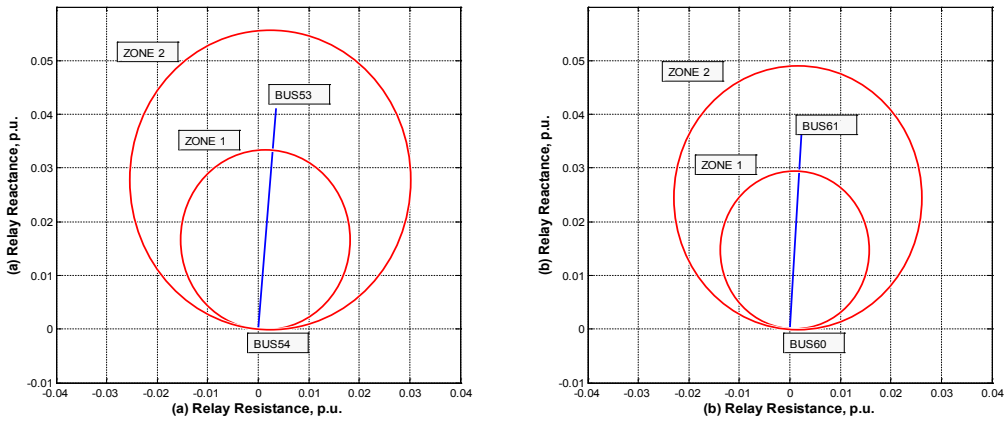

Figure 4.1: Distance relay settings for the Area #1 side of two of the main tie lines in the IEEE 68-bus system. (a) shows the setting for a relay at bus 54 looking into line 54-53; (b) shows bus 60 looking into line 60-61.

4.1.2 Incorporating Out-of-Step Relay

The relay settings shown in Figure 43 will be coordinated with the OOS relay settings in order to avoid failure to trip for faults with low current and to avoid tripping incorrectly when the power swing is stable. Discussions on these settings and trip/bloc logics can be found in Blackburn and Domin [30] as well as Anderson [12]. This process

starts with evaluating the disturbances against the distance relay settings, as shown in Figure 4.2.

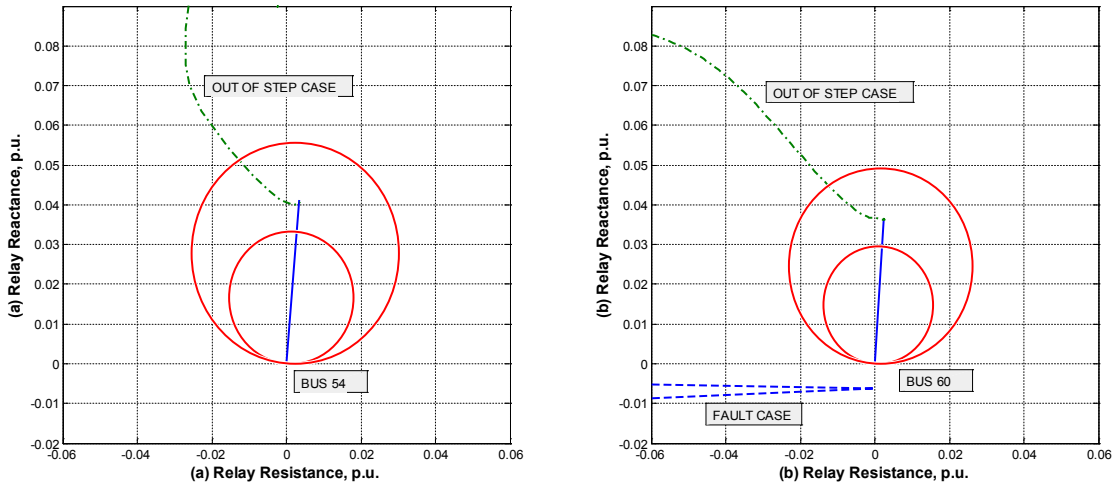

Figure 4.2: Distance relay settings from Figure 4.1 with the disturbance impedances superimposed.

From the perspective of a relay at bus 54 in Figure 4.1 (a), the fault that occurs at bus 60 doesn't register near the protection zones at all, because the fault occurs too far away from the bus to significantly influence its voltage or current flow. Bus 60 in Figure 4.2 (b) will see the fault slightly behind the relay because of the line shunt admittances and simulated fault impedance slightly distorting the measurements. If the fault is an ideal short circuit the impedance plot will approach the (0,0) coordinate in 4.2 (b).

Since the apparent impedances in both cases approach the protection zones from the positive reactance area of the plots, simply using a blinder as shown in Figure 2.14 in Chapter 2 may not be suitable because the blinder lines to the positive and negative resistance sides may not adequately cover swings when the line loading becomes reactive such as in Figure 4.2. Therefore, the OOS protection zones will be established as circles

that are concentric with the zone 2 (larger circles) of the distance relays, with twice the radii of the zone 2 settings.

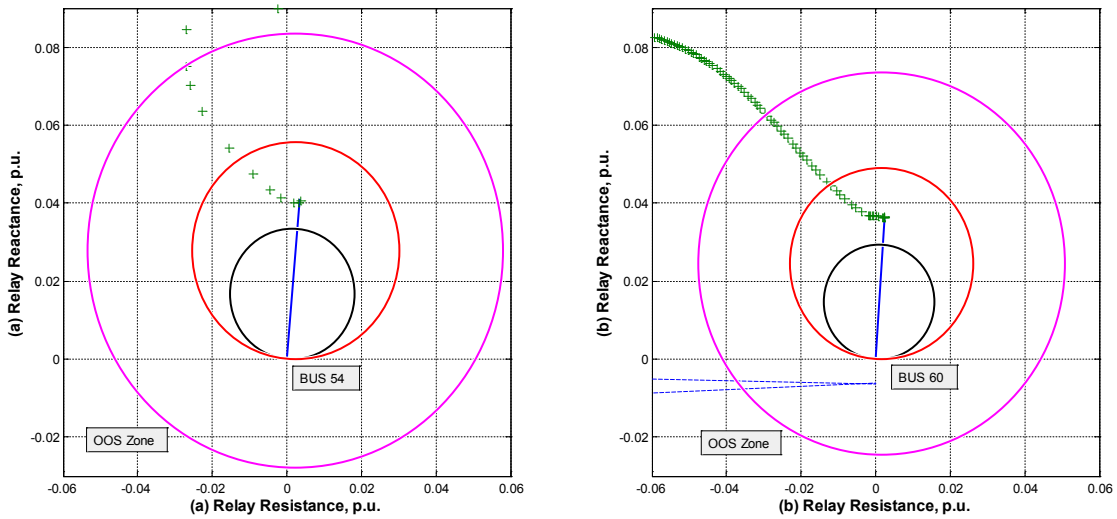

Figure 4.3: Distance relay settings from Figure 4.1 with the OOS zones added.

Another crucial element of OOS protection is time, specifically the time delays applied in order to allow other protection elements operate and the timing of the blocking signal such that the OOS can block the distance relay from operating until the stability of the swing is confirmed. The resistances and reactances of the unstable swing case (plots with "+" symbols) from Figure 4.3 are separated and plotted with respect to time in order to check the timing of the OOS zone encroachments. This plot is compressed to show the time period near the unstable condition in Figure 4.4 in the next page.

After evaluating the timing and the impedance plots in Figures 4.3 and 4.4, it becomes apparent that the unstable swing will develop at the bus near the disturbance first (bus 60) and escalates slowly until the system is no longer able to support the power flows. The bus further away from the disturbance (bus 54) will begin its swing after some

time has elapsed as the effects of the disturbance make their way across the system, and then once the stability threshold is reached, the swings destabilize quickly.

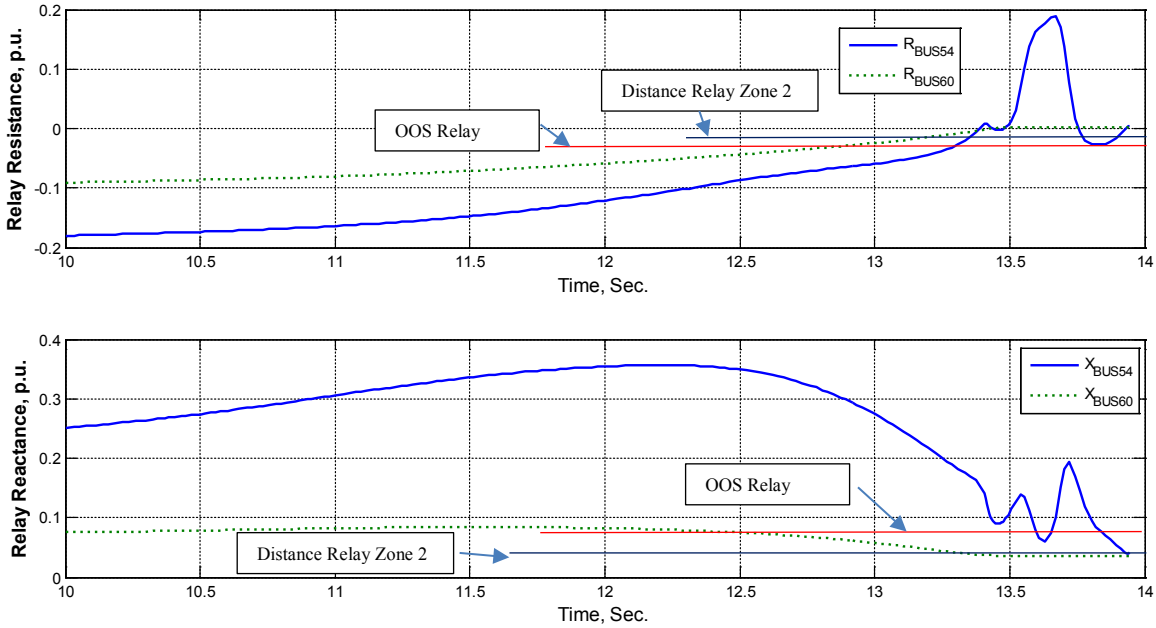

Figure 4.4: Apparent resistances (top) and reactance (bottom) plotted against time in the unstable swing cases.

Since the unstable swing at bus 54 is a consequence of the disturbance at bus 60 propagating throughout the system, the remainder of this analysis will focus on bus 60. As described by Anderson [12], a basic logic diagram of the OOS relay tripping and blocking scheme is shown in Figure 4.5 on the next page. Once the OOS zone is encroached, the normally open contact "OOS" in Figure 4.5 closes, energizing the OS timer, which in turn will delay the protection sequence in order to allow stable swings to exit the zone. If the swing stays within the OOS zone and the time delay is exhausted, *and* zone 2 of the distance relay (contact 21-2) is tripped and initiates the AR contact, then the next time delay (T1) is initiated, once again giving the power swing a chance to

exit the zone. If the power swing stays within the zones, then none of the time delays will reset causing the circuit breaker contact (52) to trip. The device designations are based on generic standard conventions [34].

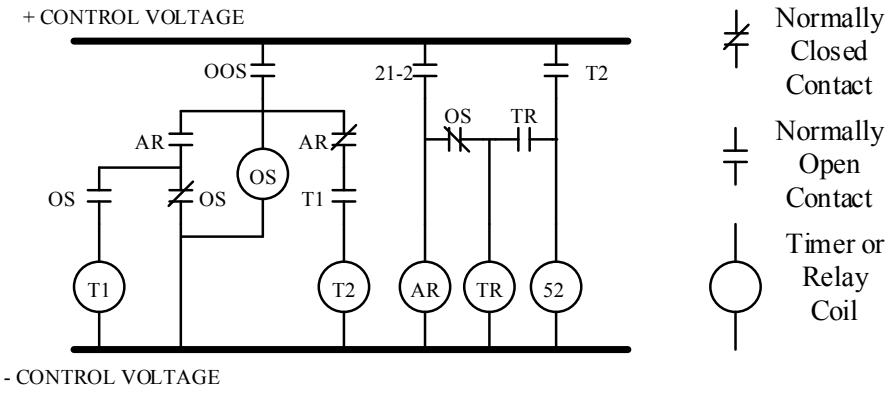

Figure 4.5: Out-of-Step Relay trip/block logic diagram.

Based on the relay zone settings and the time plot in Figure 4.4, the apparent impedance at bus 60 will enter the OOS zone at 12.89 seconds and the distance relay zone 2 at 13.24 seconds. This means that the timer T1 has to have a drop-off time of at least 350 milliseconds otherwise this unstable swing will be incorrectly blocked.

4.2 Updating Out-of-Step Relay Settings With TSA Considerations

After further reviewing the simulation results details, it is determined that the instability of the line 60-61 in the line tripping case is due to the inability of Area #2 to transfer reactive power to Area #1. Before the line trip, Area #1 has been receiving real and reactive power from Area #2. Therefore, the medial actions for this condition will begin with various methods to either reduce the power consumption requirements in Area #1 or to increase real or reactive power production in Area #1. Simply trying to push

more power through the remaining lines carries the risk of overloading the other lines and tripping other relays that further damage the system.

Load shedding is the term used for disconnecting loads in order to maintain the integrity of the overall system. Increasing real power will require changing set points on the local generators in order to drive more power into the system. Increasing reactive power may be accomplished by changing AVR outputs at the generators or, if available, bring reactive power sources such as switched shunts or synchronous condensers online.

The OOS protection logic can then be enhanced with TSA by taking the following steps. First, identify a TSA-based remedial action scheme (RAS) trip zone, which acts like a further outer ring of protection zone outside of the OOS zone. When apparent impedances reach this zone, the remedial actions available in the system may be triggered. Second, the TSA RAS contact will have a time delay similar to the OOS delay in order to allow the system to recover naturally if possible. Third, the TSA RAS will delay the OOS timer starting time in order to allow the RAS to take effect. The logic diagram is updated in Figure 4.6 in the next page. The zone setting for the RAS zone is arbitrarily selected at three times the OOS zone.

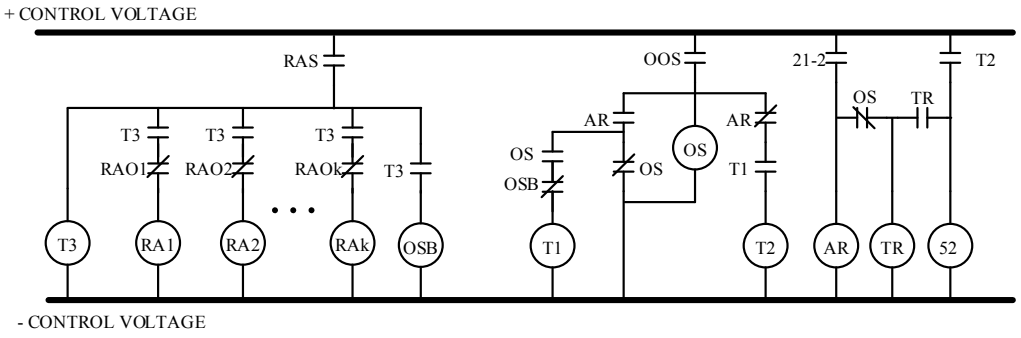

Figure 4.6: Out-of-Step Relay trip/block logic diagram updated with RAS.

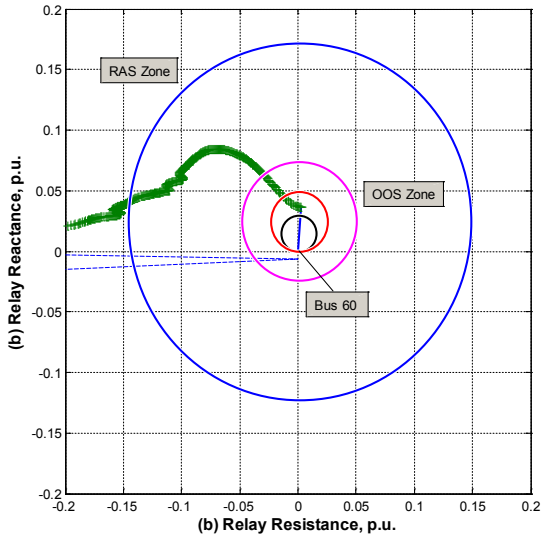

Figure 4.7: Relay settings from Figure 4.3 with the RAS zone added.

From Figure 4.6, the RAS contact is triggered when the apparent impedance reaches the RAS zone, outermost circle in Figure 4.7. The T3 timer then initiates a time delay in order to allow the swing to exit the zone within the allotted time. If the power swing stays within the zone, the remedial actions (RA) are initiated. There may be several remedial actions, so each parallel branch represents an RA option. Each of the RA contacts also have a normally closed "remedial action is available" (RAO) contact, designed to receive device status flags from the RA devices. For example, if a capacitor bank is already online, then sending a further trip signal to try to bring it online will result in no further action to support the system. The final part of the RAS block is the OSB contact that sends a blocking signal to the OOS protection.

Internal logic is added to ensure the blocking signal is removed if the RAs are not available, and the order of RA choices is based on the magnitudes of the TSA coefficients. This is done in a trial-and-error manner, because there are no set

methodologies for determining the most effective way to compare TSA coefficients with the goal of selecting control actions. Adding to this complication is the fact that there are several possible α-parameter choices, depending on the types of devices available in the system.

For the specific case (cases C & D from Chapter 3), the voltage set-point of the wind turbine does not provide sufficient information for selecting a remedial action, so simulations were run to evaluate a few additional α-parameters, including a switched shunt at bus 59 near the fault point, the generator power and reactive power outputs at a nearby synchronous machine at bus 2, and changes to a load connected near the same generator which is approximated by the ratio of power coming from the generator. These results are summarized in Table 4.1 below.

Variable	$\alpha = P_{Gen,Bus2}$	$\alpha = Q_{Gen,Bus2}$
θ_{60}	$7.9x10^{-3}$	$7.5x10^{-3}$
θ_{61}	$9.5x10^{-3}$	$8.5x10^{-3}$
θ_{60}-θ_{61}	$-2x10^{-3}$	$-1x10^{-3}$

Table 4.1: Summary of the maximum values of the tie line angle sensitivities compared to choices of α.

Based on Table 4.1, the RAS is implemented by shedding the load close to the generator at bus 2, as well as adding reactive power to the generator at the same bus. The tie line angles are shown in Figure 4.8, and the apparent impedance plot is shown in Figure 4.9 on the next page. The figures show some improvements in the tie line angles, which seems to converge to a lower angle difference than the cases without RAS or OOS.

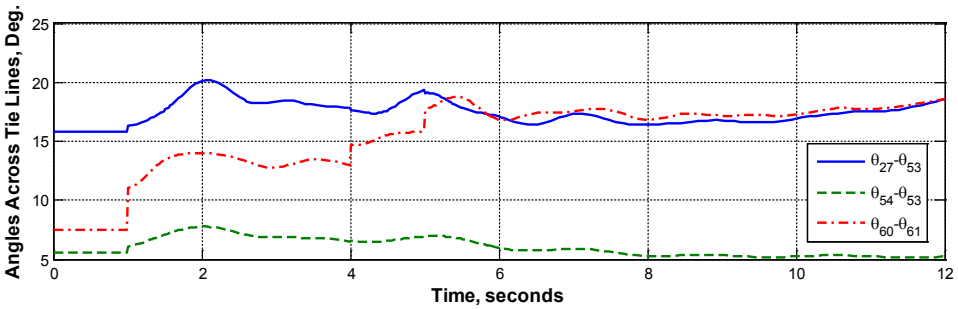

Figure 4.8: Tie line angles in the RAS case.

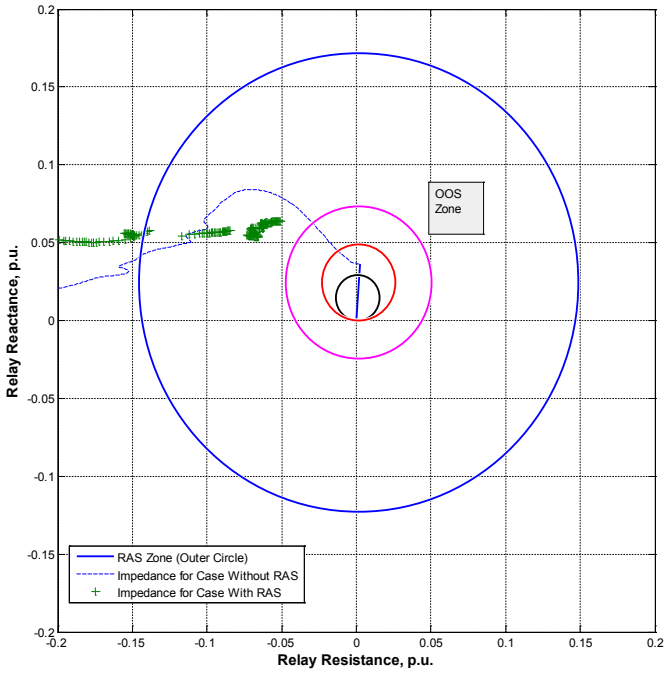

Figure 4.9: Bus 60 apparent impedances in the RAS case compared to no RAS.

Figure 4.9 shows that in the case where there is RAS operating the apparent impedance will swing back towards the original operating point before reaching the out-of-step relay zone. This means that the integrity of the tie line can be preserved at least for a longer period of time while other devices work to return balance to the system.

CHAPTER 5

CONCLUSIONS

5.1 Trajectory Sensitivity Analysis

This dissertation studied the influences of system parameters on the responses of other variables within the power system using TSA. An algorithm was achieved in the MATLAB environment based on a pre-existing power system dynamic simulation extended to handle the calculation of TSA coefficients. The proposed algorithm was then tested on the modified IEEE 68-bus system with different disturbances. The results illustrated the set of system variables that are the most sensitive to the α-parameter, which indicates the possibilities in influencing the state variables during disturbances by making adjustments to the α-parameter.

Based on the plots in the figures in Chapter 3, it can be inferred that adjusting the α-parameters associated with the DFIG will have limited influence on rest of the system. However, the α-parameter will have effects on the DFIG variables of the same machine which can be seen from analyzing the differential equations. On the other hand, changes to other candidate α-parameters can have effects on some of the state variables and system outputs that would in turn change the conditions in the system in such a way that system stability can be promoted.

5.2 Special Protection Scheme

Based on principles outlined by Frank [4], it is also possible to design controllers and remedial action schemes driven by TSA coefficients. The sensitivity coefficients can be used to determine which variables or combinations of variables are the most sensitive with respect to a controllable α-parameter and therefore become the target of control or remedial actions. Preventive protection schemes are used to extract value from TSA coefficients. This may be achieved by using TSA to analyze whether the protective actions will achieve the intended consequences, as well as check whether unintended or undesired consequences will occur. The results of the initial evaluations were incorporated into setting up a special protection scheme that is based on added a layer of TSA-driven remedial actions to an existing out-of-step relaying protection scheme.

The main off-line part of the scheme is the selection of corrective actions once the detection part of the scheme sends the request for corrective action. Each candidate for corrective action has two aspects that will be evaluated for use: the efficacy of the action, and the availability of the action. The efficacy of the action can be determined directly from the sensitivity coefficients which indicate an approximate relationship between the system variables and the α-parameters.

The merits of the special protection scheme will be determined by the amount of power system resources that can be saved, and the amount of customer loads that can be saved. If the special protection scheme can increase the stability of the system or reduce the amount of load losses compared to conventional protection, then this scheme will be a candidate for further comparison to other protection schemes. In practice, the choice of

special protection schemes will usually be determined by the amount of investment required to implement them, and the costs they impose upon the operation of the power system.

After completing the simulations and applying the protection schemes, it was demonstrated that adding the remedial action scheme can provide value to the power system in the events where out-of-step protection or unstable swings may occur. The remedial action scheme is purposefully chosen to be tripped much sooner than the out-of-step relay in order to afford the remedial action to take effect. In the end, the new special protection scheme functions as an early warning and early corrective action driver for the power system.

5.3 Practical Considerations

The sensitivity coefficients are calculated based on the state variable relationships such as the examples presented above. However, practical power systems in operation often do not measure the state variables directly. In modern power system control and management, the measured quantities usually include bus voltage magnitudes and angles, line current magnitudes and angles, bus frequencies, and power flow through equipment. These items are often measured and sampled at long intervals (1+ seconds) for state estimators. Recent developments have incorporated PMU outputs at faster measurement report rates, at 30 to 120 measurements per second, or once every 0.5 to 2 cycles.

For this proposed scheme, in order to make the application feasible in real-world applications the TSA calculations will have to be able to work with the measurements that are available, which are almost never all the measurements desired under ideal

circumstances. Furthermore, PMUs have the ability to include digital information and custom analog messages, which can be leveraged to improve the TSA analysis.

In order to make the special protection scheme effective, a more complete or automated TSA analysis must be performed by cycling through all the available system parameters. This dissertation has simplified the outcome by focusing on one subset of disturbances at particular areas within the power system, and focused on system parameters that are traditionally associated with existing methods of returning the system to stability.

Power system protection schemes are often described as an art as much as a science, because each power system has different characteristics and respond to disturbances differently, even in the same system from different operating conditions. The special protection scheme proposed in this dissertation is a new tool that may be used to cover blind spots or unexpected system responses by adding an element of sensitivity study in order to estimate possible effects of the actions that can be taken.

APPENDICES

APPENDIX A

IEEE 68-BUS TEST SYSTEM DATA

The IEEE 68-bus test system data is based primarily on the information published by Kundur [28], but additional dynamic model information is added here for the wind turbine generators. Table A.1 includes the bus data including initial condition voltages and angles as well as bus type. PV buses are buses with power sources (generators) with voltage control, PQ buses are buses with only specified loads or sources without voltage control, and the Slack bus is the bus with the reference voltage. Table A.2 includes the transmission line and transformer data.

BUS#	kV Rating	Initial Voltage	Initial Angle	BUS#	kV Rating	Initial Voltage	Initial Angle
1	20	1.000	33.89	35	230	0.889	14.43
2	20	1.000	38.97	36	230	0.927	7.71
3	20	1.000	42.28	37	230	0.922	32.38
4	20	1.000	46.16	38	230	0.927	27.58
5	20	1.000	44.94	39	230	0.878	-1.74
6	20	1.000	49.06	40	230	0.903	35.25
7	20	1.000	51.59	41	230	0.995	65.89
8	20	1.000	40.91	42	230	0.997	58.08
9	20	1.000	48.86	43	230	0.900	-1.80
10	20	1.000	35.83	44	230	0.898	-1.76
11	20	1.000	35.95	45	230	0.886	15.03
12	20	1.000	14.23	46	230	0.916	31.05
13	20	1.000	0.00	47	230	0.910	25.76
14	20	1.000	67.43	48	230	0.906	27.91
15	20	1.000	58.94	49	230	0.919	37.22
16	20	1.000	62.64	50	230	0.911	35.12
17	230	0.937	-2.70	51	230	0.894	19.81
18	230	0.977	55.59	52	230	0.918	30.67
19	230	0.931	40.25	53	230	0.918	25.44

Table A.1: IEEE 68-bus system bus data.

BUS#	kV Rating	Initial Voltage	Initial Angle	BUS#	kV Rating	Initial Voltage	Initial Angle
20	100	0.943	39.01	54	230	0.937	31.05
21	230	0.921	37.10	55	230	0.918	29.28
22	230	0.949	42.85	56	230	0.896	29.16
23	230	0.953	42.46	57	230	0.892	28.78
24	230	0.926	34.04	58	230	0.894	29.59
25	230	0.958	33.24	59	230	0.884	25.99
26	230	0.947	34.26	60	230	0.885	24.94
27	230	0.937	33.22	61	230	0.902	17.39
28	230	0.949	38.08	62	230	0.902	33.41
29	230	0.956	41.24	63	230	0.897	32.12
30	230	0.916	23.39	64	230	0.929	32.36
31	230	0.928	27.45	65	230	0.899	32.75
32	230	0.939	27.67	66	230	0.898	31.27
33	230	0.932	22.68	67	230	0.899	31.66
34	230	0.938	14.21	68	230	0.918	33.82

Table A.1: IEEE 68-bus system bus data. (Continued)

From Bus	To Bus	Rated MVA	Rated KV	Line Resistance	Line Reactance	Shunt Admittance
67	68	100	230	0.0009	0.0094	0.0855
66	67	100	230	0.0018	0.0217	0.183
65	66	100	230	0.0009	0.0101	0.08615
63	62	100	230	0.0004	0.0043	0.03645
53	54	100	230	0.0035	0.0411	0.34935
59	58	100	230	0.0006	0.0092	0.0565
58	57	100	230	0.0002	0.0026	0.0217
62	65	100	230	0.0004	0.0043	0.03645
60	57	100	230	0.0008	0.0112	0.0738
59	60	100	230	0.0004	0.0046	0.039
19	68	100	230	0.0016	0.0195	0.152
57	56	100	230	0.0008	0.0128	0.0671
56	55	100	230	0.0013	0.0213	0.1107
66	56	100	230	0.0008	0.0129	0.0691
52	37	100	230	0.0007	0.0082	0.06595
37	27	100	230	0.0013	0.0173	0.2655
52	55	100	230	0.0011	0.0133	0.1069
55	54	100	230	0.0013	0.0151	0.1286

Table A.2: IEEE 68-bus system branch data.

From Bus	To Bus	Rated MVA	Rated KV	Line Resistance	Line Reactance	Shunt Admittance
25	26	100	230	0.0032	0.0323	0.2655
55	54	100	230	0.0013	0.0151	0.1286
54	25	100	230	0.007	0.0086	0.073
25	26	100	230	0.0032	0.0323	0.2655
27	26	100	230	0.0014	0.0147	0.1198
68	21	100	230	0.0008	0.0135	0.1274
28	29	100	230	0.0014	0.0151	0.1245
26	28	100	230	0.0043	0.0474	0.3901
26	29	100	230	0.0057	0.0625	0.5145
42	41	100	230	0.004	0.06	1.125
41	40	100	230	0.006	0.084	1.575
18	42	100	230	0.004	0.06	1.125
18	50	100	230	0.0012	0.0288	0.2575
50	51	100	230	0.0009	0.0221	0.81
51	45	100	230	0.0004	0.0105	0.36
49	46	100	230	0.0018	0.0274	0.135
68	24	100	230	0.0003	0.0059	0.034
46	38	100	230	0.0022	0.0284	0.215
38	33	100	230	0.0036	0.0444	0.3465
31	38	100	230	0.0011	0.0147	0.1235
39	45	100	230	0	0.0839	0
39	44	100	230	0	0.0411	0
43	44	100	230	0.0001	0.0011	0
43	17	100	230	0.0005	0.0276	0
36	61	100	230	0.0022	0.0196	0.17
36	61	100	230	0.0022	0.0196	0.17
63	58	100	230	0.0007	0.0082	0.06945
23	22	100	230	0.0006	0.0096	0.0923
60	61	100	230	0.0023	0.0363	0.1902
61	30	100	230	0.0019	0.0183	0.145
61	30	100	230	0.0019	0.0183	0.145
32	30	100	230	0.0024	0.0288	0.244
30	53	100	230	0.0008	0.0074	0.24
30	31	100	230	0.0013	0.0187	0.1665

Table A.2: IEEE 68-bus system line data. (Continued)

From Bus	To Bus	Rated MVA	Rated KV	Line Resistance	Line Reactance	Shunt Admittance
33	32	100	230	0.0008	0.0099	0.084
34	33	100	230	0.0011	0.0157	0.101
34	36	100	230	0.0033	0.0111	0.725
45	35	100	230	0.0007	0.0175	0.695
23	24	100	230	0.0022	0.035	0.1805
44	45	100	230	0.0025	0.073	0
40	48	100	230	0.002	0.022	0.64
48	47	100	230	0.0025	0.0268	0.2
48	47	100	230	0.0025	0.0268	0.2
47	53	100	230	0.0013	0.0188	0.655
31	53	100	230	0.0016	0.0163	0.125
60	61	100	230	0.0023	0.0363	0.1902
53	54	100	230	0.0035	0.0411	0.34935
53	27	100	230	0.032	0.32	0.205
18	49	100	230	0.0038	0.05705	1.16
21	22	100	230	0.0008	0.014	0.12825
68	37	100	230	0.0007	0.0089	0.0671
17	36	100	230	0.0005	0.0045	0.16
1	54	100	20	0	0.0181	0
11	32	100	20	0	0.013	0
12	36	100	20	0	0.0075	0
13	17	200	20	0	0.00165	0
14	41	100	20	0	0.0015	0
15	42	100	20	0	0.0015	0
16	18	100	20	0	0.003	0
20	19	100	100	0.0007	0.0138	0
35	34	100	230	0.0001	0.0074	0
65	64	100	230	0.0016	0.0435	0
2	58	100	20	0	0.025	0
63	64	100	230	0.0016	0.0435	0
3	62	100	20	0	0.02	0
4	19	100	20	0.0007	0.0142	0
5	20	100	20	0.0009	0.018	0
6	22	100	20	0	0.0143	0
8	25	100	20	0.0006	0.0232	0

Table A.2: IEEE 68-bus system line data. (continued)

From Bus	To Bus	Rated MVA	Rated KV	Line Resistance	Line Reactance	Shunt Admittance
8	25	100	20	0.0006	0.0232	0
9	29	100	20	0.0008	0.0156	0
10	31	100	20	0	0.026	0
7	23	100	20	0.0005	0.0272	0

Table A.2: IEEE 68-bus system line data. (continued)

APPENDIX B

EXPANDED LOGIC AND PROCESS FLOW CHARTS

The flow charts below are expansions of the processes and logics that are described throughout the dissertation.

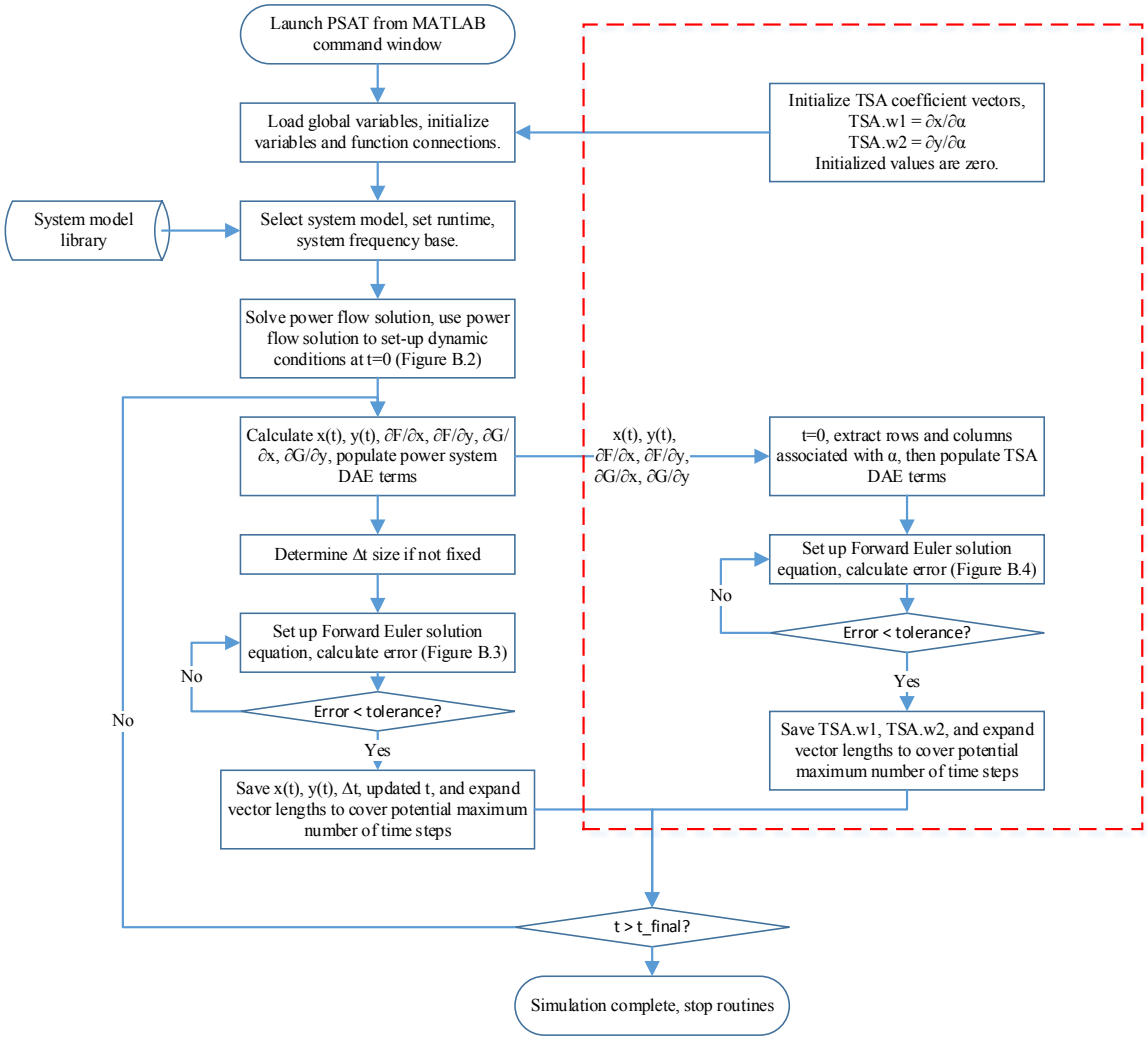

Figure B.1: Overall time domain simulation algorithm details.

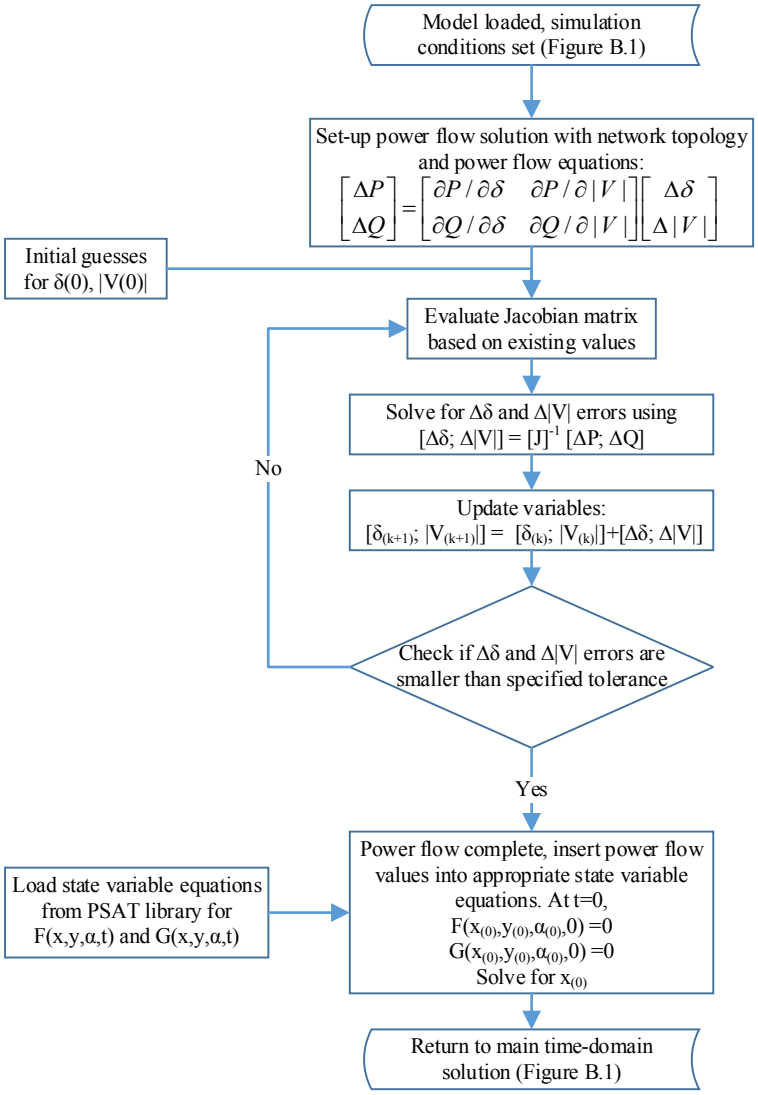

Figure B.2: Power flow and time-domain simulation initialization algorithm details.

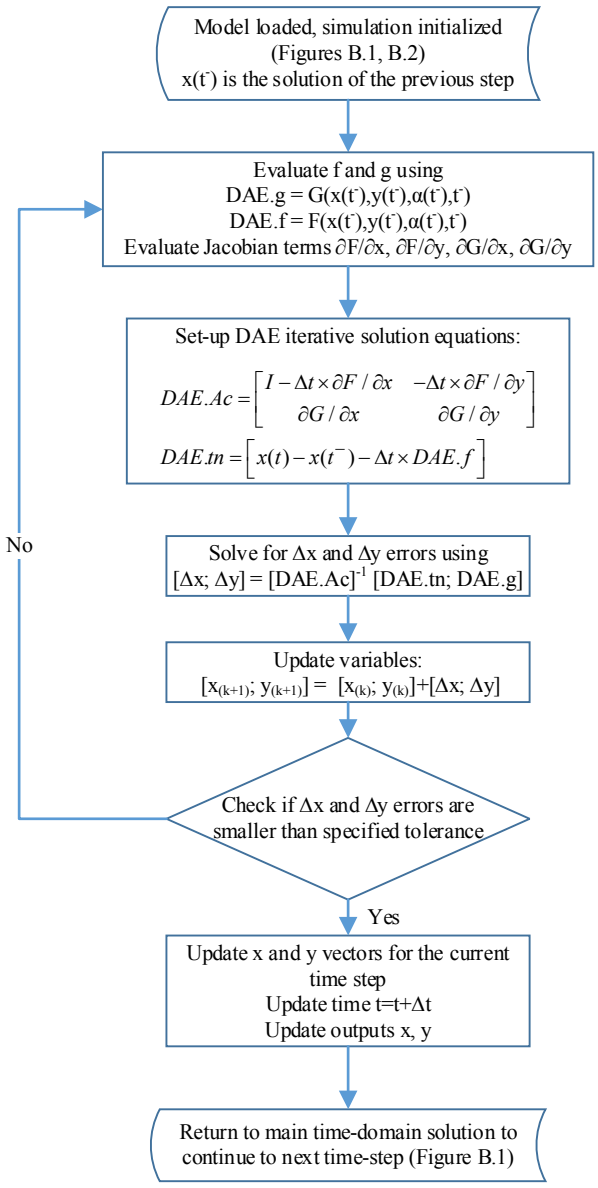

Figure B.3: Time-domain simulation Forward Euler integration algorithm details

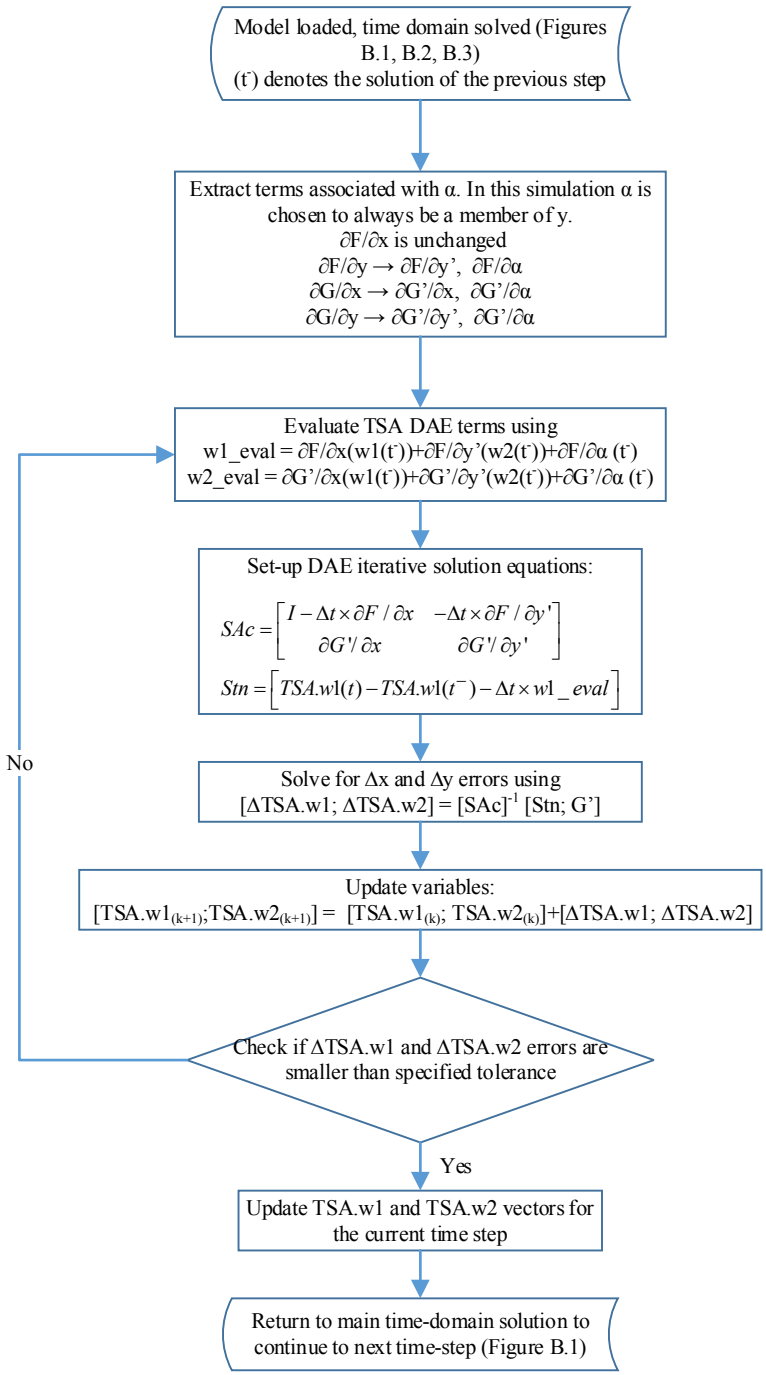

Figure B.4: TSA calculation Forward Euler integration algorithm details

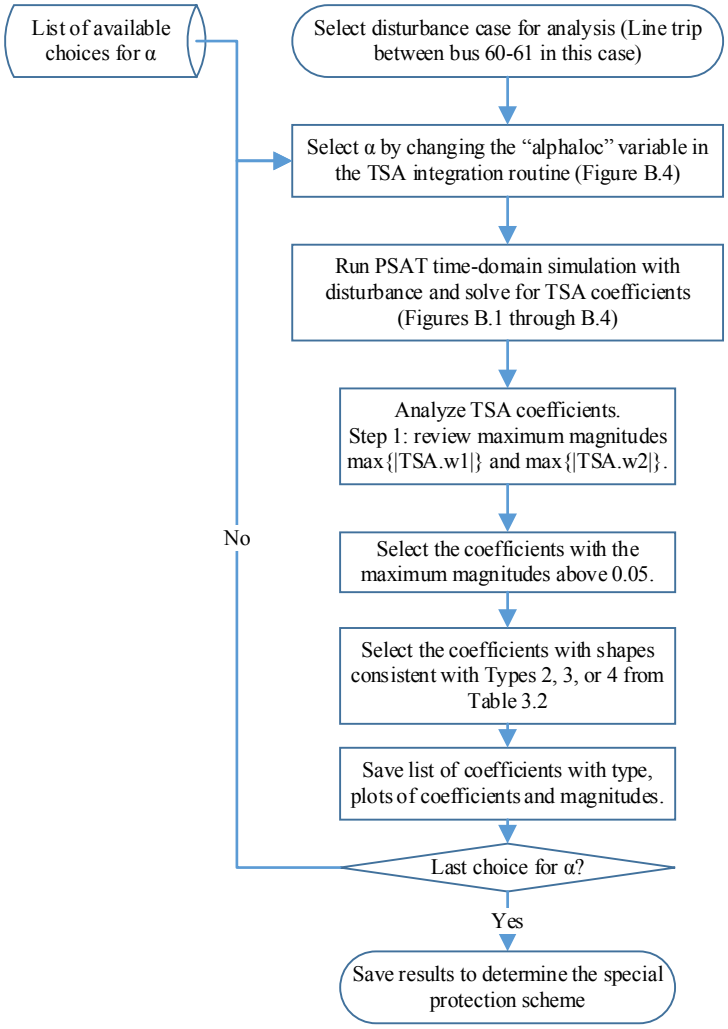

Figure B.5: Usage of TSA coefficients in special protection scheme set-up

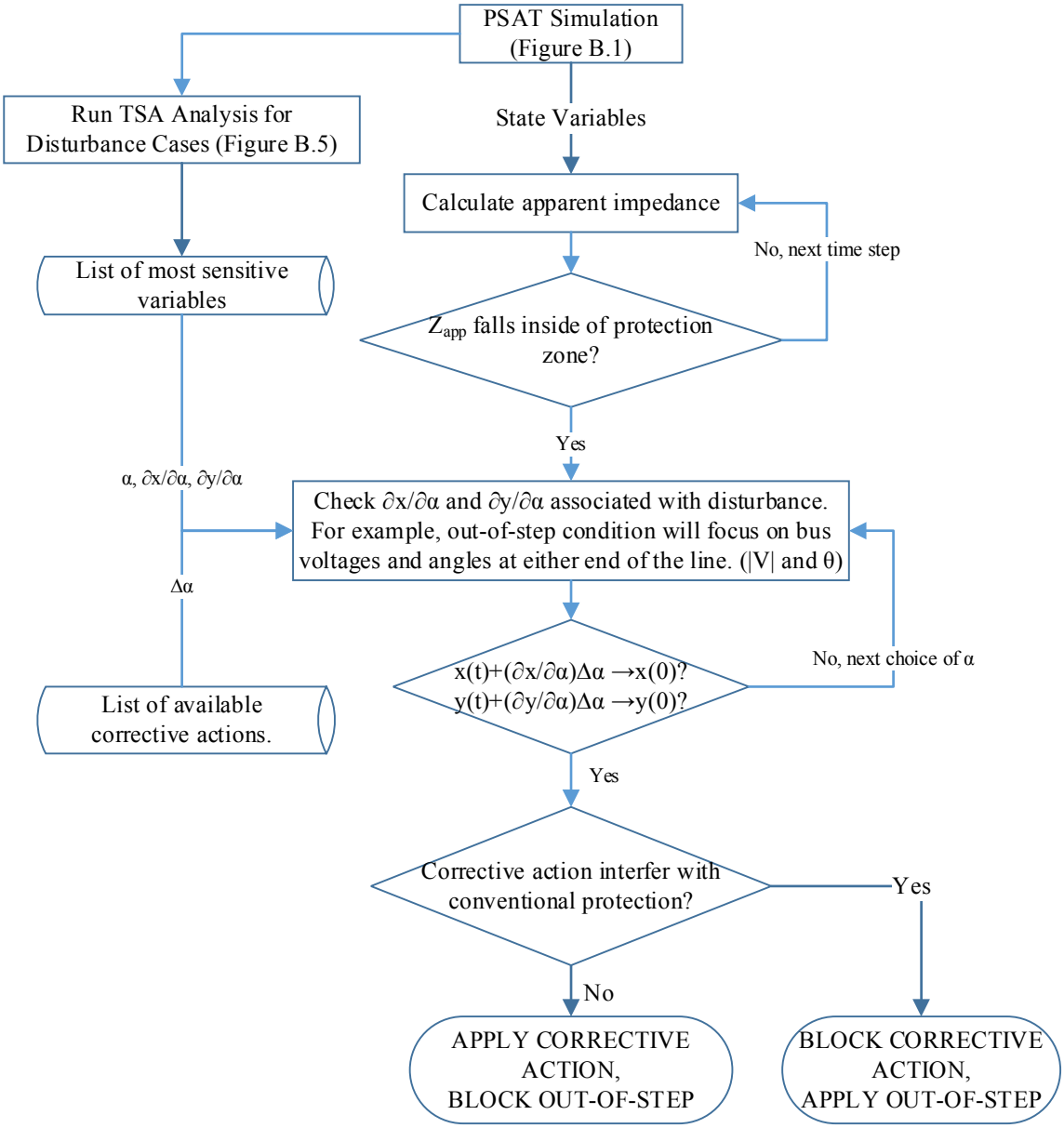

Figure B.6: Expanded trip and block logic for special protection scheme

REFERENCES:

[1] Federico Milano, “Power System Analysis Toolbox: Documentation for PSAT”, self-published, http://www.power.uwaterloo.ca/_fmilano/psat.htm, Feb. 2008

[2] P.M. Anderson and A.A. Fouad, “Power System Control and Stability”, IEEE Press Power Engineering Series, Wiley-Interscience, Second Edition, 2003.

[3] P.M. Anderson and A. Bose, “Stability Simulation of Wind Turbine Systems”, IEEE Transactions on Power Apparatus and Systems, vol. 102, no. 12, pp. 3791-3795, Dec. 1983

[4] Paul M. Frank, “Introduction to System Sensitivity Theory”, Academic Press, 1978

[5] Mark J. Laufenberg and M.A. Pai, “Sensitivity Theory in Power Systems: Application in Dynamic Security Analysis”, Proceedings of the 1996 IEEE International Conference on Control Applications, September 1996.

[6] Mark J. Laufenberg and M.A. Pai, “A New Approach to Dynamic Security Assessment Using Trajectory Sensitivities”, IEEE Transactions on Power Systems, Vol. 13, No. 3, August 1998.

[7] Guanji Hou, “Trajectory Sensitivity Based Power System Dynamic Security Assessment”, Ph.D. Dissertation, Arizona State University, May 2012.

[8] K. N. Shubhanga and A.M. Kulkarni, “Determination of effectiveness of stransient stability controls using reduced number of trajectory sensitivity computations”, IEEE Trans. Power Syst., vol. 19, no. 1, pp. 473-482, 2004

[9] L. Tang and J. McCalley, “Trajectory sensitivities: Applications in power systems and estimation accuracy refinement”, IEEE Power and Energy Society (PES). Vancouver, BC, Canada, 21-25 July, 2013.

[10] D. Chatterjee, A. Ghosh, and M.A. Pai, "Trajectory sensitivity analysis in distributed generation systems ", IEEE International Conference on Power Electronics, Drives and Energy Systems, New Delhi, India, 12-15 Dec. 2006.

[11] A. Mitra and D. Chatterjee, "A new sensitivity based approach to study impact of wind power penetration on transient stability", IEEE International Conference on Power Electronics, Drives and Energy Systems (PEDES), Bengaluru, India, 16-19 Dec. 2012.

[12] Paul M. Anderson, “Power System Protection”, IEEE Press Power Engineering Series, pp. 894-909, 2007

[13] NERC Board of Trustees, “Standard PRC-012-0 – Special Protection System Review Procedure”, North American Electric Reliability Corporation (NERC), 2005

[14] NERC Board of Trustees, “Standard PRC-014-0 – Special Protection System Assessment”, NERC, 2005

[15] NERC Board of Trustees, “Standard PRC-015-0 – Special Protection System Data and Documentation”, NERC, 2007

[16] NERC Board of Trustees, “Standard PRC-017-0 – Special Protection System Maintenance and Testing”, NERC, 2007

[17] LNF de Villiers, JM van Coller, "Placing and Setting of Out-of-Step Relays",8th IEE International Conference on Developments in Power System Protection, 2004.

[18] Kevin W. Jones, "Power Swing Relaying in the Texas Panhandle – An Out-of-Step Odyssey", 68th Annual Conference for Protective Relay Engineers, 2015

[19] D. Tholomier, D. Paraiso, A. Apostolov, "Adaptive Protection of Transmission Lines", Clemson University Power Systems Conference, 2009

[20] J. Ariza, J. Gers, "Setting and Testing of Power Swing Blocking and Out of Step Relays Considering Transient Stability Conditions", IET 9th International Conference on Developments in Power System Protection, 2008

[21] C. Sena, R. Franco, A. Giusto, "Assessment of Power Swing Blocking Functions of Line Protective Relays for a Near Scenario of the Uruguayan System", IEEE/PES Transmission and Distribution Conference and Exposition: Latin America, 2008

[22] Juergen Holbach, "New Out of Step Blocking Algorithm for Detecting Fast Power Swing Frequencies", Power Systems Conference, 2006

[23] J.S. Thorp, A.G. Phadke, S.H. Horowitz, M.M. Begovic, "Some Applications of Phasor Measurements to Adaptive Protection", IEEE Transactions on Power Systems, Vol. 3, Issue 2, 1988

[24] V. Centeno, J. De La Ree, A.G. Phadke, G. Michel, J. Murphy, R. Burnett, "Adaptive Out-of-Step Relaying Using Phasor Measurement Techniques", IEEE Computer Applications in Power, Vol. 6, Issue 4, 1993

[25] IEEE Power & Energy Society Power System Relaying Committee, "IEEE Standard for Synchrophasor Measurements for Power Systems," IEEE Std C37.118.1™ -2011 (Revision of IEEE Std C37.118.1™ -2005)

[26] IEEE Power & Energy Society Power System Relaying Committee, "IEEE Standard for Synchrophasor Data Transfer for Power Systems," IEEE Std C37.118.2™ -2011 (Revision of IEEE Std C37.118.1™ -2005)

[27] Ian A. Hiskens and M.A. Pai, "Trajectory Sensitivity Analysis of Hybrid Systems", IEEE Transactions on Circuits and Systems – Part I: Fundamental Theory and Applications, Vol. 47, No. 2, February 2000.

[28] P. Kundur, "Power System Stability and Control", McGraw Hill, First Edition, 1994

[29] Hany A. Abdelsalam, "A Centralized Wide Area Control of FACTS for Damping Power System Inter-Area Oscillation", Ph.D. Dissertation, Southern Illinois University Carbondale, USA, May 2011.

[30] J. Lewis Blackburn and Thomas J. Domin, "Protective Relaying Principles and Applications", CRC Press, Third Edition, 2007.

[31] Allan Greenberg, "Electrical Transients in Power Systems", Wiley-Interscience, Second Edition, 1991.

[32] SERC Reliability Corporation, "Automatic Underfrequency Load Shedding Requirements: PRC-006-SERC-01", SERC Standards & Regional Criteria Webpage, www.serc1.org/programs-areas/standards-regional-criteria, March 2013

[33] J. J. Grainger and W. D. Stevenson, Jr., “Power System Analysis”, McGraw-Hill , International Edition, 1994.

[34] IEEE Power & Energy Society Substations and Power System Relaying Committees, "IEEE Standard for Electrical Power System Device Function Numbers, Acronyms, and Contact Designations," IEEE Std C37.2™ -2008